Targeted Prodrugs

of a

Novel Platform Anthracycline: Doxazolidine

by:

Daniel Lee Rudnicki

B.A. *magna cum laude* University of Colorado at Boulder, 2002.

A Thesis submitted to the Faculty of the Graduate School of the University of Colorado in partial fulfillment of the requirements for the degree of Doctor of Philosophy

Department of Chemistry and Biochemistry

2012

This Thesis for Doctor of Philosophy degree by Daniel Lee Rudnicki titled

Targeted Prodrugs of a novel Platform Anthracycline: Doxazolidine

has been approved for the

Department of Chemistry and Biochemistry by:

_____

Tad Koch

_____

Dylan Taatjes

_____

Date

The final copy of this thesis has been examined by the signators and we find that both the content and the form meet acceptable presentation standards of scholarly work in the above mentioned discipline.

Targeted Prodrugs of a Novel Platform Anthracycline: Doxazolidine

Rudnicki, Daniel (Ph.D., Chemistry)

Thesis Directed by Professor Tad H. Koch

Abstract

Doxorubicin (Dox) is an antitumor drug that has been used as a chemotherapeutic agent in the clinic for over 30 years. Dox treatments have been hindered by significant dose limiting cardiotoxic effects resulting in irreversible cardiomyopathy. A Dox variant, Doxazolidine (Doxaz) is a Dox-formaldehyde conjugate discovered in the Koch lab. Doxaz operates via a distinct mechanism, and exhibits an improved therapeutic profile compared to Dox. Doxaz suffers from poor aqueous stability; however, stabilization of Doxaz has been achieved through the use of enzymatically activated carbamate prodrugs. This thesis presents the synthesis and preliminary evaluation of Doxaz prodrugs intended for commercialization. The prodrugs contain the active platform therapeutic (Doxaz), an enzyme cleavage site, a self-eliminating spacer to increase cleavage efficiency, and in some cases, a maleimide moiety for passive targeting through albumin biniding. The enzymes targeted are proteases such as plasmin and cathepsin B. Also presented are prodrugs aimed at tumor associated hypoxia and enzymes such as NQO1 and NQO2. The synthesis of these prodrugs places an emphasis on scalable manufacturing processes. These prodrugs are currently, or will be undergoing complete biological characterization and animal studies in varying species.

Although many have contributed

to the successful completion of this thesis,

I dedicate this to my one true inspiration,

my son, Macallum.

May you enjoy all that life has given you,

and

may cancer never touch you or the ones you love.

Acknowledgements

After a short excursion as a professional figure skater, I returned to the academic environment hungry for a challenge. Completion of my undergraduate degree, and some time in industry led me to the pursuit of a Ph.D. I was accepted to graduate schools around the country, however after visiting those schools, I realized that I needed to be close to my childhood home and family in Colorado. After a welcoming barbecue, and a long discussion with Professor Tad Koch, I knew I had made the right choice, and it was imperative that Dr. Koch be my advisor.

During my graduate career, Tad has supported me through the trials and tribulations of research science, the birth of my son, and a near fatal motorcycle accident. During all of this he has given me the confidence to continue at any cost. I thank Tad not only for his academic guidance, but for the fatherly guidance I so needed all too often. I find the story of Tad's research to be one of the most exciting and intriguing stories of modern research. I thank him so much for allowing me to play a part, however small. I believe the journey is only now beginning.

I would like to especially thank Dr. Ben Barthel and Price Kirby. Ben, I admire you for being so amazing at all the things I am not. You are a wonderful friend, confidant and mentor, not to mention a phenomenal scientist. I look forward to our future endeavors. Price, thank you so much for your fun-loving spirit, your superb attention to experimental detail and long nights of foosball.

I must finally thank those who stood by me in quiet emotional and financial support. Primarily, my loving wife who has given me more to smile about than any man deserves. Fiona, you and Mac are proof that only good things come from figure skating. Without you, none of this would have been possible. To my sister Denise who has nearly finished her successful battle with breast cancer, thank you for the motivation and realization of the importance of my work. To my mother, thank you for all the gifts you have given me throughout my life, and I hope that with all my faults, I am able to make you proud. And finally, to the figure skaters and wonderful friends, especially Emily Williams and Laura Smith, thank you so much for your kindness and words of encouragement. I hope your dreams come true as mine have.

Table of Contents

List of Tables

Chapter 1

None

Chapter 2

Chapter 3

Chapter 4

List of Figures

Chapter 1

Chapter 2

Chapter 3

Chapter 4

List of Schemes

Chapter 1

None

Chapter 2

Chapter 3

Chapter 4

Chapter 1 Introduction

1.1 History of Doxorubicin (Dox)

Daunorubicin, also known by its trade name Daunomycin, and related members of the anthracycline family of natural products have been prominent anti-cancer therapeutics since their discovery in the 1960's by an Italian research company, Farmitalia Research Laboratories. An interesting strain of *Streptomyces peucetius* which contained a red pigmentation that was isolated from the soil surrounding a 13th century castle, Castel del Monte, produced the red daunorubicin. The discovery was shared with a French group who discovered the compound at the same time. The two groups cooperatively named the compound daunorubicin (Dau), combining the word Dauni, a pre-Roman tribe that occupied the area of Italy where the compound was discovered, and rubis, the French word for ruby which was descriptive of the red color.[1] In the early 1960's, daunorubicin had some success as a lymphoma and acute leukemia therapeutic until it became apparent that daunorubicin had a debilitating side effect, namely chronic cardiotoxicity.[2]

During this time, Farmitalia Research Laboratories discovered that small changes to the daunorubicin functional groups had a measurable effect on the biological activity. Using *N*-nitroso-*N*-methyl urethane, *Streptomyces peucetius* was mutated to produce a new strain, *Streptomyces peucetius* var *caesius* which afforded a different, biologically active, red colored antibiotic. Arcamone *et al*. initially referred to this new compound as Adriamycin, after the Adriatic Sea, but later changed the name to doxorubicin to conform to the previous conventions.[3] Doxorubicin showed better cytotoxicity toward both murine and human tumors,

especially solid tumors.[2-4] The structures of some common anthracyclines, doxorubicin, daunorubicin and epirubicin are provided in Figure 1.1.1.

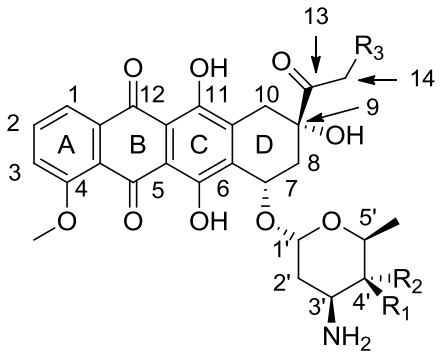

Doxorubicin: R_1=R_3=OH; R_2=H
Daunorubicin: R_1=OH; R_2=R_3=H
Epirubicin: R_1=H; R_2=R_3=OH

Figure 1.1.1 Common Anthracycline Structures. The recognized ring and crbon numbering system of some common anthracyclines.

Doxorubicin was approved by the U.S. Food and Drug Administration in the 1970s and has historically been one of the most successful agents for the treatment of several types of cancers including leukemia, lymphoma, sarcoma, and solid tumors of the lung, ovaries and breast.[5] Currently doxorubicin is used as a clinical therapeutic in many multidrug protocols in an attempt to improve its therapeutic index, and continues to be a lucrative pharmaceutical. For example, sales of CAELYX (pegylated liposomal doxorubicin hydrochloride) approved for the treatment of ovarian cancer, metastatic breast cancer and Kaposi's sarcoma, were $75 million for the fourth quarter and $284 million for the full year of 2010 as reported by Merck. The marketing rights for CAELYX returned to Johnson & Johnson on Dec. 31, 2010.[6]

1.2 Doxorubicin Cardiotoxicity

Despite its vast utility in clinical oncology, doxorubicin hydrochloride or Adriamycin use is limited by a potentially fatal cardiomyopathy. In early trials, the onset of congestive heart failure was observed to be abrupt with a very poor prognosis. Fatality was reported in 70 – 80% of cases.[7,8] Physicians currently monitor risk factors such as age,[9] preexisting cardiac disease[9,10,11] dosing regimen,[9,12,13] and concomitant medications such as mitomycin, vinblatine sulfate, vincistine sulfate, decarbazine, bleomycin sulfate, etoposide, amascrine and megestrol acetate[10,14-20] as they could contribute to the deleterious side effect. Most importantly, the total dose of Dox given has the greatest impact on Dox induced cardiomyopathy. Many groups have shown that the incidence of cardiomyopathy sharply increases at lifetime doses above 550 mg/m^2 of body surface area.[9,10,21] The current, clinically accepted lifetime limit of anthracyclines is 550 mg/m^2.

To date, the mechanism of Dox dose and treatment limiting cardiotoxicies are poorly understood. *In vitro* and *in vivo*, anthracyclines have been shown to stimulate superoxide production via the reduced form of nicotinamide-adenine dinucleotide phosphate (NADPH).[22-24] The mechanism of this oxidative stress is hypothesized to be preceded by reduction of the anthracycline quinone to a semiquinone radical, with subsequent reaction with dioxygen to produce the superoxide.[22] Superoxide radicals are toxic to tissues, and their initiation of a peroxide radical chain reaction can lead to the conversion of unsaturated fatty acids to lipid peroxides. Lipid peroxides rapidly decompose to yield many products most notably malondialdehyde.[24] Malondialdehyde was not detected in untreated heart tissue; however, after doxorubicin treatment, malondialdehyde was detected two to six days after

administration in rats. Malondialdehyde was also observed in human platelet-rich plasma after doxorubicin treatment.[25]

The protection of cells from oxygen radicals such as superoxide and peroxides encompasses many enzymes such as the glutathione and selenium dependent glutathione peroxidase,[26,27] catalase,[23,26] and superoxide dismutase.[28] It has been shown in animal models that cardiac concentrations of these protective enzymes are much lower than in other organs,[22,23] and doxorubicin acutely depresses the protective glutathione peroxidase[23] which renders the cell vulnerable to lipid peroxides and hydrogen peroxide. The inhibition of enzymes meant to deplete toxic oxygen radicals causes doxorubicin to potentiate its own toxicity. Thus, the lower concentration of detoxifying enzymes in cardiac tissue appears to elevate the risk of heart damage. In addition, an acute reduction of glutathione in the heart after treatment with doxorubicin has been observed.[29] The exact role of reduced glutathione in the myocardium is not entirely known; however, it has been found to have a significant role in muscle contraction, implicating that its depletion due to doxorubicin could lead to heart failure.[30]

Mitochondrial damage through the inhibition of coenzyme Q_{10} or ubiquinone, has also been postulated as a cause of doxorubicin induced cardiotoxicity. Coenzyme Q_{10} is a coenzyme of mitochondrial succinoxidase and nicotinamide-adenine dinucleotide oxidase, which are involved in the electron-transfer process of respiration and coupled phosphorylation.[31] Doxorubicin can interfere with these enzyme systems.[32] The high concentration of mitochondria in myocardial tissue coupled with the doxorubicin induced alteration of mitochondria implicates this mechanism. The ability of doxorubicin to bind the apoenzyme has

been used as an explanation of the observed inhibitory effect because the doxorubicin apoenzyme conjugate disallows the binding of the true coenzyme Q_{10} due to structural similarity.

Additionally, Dox has been shown to play a role in iron depletion and iron homeostasis in cytosolic fractions of myocardia obtained from patients after surgery.[33] Iron acts as a cofactor in many enzyme systems as varied as respiration and DNA synthesis.[34] Iron Regulatory Protein 1 (IRP-1) is the cytosolic form of mitochondrial aconitase and is a bifunctional protein that regulates the concentration of metabolically available low molecular weight iron and modulates the iron uptake versus sequestration.[37,38] IRP-1 can also be inactivated by a secondary alcohol metabolite of Dox, DOXol.[33] DOXol is formed from Dox by reduction of the C-13 carbonyl group to a secondary alcohol by NADPH-dependent aldo-keto reductases that are present in cytosolic fractions of human myocardium.[35] This reduction is shown schematically in Figure 1.2.1. DOXol inactivates IRP-1 by initiating redox mechanisms that sequester iron from the [4Fe-4S] cluster in aconitase forming Dox and Dox-Fe(II).[33] This Dox-iron conjugate upsets the equilibrium between aconitase and IRP-1 by the irreversible modification of cysteine residues on IRP-1. The disruption of this equilibrium is critical to iron homeostasis because under normal conditions, aconitase acts as an isomerase and uses the [4Fe-4S] center to convert citrate to isocitrate in the Krebs cycle. When cellular iron levels fluctuate, the [4Fe-4S] center assembles or disassembles. Under low iron levels, the [4Fe-4S] center disassembles and aconitase takes on the role of IRP-1, a translational regulator of both ferritin and the transferrin receptor (TfR). IRP-1 negatively affects the transcription of the iron storage protein ferritin, and positively affects the iron uptake protein TfR. Disruption of this equilibrium causes cardiac cells

to lose their ability to regulate iron, causing the malformation of many iron dependent enzymes such as catalase, lipoxygenase, cytochromes and myoglobin.[36]

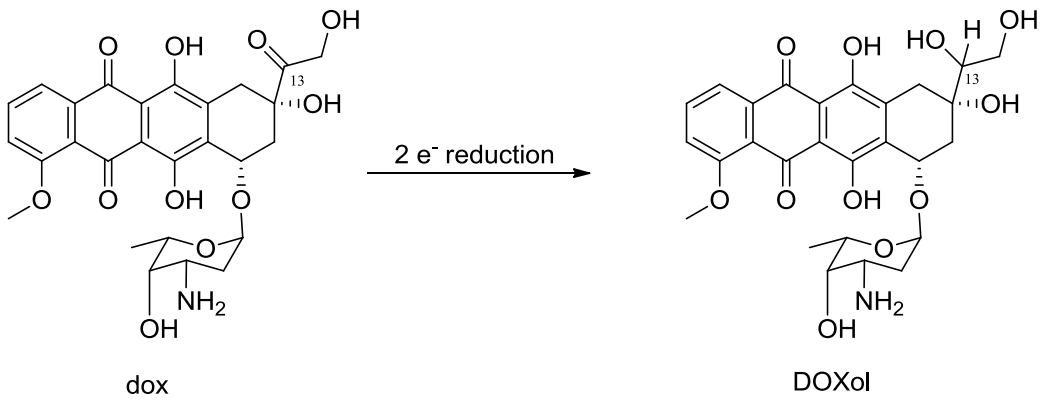

Figure 1.2.1 Reduction of Dox to DOXol. The ketone at position 13 is reduced to an alcohol.

1.3 Mechanism of Doxorubicin Antitumor Activity

Multiple mechanisms have been proposed for the efficacy of doxorubicin, but, like the observed Dox induced cardiotoxicity, the exact mechanism is still unclear. Although the primary function has been ascribed to drug interference with DNA topoisomerase II, inhibition of DNA-dependent functions through intercalation of DNA, direct DNA damage, free radical formation and membrane interactions are also implicated. A schematic representation of these processes is provided in Figure 1.3.1. A mechanism studied by the Koch group amongst others is doxorubicin crosslinking of DNA via first its induction of formaldehyde through complexation with iron and production of reactive oxygen species and second its use of the formaldehyde to create a covalent bond between Dox and a DNA G-base.

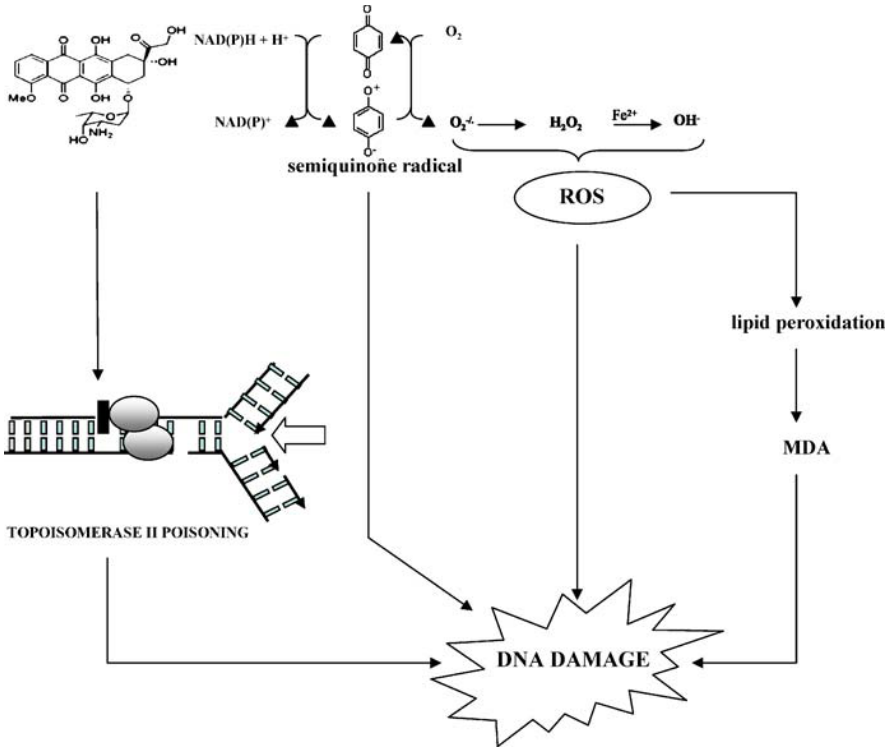

Figure 1.3.1 Doxorubicin induced DNA damage. Dox can damge DNA via induction of reactive oxygen species and formation of DNA strand breaks as a topoisomerase II poison.

DNA is recognized as the primary pharmacological target of doxorubicin. The planar tetracyclic chromophore can insert itself between adjacent base pairs, while the electrostatic interactions between the phosphate groups of DNA and the positively charged amino group of the sugar moiety stabilize the DNA-Dox conjugate in the minor groove. The cytotoxic activity is not only dependent on the drug's ability to bind to DNA, based on the observation that the site of binding is more important than the binding affinity. Effective intercalating agents have been found to possess an additional function: the ability to interfere with the function of Topoisomerase II (Topo II).[40,41] Antitumor activity of Topoisomerase II inhibitors is achieved by forming DNA-drug-enzyme complexes that stabilize the cleavable complex.[42] The ability of doxorubicin to intercalate into DNA places it at the interface of the enzyme active site and the

DNA cleavage site, preventing DNA religation. The resulting double stranded DNA breaks are lethal to the cell.

In addition to Topoisomerase II poisoning, free radical formation through the reduction-oxidation pathway of the anthracycline quinone, as previously described, can cause DNA damage. The intercalation of the semiquinone radical has been hypothesized to cause direct DNA damage; however, the free radical effect can only be detected at high drug levels.[43] Interestingly, the addition of Dox and antioxidants to tumor cells offered no protection against the cytotoxic potential of Dox. It is therefore likely that the production of reactive oxygen species is not the only source of antitumor toxicity.[44-47]

The availability of formaldehyde as a result of doxorubicin and iron induced reactive oxygen species allows for the formation of a Dox-formaldehyde-DNA conjugate. Crystal structures of both daunorubucin and epirubicin bound to DNA[48,49] illustrate how the formaldehyde derived CH_2 forms a bridge between the exocyclic amine of guanine to the 3'-amino substituent of the anthracycline. The sequence 5'-NGC-3' is the most effective sequence to afford the covalent bond of the anthracycline to the guanine, while situating the anthracycline in a position to hydrogen bond to the guanine of the complementary strand.[49,50] This so called "virtual crosslink" thereby activates cell apoptosis via a Topoisomerase II independent mechanism[51] and will be discussed further in section 1.6.

1.4 Resistance to Doxorubicin

While being broadly used in clinical settings, doxorubicin still has deficiencies in addition to dose limiting cardiotoxicity, namely, the propensity for the majority of cancers to develop

resistance to doxorubicin therapy.[52] The modest lipophilicity and net positive charge at physiological pH make anthracyclines efficient substrates for active transport drug efflux pumps such as P-glycoprotein.[52] P-glycoprotein is expressed in normal tissues such as liver, colon, kidney and adrenal gland. It is therefore not tumor specific, and functions as a transporter of hydrophobic metabolites, xenobiotics, and/or hormones.[53] Tumors derived from tissues naturally expressing P-glycoprotein could be an explanation for their elevated resistance. P-glycoprotein is a member of the ATPase binding cassette (ABC) superfamily of transmembrane ATP-dependent transporters,[54] and multidrug resistant cancers often overexpress this well characterized transmembrane protein.[53]

1.5 Doxorubicin Modification and Delivery Methods

Decades have been dedicated to improving the therapeutic index of Dox. Volumes of work have been published outlining the multitude of functional group variations and delivery methods. Arcamone *et al*. explored many synthetic and biosynthetic variants of doxorubicin, including, but not limited to modification of functional groups, removal and/or modification of the sugar moiety and modification of the aglycone.[55] The most clinically relevant molecules to arise from these investigations have been epirubicin,[556,57] idarubicin,[58] Iodo-doxorubicin,[59] Mitoxantrone,[60] and Valrubicin.[61] Each variant may have some advantage to Dox for certain indications, some even offering oral bioavailability;[62] however none have surpassed Dox as a widely prescribed therapeutic.

The most clinically relevant advances surrounding Dox have been the reformulation of Doxorubicin HCl into liposomal drug delivery systems such as Myocet and Doxil. These so called

"stealth" liposomes protect Dox from the immune system, and anecdotal evidence suggest they may have some tumor targeting qualities. Doxil liposomes are functionalized with polyethylene glycol, and have in some instances been further modified to target folate receptor[63] with some success.[64] Passive targeting of liposomal Dox has been demonstrated using $\alpha v\beta 3$ integrin targeting RGD peptides[65,66] and steric modification of stealth liposomes has been attempted to take advantage of the enhanced permeability and retention effect (EPR), also with limited success.[67,68]

The EPR effect was first reported in 1986 by Matsumura and Maeda[68] and has subsequently been reviewed by Maeda and others[68,69] The combination of poor blood vessel architecture and the production of large amounts of various vascular permeability factors in solid tumors was observed. These factors ensure that the tumor has a sufficient supply of oxygen and nutrients to perpetuate rapid growth. Macromolecules larger than 40 kDa can therefore leak through vessels near the tumor and accumulate in tumor tissues, while smaller molecules, such as cancer therapeutics, can easily diffuse back into the blood. Constrained lymphatic vessels in the tumor area exacerbates the situation, allowing the tumor to accumulate many macromolecules. In normal tissues, there is no such accumulation, and the EPR effect has therefore become an attractive principle in tumor-targeting chemotherapy. A schematic representation of the EPR effect is shown in Figure 1.5.1. The Koch group has designed albumin binding prodrugs to exploit the EPR effect, and discussion of these compounds can be found in Chapter 5.

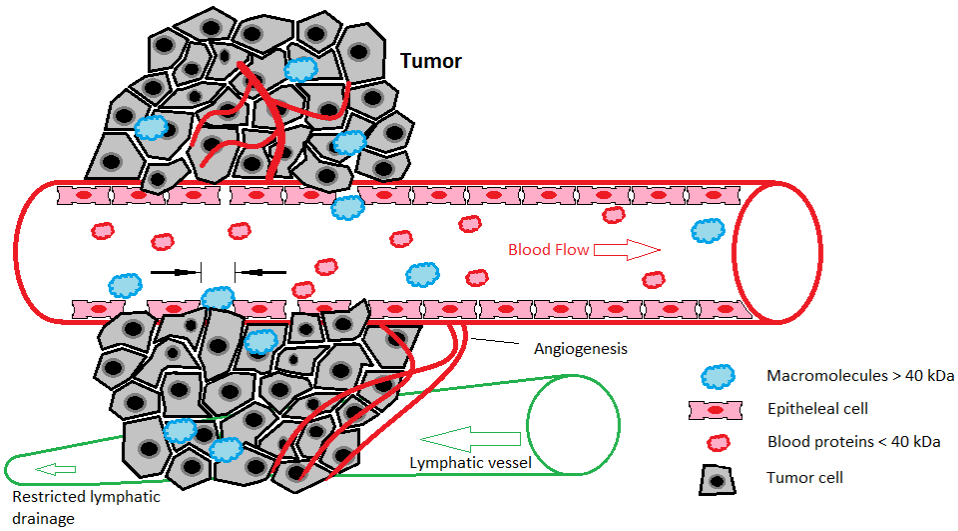

Figure 1.5.1 Schematic representation of the EPR effect. Macromolecules larger than 40 kDa accumulate in the leaky vasculatre formed during angiogenisis.

Covalent modification of doxorubicin with targeting moieties to guide the prodrug to tumor expressed surface proteins has been widely investigated and has been reviewed elsewhere.[70] Briefly, conjugates of monoclonal antibodies to deliver Dox to the tumor target have been reviewed[71] and one of these targeting moieties conjugated to the highly potent cytotoxin calicheamicin has been approved by the FDA. Other Dox-immunoconjugates seek to take advantage of cathepsin cleavable moieties upon internalization of the conjugate by the endosome/lysosome.[72] Many other examples of prodrug therapies such as Antibody-Directed Enzyme Prodrug Therapy (ADEPT), Bacterial-directed enzyme prodrug therapy (BDEPT), Gene-directed enzyme prodrug therapy (GDEPT) and Lectin-directed enzyme-activated prodrug therapy (LEAPT) have been investigated and will not be discussed here, however These strategies have been reviewed by Florent and Monneret.[70]

Tumor associated enzymes have been targeted as well.[73] Dox conjugates with peptide moieties cleaved by prostate specific sntigen (PSA),[74] plasmin,[75,76] matrix metalloproteinases

(MMP),[77] and endopeptidase lugumain,[78] just to name a few, have been synthesized. In all cases, in vitro analysis has shown that addition of extracellular enzyme raises the cytotoxicity of the prodrug, implying that the peptide moieties are indeed cleaved by the desired enzyme, releasing Dox. Not all investigators examined the cardiotoxic effects of the prodrugs; however, those that did found that the prodrugs exhibited lower cytotoxicity than Dox alone.

1.6 A Modification of Doxorubicin: Doxazolidine

With the vast collection of research surrounding the most profitable cytotoxin in history, the discovery of additional effectual modifications seemed unlikely. However, while examining the interaction of Dox with DNA, Koch *et al*. made an astonishing discovery. Building on the observation by Wang *et al.* that daunorubicin and doxorubicin, using formaldehyde, can create a virtual crosslink to DNA, [48] Koch *et al.* showed that the combination of daunorubicin or doxorubicin and DNA in transcription buffer containing ferric ion and dithiothreitol produced the same viritual crosslink,[39] as shown in Figure 1.6.1.[80] The cellular mechanism for the formation of formaldehyde is not entirely clear;[39] however, MCF-7 human breast cancer cells with daunorubicin or doxorubicin causes an internal increase in the concentration of formaldehyde.[81] These observations prompted the synthesis of doxorubicin conjugates that already contained a formaldehyde equivalent. The two compounds were called Doxoform (DoxF)[82] and Doxsaliform (DoxSF)[83] and are shown in Figure 1.6.2. Note that due to the use of excess formaldehyde, DoxF is composed of two doxorubicin molecules bound together by three formaldehyde derived methylene equivalents.

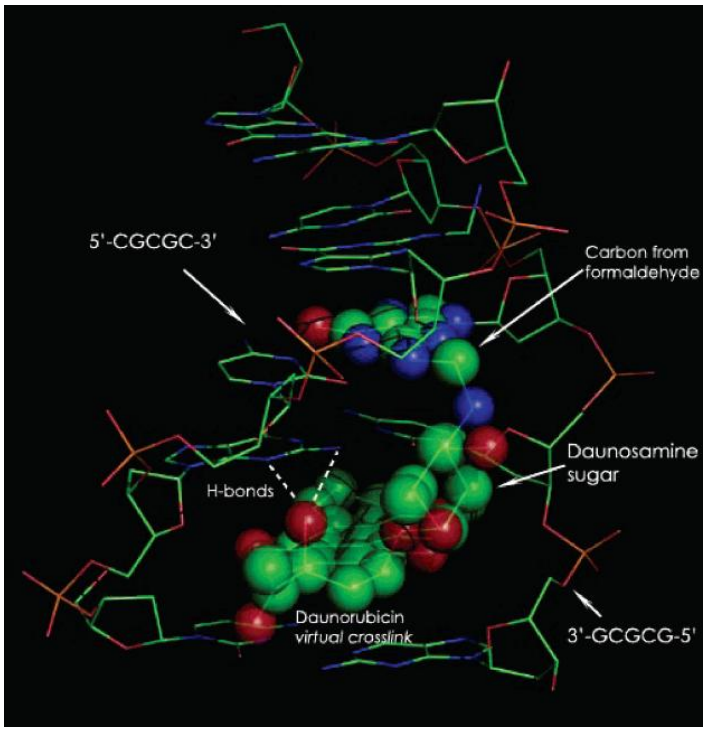

Figure 1.6.1 Crystal Structure of DNA-daun virtual crosslink. Covalent bonds to one DNA strand and Hydrogen bonds to the other creates a virtual crosslink[80].

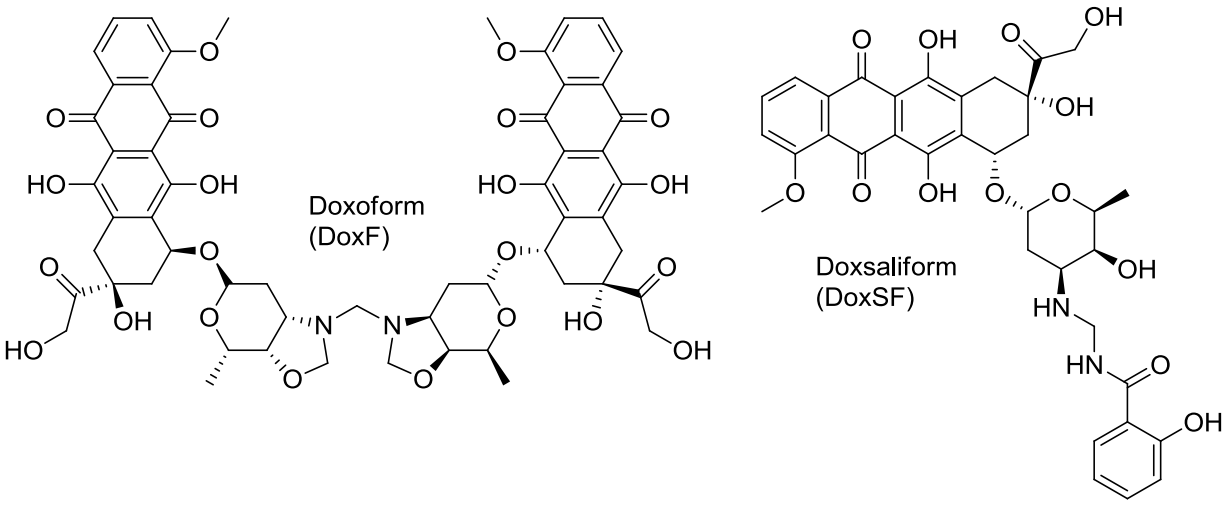

Figure 1.6.2 Structures of DosF and DoxSF

DoxF was shown to have a short half life of only a few minutes at 25°C in RPMI 1641 cell culture medium, ultimately hydrolyzing to Dox.[82] Regardless of the rapid hydrolysis, DoxF was shown to inhibit the growth of both sensitive and multidrug-resistant tumor cells approximately

equally, exhibiting a 10 to 10,000 time higher effectiveness when compared to Dox control,[82] eluding to the possibility that this compound was somehow escaping the multidrug resistance P-170 glycoprotein. The Koch group showed that DoxF reacts with DNA to yield the same virtual cross-links observed with the reaction of Dox, DNA and formaldehyde.[82] They concluded that DoxF was acting as a prodrug, releasing a monomeric species, dubbed doxazolidine (Doxaz), capable of forming DNA cross links.[80] The half life of doxazolidine hydrolysis to Dox was determined to be 3-4 minutes at pH 7.4 and 37 °C,[80] which has direct implications on the effectiveness of Doxaz as a standalone cancer therapeutic. The structure of doxazolidine is provided in Figure 1.6.3.

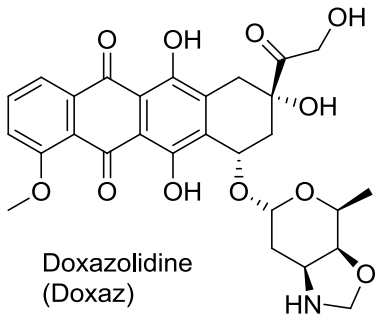

Doxazolidine
(Doxaz)

Figure 1.6.3 Structure of doxazolidine (Doxaz).

In an attempt to deliver doxorubicin and a formaldehyde equivalent in a hydrolytically stable prodrug, Koch *et al*. exploited the formation of an N-Mannich base by condensing the dox 3' primary amine with various alkyl and aryl primary amines in the presence of formaldehyde.[83] A molecule of particular interest, doxsaliform (DoxSF) emerged from these studies as a compound capable of releasing dox bearing a formaldehyde equivalent in a time dependent manner under physiological conditions.[83] The proposed hydrolytic mechanism is shown in Figure 1.6.4. This mechanism suggests that the protonation of the carbonyl oxygen by the phenolic hydrogen of salicylamide allows the free electron pair of the amine to participate

in the elimination of the salicylimidic acid while forming the dox-Schiff base. The imidic acid subsequently tautomerizes to salicylamide, and most importantly, the dox-Schiff base retains the formaldehyde equivalent and equilibrates between dox-Schiff and the dox-aminol (see Figure 1.6.4). With a cogent time release trigger in hand, Koch *et al*. sought effective tumor targeting of DoxSF. The $\alpha_v\beta_3$ integrin has been an attractive target for cancer therapeutics, and the utility of this integrin has recently been reviewed.[84] Conjugation of DoxF to short RGD motif containing peptides, RGD-4C and cyclic-(N-Me-VRGDf) known to preferentially bind the $\alpha_v\beta_3$ integrin[84] via a short hydroxylamine ether tether afforded the first prodrugs designed by Koch *et al*. to contain both a targeting motif and a time release trigger. They hypothesized that that a prodrug with this design would bind $\alpha_v\beta_3$ and localize in/or near the tumor and vascular endothelial cells of the developing blood supply. Upon hydrolysis of the N-Mannich base, the conjugate would release the doxorubicin active metabolite locally. It was found that the cyclic RGD peptide exhibited better binding affinity, and the prodrug as a whole was more effective than Dox at inhibiting growth of MDA-MB-435 cells *in vitro,* but less active than doxsaliform alone. No *in vivo* studies were performed with these molecules. The focus of the group was instead directed at the functionalization of Doxaz and the exploration of enzymatically activated triggers, largely due to the superior activity of Doxaz and Doxf.[80]

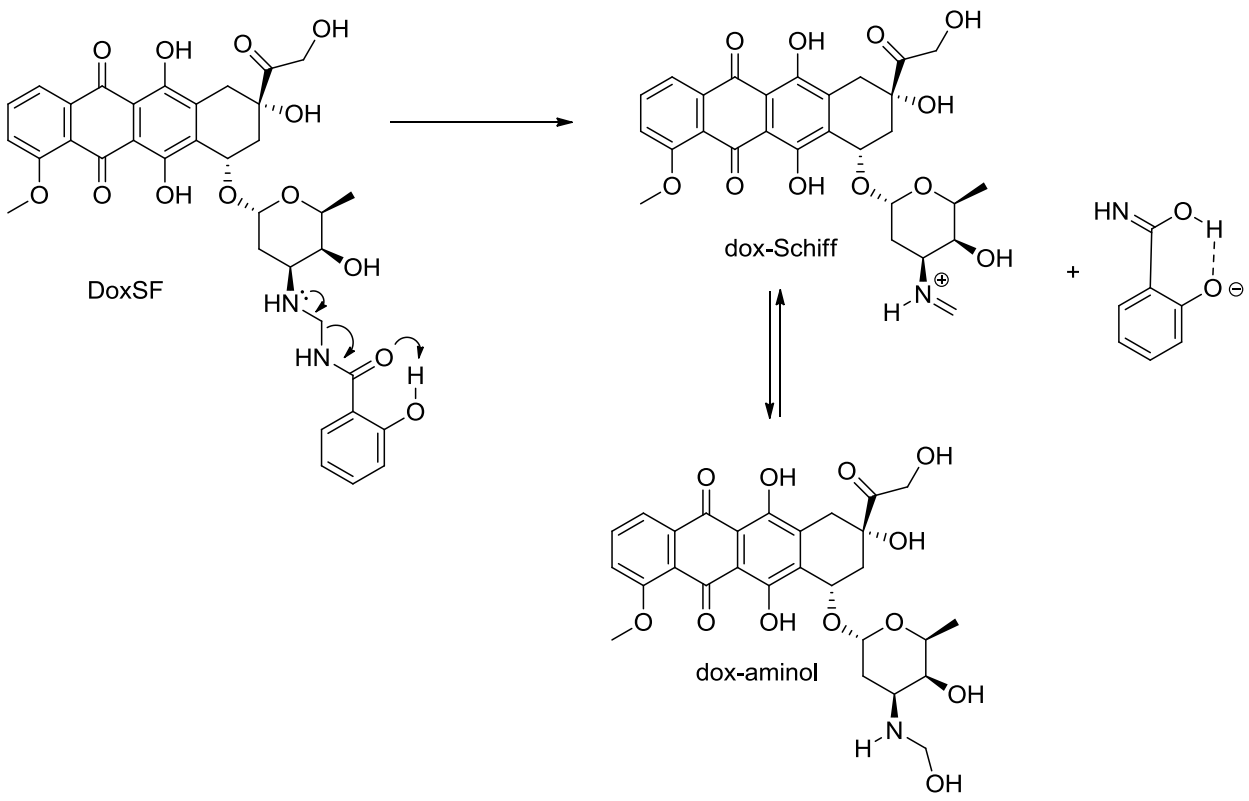

Figure 1.6.4 Mechanism of the DoxSF time release trigger.

The proposed model for doxazolidine binding to DNA proceeds through a tautomer of a G base that, in this tautomeric state, the nitrogen has a lone pair of electrons on the exocyclic amine available to approach the oxazolidine carbon in a S_N2 fashion, and is depicted in Figure 1.6.5. Subsequent proton rearrangement and intercalation completes the virtual crosslink.[80]

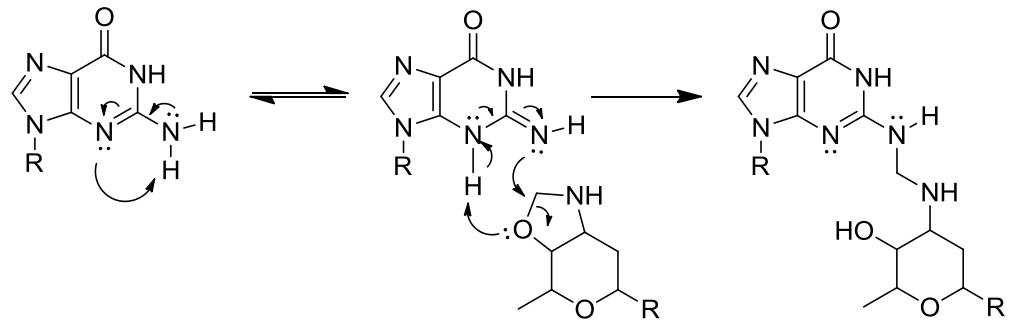

Figure 1.6.5 Doxazolidine covalently bonds one strand of DNA. A G-base on one strand of DNA must tautomerize to allow a concred ring opening mechanism and formation of a covalent

In an attempt to explain the difference in Doxaz and Dox activity, experiments designed to investigate cell cycle distribution profiles were performed comparing the two drugs. Dox induced cell cycle arrest at the G2/M transition state, while Doxaz induced apoptosis. In addition, Dox was less effective against Topo II deficient cells than Doxaz, implicating a Topo II independent mechanism for Doxaz.[85] Comparative analysis of data from experiments at the National Cancer Institute measuring the toxicity of Doxaz demonstrated that the activity of Doxaz correlated more closely with DNA crosslinking agents than with the parent Dox molecule.[85] The exciting conclusion is that Doxaz is a potent cytotoxin with a mechanism of action different from that of Dox.[85]

1.7 Doxazolidine as a Prodrug

The hydrolytic instability of Doxaz needed to be addressed to provide a commercially viable therapeutic. The hypothesized solution was to stabilize the oxazolidine moiety by forming a carbamate. Not only would this stabilize the vulnerable oxazolidine, but it would provide a tumor specific targeting moiety to evade release of the cytotoxic Doxaz in normal tissues, and especially the heart. The pursuit of this solution is indeed the focus of this thesis, and unexpectedly, the synthetic routes to a doxazolidine prodrug have proven to be difficult.

Learning about irinotecan and capecitabine suggested our use of a carbamate functional group, and will be discussed further in Chapter 4.

1.8 Investigations Presented in this Thesis

Presented in this thesis are the synthesis and biological evaluation of prodrugs designed to exploit tumor associated enzymes. Proteases involved in tissue remodeling, enzymes associated with hypoxic processes in solid tumors and a serine esterase have been selected as possible targets. Presented also is an albumin binding prodrug capable of becoming ensnared in the leaky vasculature surrounding a newly forming tumor actively involved in angiogenesis. Both the successful and unsuccessful synthetic routes to obtain these surprisingly elusive prodrugs will be presented, as well as the biological activity and potential for commercial development.

1.9 Chapter 1 References

1. Weiss, R.B. The anthracyclines: will we ever find a better doxorubicin?. *Semin. Oncol.* **1992**, 19, 670-686.

2. Tan, C.; Tasaka, H.; Yu, K.P.; Murphy, M.L.; *et al.* Daunomycin, an antitumor antibiotic, in the treatment of neoplastic disease. Clinical evaluation with special reference to childhood leukemia. *Cancer.* **1967**, 20, 333-353.

3. Arcamone, F.; Cassinelli, G.; Fantini, G.; *et al.* Adriamycin, 14-hydroxydaunomycin, a new antitumor antibiotic from *S. peucetius* var. *caesius*. *Biotechnol. Bioeng.* **1969**, 11, 1101-1110.

4. Di Marco, A.; Gaetani, M.; Scarpinato, B. Adriamycin (NSC-123,127): a new antibiotic with antitumor activity. *Cancer. Chemother. Rep.* **1969**, 53, 33-37.

5. Young, R.C.; Ozols, R.F.; Myers, C.E. The anthracycline antineoplastic drugs. *N. Engl. J. Med.* **1981**, 305, 139-153.

6. Merck pharmaceuticals Home Page. http://Merck.com (accessed January 2012).

7. Von Hoff, D.D.; Layard, M. Risk factors for the development of daunorubicin cardiotoxicity. *Cancer. Treat. Rep.* **1982**, 65, 19-24.

8. Bristow, M.R.; Mason, J.W.; Billingham, M.E.; *et al*: Doxorubicin cardiomyopathy: Evaluation by phonocardiography, endomyocardial biopsy, and cardiac catheterization. *Ann. Intern. Med.* **1978**, 88, 168-175.

9. Von Hoff, D.D.; Layard, M.W.; Basa, P.; *et al*. Risk factors for doxorubicin-induced congestive heart failure. *Ann. Intern. Med*. **1979**, 91, 710-717.

10. Praga, C.; Beretta, G.; Vigo, P.L.; *et al*. Adriamycin cardiotoxicity: A survey of 1,273 patients. *Cancer. Treat. Rep*. **1979**, 63, 827-834.

11. Suzuki, T.; Kanda, H.; Kawai, Y.; *et al.* Cardiotoxicity of anthracycline antineoplastic drugs-Clinicopathological and experimental studies. *Jpn. Circ. J*. **1979**, 43, 1000-1008.

12. Gralla, E.J.; Fleischman, R.W.; Luthra, Y.K.; *et al*. The dosing schedule dependent toxicities of Adriamycin in beagle dogs and rhesus monkeys. *Toxicology*. **1979**, 13, 263-273.
13. Chlebowski, R.T.; Paroly, W.S.; Pugh, R.P.; *et al*. Adriamycin given as a weekly schedule without a loading dose: Clinically effective with reduced incidence of cardiotoxicity. *Cancer. Treat. Rep*. **1980**, 64, 47-51.

14. Minow, R.A.; Benjamin, R.S.; Gottlieb, J.A. Adriamycin (NSC-123127) cardiomyopathy-An overview with determination of risk factors. *Cancer. Chemother. Rep*. **1975**, 6, 195-201.

15. Buzdar, A.U.; Legha, S.S.; Tashima, C.K.; *et al*. Adriamycin and mitomycin C: Possible synergistic cardiotoxicity. *Cancer. Treat. Rep*. **1978**, 62, 1005-1008.

16. Bhanot, P.; Cushing, B.; Philippart, A.; *et al*. Hepatic irradiation and adriamycin cardiotoxicity. *J. Pediatr*. **1979**, 95, 561-563.

17. Beretta, G.; Villani, F. Cardiomyopathy in adults after combination Adriamycin and D1IC (Letter). *Cancer. Treat. Rep*. **1980**, 64, 353.

18. Mosijczuk, A.D.; Ruymann, F.B.; Mease, A.D.; *et al*. Anthracycline cardiomyopathy in children:report of two cases. *Cancer*. **1979**, 44, 1582-1587.

19. Steinherz, L.J.; Steinherz, P.G.; Mangiacasale, D.; *et al*. Cardiac abnormalities after AMSA administration. *Cancer. Treat. Rep*. **1982**, 66, 483-488.

20. Gottlieb, S.L.; Edmiston, A.; Haywood, l.J. Late, late doxorubicin cardiotoxicity. *Chest* **1980**, 78, 880-882.

21. Lefrak, E.A.; Pitha, J.; Rosenheim, S., *et al*. Adriamycin (NSC-123127) cardiomyopathy. *Cancer. Chemother. Rep*. **1975**, 6, 203-208.

22. Doroshow, J.H.; Locker, G.Y.; Myers, C.E. Experimental animal models of adriamycin cardiotoxicity. *Cancer. Treat. Rep*. **1979**, 63, 855-860.

23. Doroshow, J.H.; Locker, G.Y.; Myers, C.E. Enzymatic defenses of the mouse heart against reactive oxygen metabolites: alterations produced by doxorubicin. *J. Clin. Invest*. **1980**, 65, 128-135.

24. Myers, C.E.; McGuire, W.P.; Liss, R.H.; *et al*. Adriamycin: The role of the lipid peroxidation in cardiac toxicity and tumor response. *Science.* **1977**, 197, 165-167.

25. Stuart, M.J.; deAlarcon, P.A.; Oski, F.A. Inhibition of Adriamycin(ADR) induced lipid peroxidation by α-tocopherol (α-T) and acetylsalicylic acid (ASA) (abstr). *Pediatr. Res*. **1978**, 12, 474.

26. Flohé, L.; Zimmermann, R. The role of GSH peroxidase in protecting the membrane of rat liver mitochondria. *Biochem. Biophys. Acta*. **1970**, 223, 210-213.

27. Chow, C.K.; Tappel, A.L. Response of glutathione peroxidase to dietary selenium in rats. *J. Nutr*. **1974**, 104, 444-451.

28. Thayer, W.S. Adriamycin stimulated superoxide formation in submitochondrial particles. *Chem. Biol. Interact*. **1977**, 19, 265-278.

29. Olson, R.D.; MacDonald, J.S.; vanBoxtel, C.J.; *et al*. Regulatory role of glutathione and soluble sulfhydryl groups in the toxicity of adriamycin. *J. Pharmacol. Exp. Ther*. **1980**, 215, 450-454.

30. Kosower, E.M. A role for glutathione in muscle contraction. *Experientia.* **1970**, 26, 760-761.

31. Kishi, T.; Folkers, K. Prevention by coenzyme Q1O (NSC-140865) of the inhibition by adriamycin (NSC-123127) of coenzyme Q10 enzymes (Letter). *Cancer. Treat. Rep*. **1976**, 60, 223-224.

32. Kishi, T.; Watanabe, T.; Folkers, K. Bioenergetics in clinical medicine: Prevention by forms of coenzyme Q of the inhibition by adriamycin of coenzyme Q10-enzymes in mitochondria of the myocardium. *Proc. Natl. Acad. Sci .USA*. **1976**, 73, 4653-4656.

33. Minotti, G; Recalcati, S; Mordente, A.; *et al*. The secondary alcohol metabolite of doxorubicin irreversibly inactivates aconitase/iron regulatory protein-1 in cytosolic fractions from human myocardium. *Faseb J.* 1998, 12, 541-552.

34. Hentze, M.W.; Kühn, L.C. Molecular control of vertebrate iron metabolism: mRNA-based regulatory circuits operated by iron, nitric oxide, and oxidative stress. *Proc. Natl. Acad. Sci. USA.* **1996**, 93, 8175–8182.

35. Minotti, G.; Cavaliere, A.F.; Mordente, A.; *et al*. Secondary alcohol metabolites mediate iron delocalization in cytosolic fractions of myocardial biopsies exposed to anticancer anthracyclines Novel linkage between anthracycline metabolism and iron-induced cardiotoxicity. *J. Clin. Invest.* **1995**, 95, 1595–1605.

36. Minotti, G.; Cairo, G.; Monti, E. Role of iron in anthracycline cardiotoxicity: new tunes for an old song?. *Faseb J*. **1999**, 13, 199-212.

37. Kühn, L.C.; Hentze, M.W. Coordination of cellular iron metabolism by post-transcriptional gene regulation. J*. Inorg. Biochem*. **1992**, 47, 183-195.

38. Mascotti, D.P.; Rup, D.; Thach, R.E. Regulation of iron metabolism: translational effects mediated by iron, heme, and cytokines. *Annu. Rev. Nutr.* **1995**, 15, 239-261.

39. Taatjes, D.J.; Gaudiano, G.; Koch, T.H. Production of formaldehyde and DNA-adriamycin or DNA-daunomycin adducts, initiated through redox chemistry of dithiothreitol/iron, xanthine oxidase/NADH/iron, or glutathione/iron. *Chem. Res. Toxicol.* **1997**, 10, 953-961.

40. Capranico, G.; Zunino, F. DNA topoisomerase-trapping antitumor drugs. *Eur. J. Cancer*. **1992**, 28, 2055-2060.

41. Zunino, F.; Capranico, G. Sequence-selective groove binders. In: Tericher B (ed) Cancer therapeutics: experimental and clinical agents(Humana press, Totowa New Jersey 1997).

42. Capranico, G.; Binaschi, M.; Borgnetto, M.E.; *et al*. A protein-mediated mechanism for the DNA sequence-specific action of topoisomerase II poisons. *Trends. Pharmacol. Sci.* **1997**, 18, 323-329.

43. Gewirtz, D.A. A critical evaluation of the mechanisms of action proposed for the antitumor effects of the anthracycline antibiotics adriamycin and daunorubicin. *Biochem. Pharmacol.* **1999**, 57, 727-741.

44. Yoda, Y.; Nakazawa, M.; Abe T.; *et al.* Prevention of doxorubicin myocardial toxicity in mice by reduced glutathione. *Cancer. Res*. **1986**, 46, 2551-2556.

45. Cervantes, A.; Pinedo, H.M.; Lankelma, J.; Schuurhuis, G.J. The role of oxygen-derived free radicals in the cytotoxicity of doxorubicin in multidrug resistant and sensitive human ovarian cancer cells. *Cancer. Lett*. **1988**, 41, 169-177.

46. Shimpo, K.; Nagatsu, T.; Yamada, K.; *et al.* Ascorbic acid and adriamycin toxicity. *Am. J. Clin. Nutr*. **1991**, 54, 1298S-1301S.

47. Myers, C.; Bonow, R.; Palmeri, S.; *et al.* A randomized controlled trial assessing the prevention of doxorubicin cardiomyopathy by N-acetylcysteine. *Semin. Oncol.* **1983**, 10, Suppl 1, 53-55.

48. Wang, A.H.; Gao, Y.G.; Liaw, Y.C.; Li, Y.K. Formaldehyde cross-links daunorubicin and DNA efficiently: HPLC and X-ray diffraction studies. *Biochemistry*. **1991**, 30, 3812-3815.

49. Podell, E.R.; Harrington, D.J.; Taatjes, D.J.; Koch T.H. Crystal structure of epidoxorubicin-formaldehyde virtual crosslink of DNA and evidence for its formation in human breast-cancer cells. *Acta. Crystallogr. D. Biol. Crystallogr*. **1999**, 55, Pt 9, 1516-1523.

50. Taatjes, D.J.; Gaudiano, G.; Resing, K.; Koch T.H. Alkylation of DNA by the anthracycline, antitumor drugs adriamycin and daunomycin. *J. Med. Chem*. **1996**, 39, 4135-4138.

51. Swift, L.P.; Rephaeli, A.; Nudelman, A.; *et al.* Doxorubicin-DNA adducts induce a non-topoisomerase II-mediated form of cell death. *Cancer. Res*. **2006**, 66, 4863-4871.

52. Nielsen, D.; Maare, C.; and Skovsgaard, T. Cellular resistance to anthracyclines. *Gen. Pharmacol.* **1996**, 27, 251-255.

53. Longley, D.B.; Johnston, P.G. Molecular mechanisms of drug resistance. *J. Pathol*. **2005**, 205, 275-292.

54. Higgins, C.F. ABC transporters: from microorganisms to man. *Annu. Rev. Cell. Biol*. **1992**, 8, 67-113.

55. Gottesman, M.M.; Pastan, I. Biochemistry of multidrug resistance mediated by the multidrug transporter. *Annu. Rev. Biochem*. **1993**, 62, 385-427.

56. Arcamone, F. Doxorubicin Anticancer Antibiotics: Medicinal Chemistry, a Series of Medicinal Chemistry, Vol 17, (Academic Press, New York, 1981)

57. Kharsaw, M.; Bell, R.; Dang, C. Epirubicin: Is it like doxorubicin in breast cancer? A clinical review. *Breast*. **2012**, 21, 142-149. Jan 17 [Epub ahead of print].

58. Fields, S.M.; Koeller, J.M. Idarubicin: a second-generation anthracycline. *Dicp*, **1999,**. 25, 505-517.

59. Mross, K.B.; Langenbuch, T.; Burk, K.;. Hossfeld, D.K. [Iodo-doxorubicin, a new anthracycline derivative. Current state of progress]. *Onkologie*, **1990,** 13, 346-351.

60. Koeller, J.; Eble, M. Mitoxantrone: a novel anthracycline derivative. *Clin Pharm*, **1988**, 7 574-581.

61. Onrust, S.V. and H.M. Lamb, Valrubicin. *Drugs Aging*, **1999,** 15, 69-75.

62. Goebel, M., Oral idarubicin--an anthracycline derivative with unique properties. *Ann Hematol*, **1993,** 66, 33-43.

63. Yoo, H.S.; Park, T.G. Folate receptor targeted biodegradable polymeric doxorubicin micelles. *J. Control. Release.* **2004**, 96, 273-283.

64. Shmeeda, H.; Mak, L.; Tzemach, D.; *et al.* Intracellular uptake and intracavitary targeting of folate-conjugated liposomes in a mouse lymphoma model with up-regulated folate receptors. *Mol. Cancer. Ther*. **2006**, 5, 818-824.

65. Xiong, X.B.; Huang, Y.; Lu, W.L.; *et al.* Enhanced intracellular delivery and improved antitumor efficacy of doxorubicin by sterically stabilized liposomes modified with a synthetic RGD mimetic. *J. Control. Release.* **2005**, 107, 262-275.

66. Schiffelers, R.M.; Koning, G.A.; ten Hagen, T.L.; *et al.* Anti-tumor efficacy of tumor vasculature-targeted liposomal doxorubicin. *J. Control. Release*. **2003**, 91, 115-122.

67. Dvorak, H.F. Leaky tumor vessels: consequences for tumor stroma generation and for solid tumor therapy. *Prog. Clin. Biol. Res.* **1990**, 354A, 317-330.

68. Maeda, H.; Wu, J.; Sawa, T.; *et al.* Tumor vascular permeability and the EPR effect in macromolecular therapeutics: a review. *J. Control. Release*. **2000**, 65, 271-284.

69. Fang, J.; Nakamura, H.; Maeda, H. The EPR effect: Unique features of tumor blood vessels for drug delivery, factors involved, and limitations and augmentation of the effect. *Adv. Drug. Deliv. Rev.* **2011**, 63, 136-151.

70. Florent, J.C.; Monneret, C. Doxorubicin Conjugates for Selective Delivery to Tumors. *Top. Curr. Chem.* **2008**, 283, 99-140.

71. Trail, P.A.; King, H.D.; Dubowchik, G.M. Monoclonal antibody drug immunoconjugates for targeted treatment of cancer. *Cancer. Immunol. Immunother*. **2003**, 52, 328-337.

72. Dubowchik, G.M.; Radia, S.; Mastalerz, H.; *et al.* Doxorubicin immunoconjugates containing bivalent, lysosomally-cleavable dipeptide linkages. *Bioorg. Med. Chem. Lett*. **2002**, 12, 1529-1533.

73. Denny, W.A. Tumor activated prodrugs-a new approach to cancer therapy. *Cancer. Invest*. **2004**, 22, 604-619.

74. Dang, L.H.; Bettegowda, C.; Huso, D.L.; *et al.* Combination bacteriolytic therapy for the treatment of experimental tumors. *Proc. Natl. Acad. Sci. USA*. **2001**, 98, 15155-15160.

75. Chakravarty, P.K.; Carl, P.L.; Weber, M.J.; and Katzenellenbogen, J.A. Plasmin-activated prodrugs for cancer chemotherapy. 2. Synthesis and biological activity of peptidyl derivatives of doxorubicin. *J. Med. Chem*. **1983**, 26, 638-644.

76. de Groot, F.M.; de Bart, A.C.; Verheijen, J.H.; *et al.* Synthesis and biological evaluation of novel prodrugs of anthracyclines for selective activation by the tumor-associated protease plasmin. *J. Med. Chem*. **1999**, 42, 5277-5283.

77. Albright, C.F.; Graciani, N.; Han, W.; *et al.* Matrix metalloproteinase–activated doxorubicin prodrugs inhibit HT1080 xenograft growth better than doxorubicin with less toxicity. *Mol. Cancer. Ther*. **2005**, 4, 751-760.

78. Liu, C.; Sun, C.; Huang, H.; *et al.* Overexpression of legumain in tumors is significant for invasion/metastasis and a candidate enzymatic target for prodrug therapy. *Cancer. Res*. **2003**, 63, 2957-2964.

79. Kato, S.; Burke, P. J.; Koch, T.H.; *et al.* Mass spectrometric measurement of formaldehyde generated in breast cancer cells upon treatment with anthracycline antitumor drugs. *Chem. Res. Toxicol.* **2000**, *13*, 509-516.

80. Post, G. C.; Barthel, B. L.; Koch, T.H.; *et al.* Doxazolidine, a proposed active metabolite of doxorubicin that cross-links DNA. *J. Med. Chem.* **2005**, *48*, 7648-7657.

81. Kato, S.; Burke, P. J.; Koch, T.D.; *et al.* Mass spectrometric measurement of formaldehyde generated in breast cancer cells upon treatment with anthracycline antitumor drugs. *Chem. Res. Toxicol.* **2000**, *13*, 509-516.

82. Fenick, D. J.; Taatjes, D. J.; Koch, T. H. Doxoform and Daunoform: Anthracycline-formaldehyde conjugates toxic to resistant tumor cells. *J. Med. Chem.* **1997**, *40*, 2452-2461.

83. Cogan, P. S.; Fowler, C. R.; Post, G. C.; Koch, T. H. Doxsaliform: A novel N-Mannich base prodrug of a doxorubicin formaldehyde conjugate. *Lett. Drug Des. Dis.* **2004**, *1*, 247-255.

84. Meyer, A.; Auernheimer, J.; Modinger, A.; *et al.* Targeting RGD recognizing integrins: drug development, biomaterial research, tumor imaging and targeting. **2006**, 12, 2723-2747.

85. Kalet, B.T.; McBryde, M.B.; Espinosa, J.M.; Koch, T.H. Doxazolidine induction of apoptosis by a topoisomerase II independent mechanism. *J. Med. Chem*. **2007**, 50, 4493-4500.

Chapter 2 Protease Activated Prodrugs of Doxazolidine

2.1 Introduction

Proteases act through a regulatory process known as proteolysis, and play important roles in many biological and pathological systems. The human degradome, a complete list of proteases synthesized by human cells, is made up of more than 569 (and growing) proteases that are sorted into five broad classes: metalloproteinases, serine, cysteine, threonine and aspartic proteases.[1] Due to the strong evidence linking protease involvement to diseases, proteases serve an important role in drug development.

Contrary to normal tissues, cancerous tumors are growing quickly and have heightened metabolic activity, requiring additional nutrients, and physical space for growth. The overexpression of extracellular proteases aids the tumor by degrading the extracellular matrix (ECM) and paving the way for vascularization through angiogenesis. Proteases can also assist tumor cells in breaking free of the primary tumor and metastasizing to other tissues and regions of the body. The overexpression of proteases has been observed in cancerous cells at many times higher than in healthy cells,[2] and has also been observed in non cancerous cells recruited to the tumor site.[3] Currently, it is believed that urokinase plasminogen activator (uPA), cathepsin B, and membrane-type matrix metalloproteinase (MMP) activate pro-MMP's which allow ECM degradation by extracellular serine proteases such as uPA, urokinase plasminogen activator receptor (uPAR), plasminogen, and MMP's. These activities foster cellular motility, invasiveness and can release growth factors sequestered in the ECM such as vascular endothelial growth factor (VEGF), fibroblast growth factor (FGF) 2, and transforming

growth factor (TGF)- β causing a cascade of tumor growth factors in a disasterous feedback loop promoting tumor growth.[2,4-8]

The plasminogen activator uPA originates in kidney cells and was first discovered in urine, hence the urokinase designation.[9,10] Originating as a single chain known as pro-kinase, rapid conversion of uPA by plasmin to the two chain form with a bridging disulfide bond occurs. Both the single chain and single chain forms bind to the uPA receptor (uPAR),[11] forming a complex that facilitates plasminogen activation by uPA to plasmin. uPAR is anchored to the cell surface by a glycosyl-phophatidylinositol domain,[12] and has a high affinity for uPA. An inhibitor of uPA, plasmin activator inhibitor (PAI-1), can bind uPA, however uPAR can bind uPA already bound to PAI-1, forming a complex. This complex is rapidly internalized, degraded and uPAR is recycled to the cell surface in a different area.[13] This complex is therefore implicated in cell migration due to the directional nature of the recycling to the cell surface.[12] The enzymes in the plasmin system, uPA, uPAR and PAI-1 have been extensively studied as prognostic markers for many types of invasive and metastatic cancers.[14-16] A schematic representation of the plasmin system is shown in Figure 2.1.1

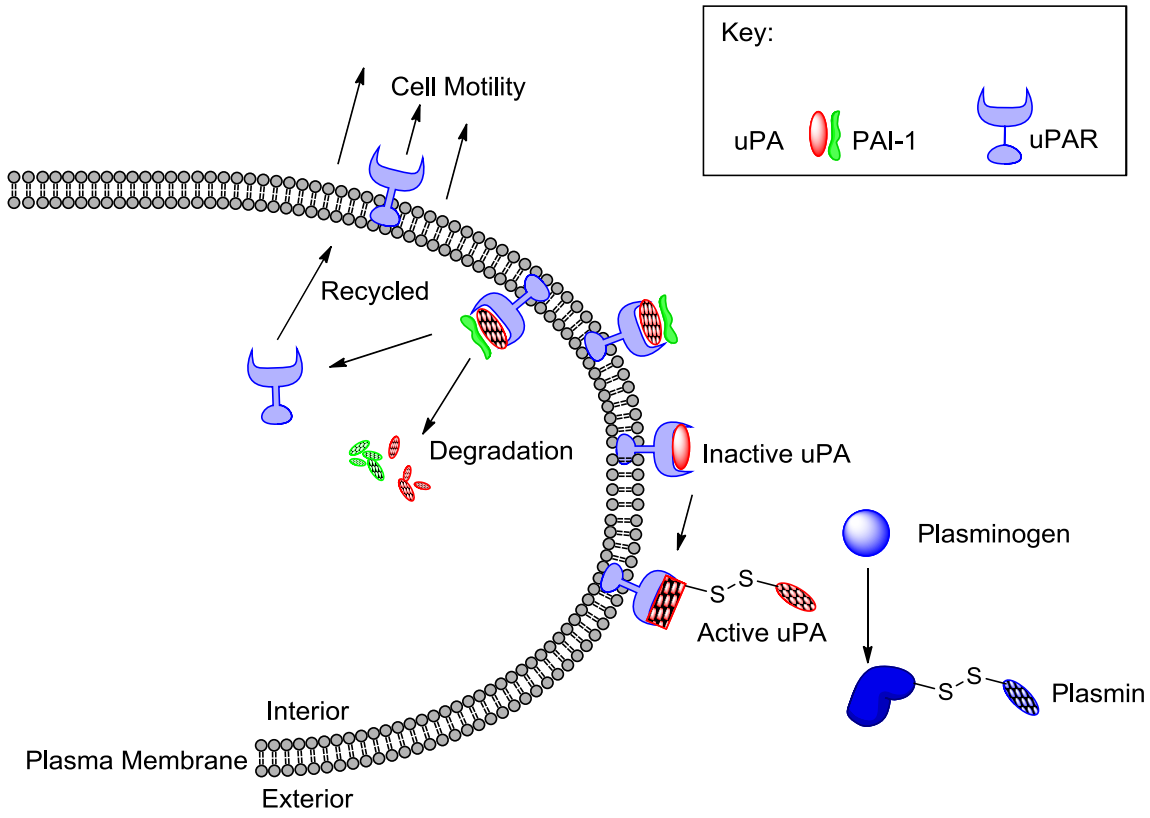

Figure 2.1.1 The Plasminogen-plasmin system. uPAR can bind uPA; when uPA is bound to PAI-1, the complex is internalized and uPA and PAI-1 are degraded while uPAR is recycled to the surface, and assists in cell motility. When free uPA binds uPAR, uPA is activated and can convert plasminogen to plasmin.

The plasminogen-plasmin system role in tumor biology is complex and involves several important steps. Many factors assist plasminogen and plasmin in tumor progression. The major ways in which the plasminogen-plasmin system affects tumors are cell proliferation, apoptosis, cell migration/invasion and angiogensis.[17-20]

The membrane bound uPAR when bound to uPA has the ability to bind growth factors and ECM proteins such as vitonectin or fibronectin, and can cause growth stimulation.[21,22] In this respect the uPA bound to uPAR is mitogenic. The role of PAI-1 and PAI-2 is not completely understood. Added PAI-1 has been shown to inhibit apoptosis[23] and enhance tumor growth by inhibiting uPA.[24] Likewise, PAI-2 is poorly understood, and this remains an area of investigation.

Cell migration is influenced by uPA, uPAR and PAI-1 by the aforementioned method of uPAR recycling. When uPAR is recycled to a localized position, enhanced activation of plasminogen to plasmin can occur. With heightened plasmin activity, the ECM is preferentially degraded, and frees the cell from adhesion in this area, allowing cell migration.[12,13] Vitronectin can influence the distribution of uPAR. Both monomeric and dimeric forms of uPAR are present on the cell surface,[25,26] and vitronectin prefers the dimeric form.[27] The uPA-uPAR-PaI-1 complex can bind vitronectin on the cell surface, changing the cell shape and cell adhesion to the ECM. When the complex is internalized, adhesion is affected (detached), and when the uPAR is recycled to the cell surface, adhesion resumes,[26] thus the cell migration is controlled. The plasminogen-plasma system also plays a role in angiogenisis. Complexing with tumor derived cytokines and VEGF, uPA and PAI-1 can modulate endothelial cell proliferation, thus encouraging angiogenesis. The uPA mediated activation of plasminogen to plasmin can also be anti-angiogenic.[28] Plasmin can be reduced by plasmin reductase and co-factors to free kringle structures. Kringle structures are loop domains within proteins containing architectures influenced by disulfide bonds, and are exemplified by angiostatin. Angiostatin has powerful inhibitory activity agains the proliferation of microvascular endothelial cells.[29]

Prodrugs designed to be activated by proteases have had various success, some currently in clinical trials.[28] A very interesting prodrug using unnatural amino acids homophenylalanine and citrulline showed 20-fold greater dosage acceptance the the maximum tolerated dose of dox.[30] A xenograft model of mice containing MMP-positive HT1080 human fibrosarcoma cells showed that the prodrug exhibited significant activity when compared to dox. Additional prodrugs aimed at MMP's and coupled to dox have had limited success[31,32]

however recent prodrugs aimed at MMP's and utilizing passive albumin targeting have shown more success, and will be discussed in Chapter 4. Use of paclitaxel, mitomycin C[33] and methotrexate[34] with protease triggers aimed at both plasmin and cathepsin B have also been evaluated. These prodrugs contained a D-Ala-Phe-Lys (aFK) peptide sequence known to be cleaved by plasmin and cathepsin B. A dox prodrug with the same aFK sequence was later synthesized and evaluated, with positive results.[35-37]

It was the aFK trigger that was most appealing to the Koch group, and based on *in vivo* efficacy of the plasmin-activated aFK Dox prodrug, development of a doxaz variant was undertaken. The doxaz prodrug was designed to employ the aFK trigger and the Katzenellenbogen spacer. The following chapter describes the synthesis and evaluation of this molecule, and subsequent modifications to develop a scalable doxaz prodrug.

2.2 Experimental Methods

2.2.1 General Remarks

Clinical samples of doxorubicin hydrochloride formulated with lactose were gifted by FeRx (Aurora, CO). Unless otherwise noted, all reagents and amino acids for solid-phase peptide synthesis were purchased from Nova Biosciences (La Jolla, CA) and other chemicals and reagents were acquired from Aldrich (Milwaukee, WI). Analytical HPLC was performed on Agilent 1050/1100 hybrid instruments equipped with a 1050 series autoinjector, a 1100 series UV/visible diode-array detector, and a 1046A fluorescence detector. An Agilent Zorbax octadecylsilyl (C18) reverse phase column (4.6 mm i.d. x 150 mm, 5 µm) was used for chromatography. Unless specifically indicated, elution was performed at 1 mL/min and room temperature with gradients of acetonitrile and 20 mM sodium phosphate buffer, pH 4.6,

containing 0.02% sodium azide. Method 1 had acetonitrile percentages of: 20% from 0 to 1.5 min, 30% at 5 min, 80% from 15 to 20 min, 20% at 24 min. Method 2 consisted of acetonitrile percentages: 20% to 40% from 0 – 5 min, 50% from 8 – 9 min, and 20% at 11 min. The presence of anthracycline-containing molecules was monitored by absorbance at 480 nm and retention times are noted individually. All NMR spectra were taken at 400 or 500 MHz on a Varian Unity INOVA spectrometer (Palo Alto, CA) or a Bruker-Avance III 300 MHz spectrometer (Billerica, MA) in deuterated solvents from Cambridge Isotope Laboratories, Inc (Andover, MA). Chemical shifts are reported in δ values of ppm and were standardized by the residual solvent peak in MestReNova NMR software (Mestrelab Research, Santiago de Compostela, Spain). UV-vis spectroscopy was performed on a Hewlett-Packard /Agilent 8452A diode array instrument. Electrospray mass spectra were obtained with a Perkin-Elmer Sciex API III$^+$ (Waltham, MA) or ABI Pulsar QqT high resolution instrument (Foster City, CA), equipped with an ion-spray source at atmospheric pressure. Purification by radial chromatography purification was done with a Harrison Research Model 7924T Chromatotron (Palo Alto, CA). Analysis by flow cytometry was performed with a Becton-Dickinson Biosciences FACscan (San Jose, CA) and a PowerWave X plate reader (BIO-TEK Instruments, Winooski, VT) was used for analyzing 96-well plate growth inhibition assays.

General Tissue Culture. All tissue culture reagents were acquired from Gibco Life Sciences (Grand Island, NY) and plates from Sarstedt, Inc (Newton, NC) or Corning, Inc. (Corning, NY) unless otherwise noted. All cells were acquired from the American Type Culture Collection (Rockville, MD) except for NCI/RES-Adr (a gift from William Wells, Michigan State University, Lansing, MI), L3.3, L3.5, and L3.6PL (all gifts of Wells Messersmith, University of Colorado,

Anschutz Medical Campus, Denver, CO). NCI/RES-Adr and SHP77 were maintained in RPMI-1640, supplemented with 10% (v/v) fetal calf serum and 1% (v/v) pencillin-streptomycin stock solution. MCF-7, MiaPaCa2, BxPC3, L3.3, L3.5, L3.6PL, and the non-tumor-derived HEK-293T were grown in Dulbecco's modified essential medium (DMEM) containing the same above supplements and the same concentrations. All of the above cells were grown in a humidified incubator under an atmosphere of 5% CO_2/95% air at 37 ºC.

2.2.2 Synthesis of Doxazolidine

Doxorubicin Free Base from Clinical Samples. Lyophilized pellets of expired clinical samples of doxorubicin HCl (20 – 50 mg) containing 100 – 250 mg lactose monohydrate (Bedford Laboratories, Bedford, OH) were dissolved in methanol to a final concentration of 2 mg/mL and combined in a separatory funnel. The methanol solution was diluted with 100 mM sodium phosphate buffer, pH 8.5, for a final concentration of 0.4 mg/mL dox HCl as a mixture of precipitated and solubilized material. The free base of dox was extracted from the solution by two washes with equal volumes of chloroform, leaving almost no red color in the aqueous fraction. The chloroform was dried with anhydrous sodium sulfate, filtered, and removed by rotary evaporation to yield a red solid. The solid was dried thoroughly under high vacuum (10^{-2} torr) for at least 2.5 h to yield pure dox free base in a final yield of 98%, as indicated by optical density at 480 nm and a molar extinction coefficient of 11,500 M^{-1} cm^{-1} in 75% DMSO/25% water.

Doxazolidine. Dox free base was dissolved to a final concentration of 5 – 10 mg/mL in deuteriochloroform and 1.1 – 2 equiv. of prilled paraformaldehyde (Aldrich, Milwaukee, WI) was added. The reaction mixture was monitored by ^{1}H NMR, with complete consumption of

dox occurring after 2 – 3 days, as evidenced by the appearance of the doxaz methylene AX pattern at 4.31 and 4.68 ppm and doxf AX pattern at 4.21 and 4.73 ppm in the ^{1}H NMR spectrum. Loss of dox was evident by the dox-specific aromatic triplet pattern for the proton at the 2-position, which appears at 7.81 ppm (as compared to 7.78 for doxaz and 7.70 for doxf). The amount of paraformaldehyde added determines the doxaz/doxoform ratio, since doxaz reacts with an additional equiv of formaldehyde to form doxf. Complete assignments of the ^{1}H NMR spectra for doxaz and doxf have been published.[38] The reaction mixture was then filtered and the deuteriochloroform removed by rotary evaporation. The doxaz/doxf mixture was used without further purification, since doxf readily hydrolyzes to produces 2 equiv of doxaz.

2.2.3 Synthesis of Ac-Gly-D-Ala-L-Phe-L-Lys(alloc)-PABA (Ac-GaFK(alloc)-PABA) coupled to the polystyrene resin.

Fmoc-p-aminobenzyl alcohol (Fmoc-PABA,). N-(Fluorenylmethyloxycarbonyloxy)-succinimide (N-Fmoc-N-hydroxysuccinimide, 6.0 g, 17.8 mmol) in p-dioxane (60 mL) was added dropwise to p-aminobenzyl alcohol (PABA, 2.5 g, 20.5 mmol) in p-dioxane (30 mL). After 48 h of stirring, 90 ml of deionized H_20 was added and the desired product immediately precipitated. The product was isolated by filtration, and washed 4 times with deionized H_20 (60 mL). Fmoc-PABA (5.9 g, 95%) was isolated that showed the following spectral properties: ^{1}H NMR ($CDCl_3$): δ 4.26 (t, 1H, J = 7 Hz, Fmoc-CH), 4.53 (d, 2H, J = 7 Hz, Fmoc-CH_2), 4.63 (s, 2H, PABA-CH_2), 6.62 (bs, 1H, NH), 7.30 (t, 2H, J = 7 Hz, Fmoc), 7.34 (d, 2H, J = 7 Hz, PABA), 7.36 (b, 2H, PABA), 7.40 (t, 2H, J = 7 Hz, Fmoc), 7.60 (d, 2H, J = 7 Hz, Fmoc), 7.77 ppm (d, 2H, J = 7 Hz, Fmoc); ESI-MS, observed m/z = 384.1014; calculated m/z for ($M + K^{+}$) = 384.0996.

Loading of Fmoc-PABA to 2-Chlorotrityl Resin. Fmoc-PABA (2 equiv) was added to 1.0 g of 2-chlorotrityl polystyrene resin in 10 mL dry THF followed by 4 equiv of dry pyridine. The solution was stirred and heated at 60 ºC in an oil bath for 16 h under argon. The solution was filtered through a coarse sintered glass frit, and the resin was washed with DCM/MeOH/DIEA 17:2:1 mL (3x), followed by DCM 10 mL (2x), DMF 10 mL (2x), DCM 10 mL (3x). The resin was dried under high vacuum (10^{-2} torr) overnight and then checked for loading level according to previous published methods.[39]

Solid Phase Peptide Synthesis. The peptide was synthesized by the solid phase method using Fmoc strategy starting with preloaded Fmoc-PABA. The peptide was prepared on a 0.25 mmol scale by single amino acid couplings using a 4-fold excess of N-acetyl-Gly and the Fmoc-protected amino acids D-Ala (Chem-Impex, International, Wood Dale, IL), L-Phe, and L-Lys-alloc. Activation was done with 2-(1H-benzotriazole-1-yl)-1,1,3,3-tetramethyluronium hexafluoro-phosphate (HBTU)/N-hydroxy-benzotriazole (HOBT) and the synthesis was performed on an ABI 433A peptide synthesizer (Applied Biosystems, Carlsbad, CA). Owing to the poor nucleophilicity of the aniline nitrogen of PABA, the coupling of the first amino acid, Fmoc-Lys(alloc), required an extended coupling time by modifying the software instructions to vortex the reaction for 60 sec, then allow it to sit for 10 min. This cycle was repeated 88 times. Fmoc groups were removed by sequential treatment (3x) with 20% piperidine/DMF, and all other amino acid couplings followed standard conditions, to yield Ac-Gly-D-Ala-L-Phe-L-Lys(alloc)-PABA (Ac-GaFK(alloc)-PABA) coupled to the polystyrene resin.

2.2.4 Synthesis of Ac-GaFK(alloc)-PABA-pNP Carbonate Ester.

Cleavage of Ac-GaFK(alloc)-PABA (8) from the Resin and Activation to Ac-GaFK(alloc)-PABA-pNP Carbonate Ester (9). The resin was placed into a medium-grain fritted funnel and washed twice with DCM (20 mL). Pyridine/MeOH (10% v/v, 20 mL) was added to the receiving flask to protect the peptide after cleavage. TFA/DCM (2% v/v, 10 mL) was then added and swirled for 1 min. The mixture was then gently vacuum filtered, without allowing the resin to proceed to dryness. This step was repeated 3 times followed by a 20 mL DCM wash. The filtrate contained the peptide and pyridine/TFA salt and was rotary-evaporated to ~10% of the original volume. Approximately 40 mL of deionized water was added to the flask. Upon swirling, the peptide began to precipitate. The solution was allowed to cool in an ice bath for at least 10 min. The precipitate was collected on a fritted funnel and washed with deionized water 10 mL (3x), followed by ether 10 mL (2x). An oven dried round bottom flask equipped with a magnetic stir bar was cooled under argon and charged with 25.0 mL of tetrahydrofuran (distilled from sodium metal and benzophenone) and **8** (376.6 mg, 0.577 mmoles). To the stirring heterogeneous mixture, 1.1 equiv p-nitrophenyl chloroformate (127.9 mg) was added followed immediately by 1.1 equiv pyridine (51.33 µL). Over the course of 20 min, all solids went into solution, after which the reaction progress was monitored by RP-HPLC (Method 1) until complete, as evidenced by the disappearance of starting material (eluting at 13.4 min), which typically required overnight reaction. The reaction mixture was then diluted with 250 mL of ethyl acetate and washed once with 150 mL deionized water, followed by extractions with 150 mL of saturated sodium bicarbonate until the aqueous layer no longer turned yellow (typically 5 extractions). The organic layer was dried over sodium sulfate and concentrated by

rotary evaporation to yield 400 mg of a pale yellow solid that was used without further purification, with a final yield of 85%. Ac-GaFK(alloc)-PABA-pNP was characterized by the following spectroscopic data with NMR assignments made from ^{1}H NMR(DMSO, 500 MHz): δ 0.94 (d, 3H, *J*=7.0 Hz, Ala-CH_3), 1.32 – 1.27 (m, 1H, Lys-γ'), 1.40 – 1.33 (m, 1H, Lys-γ), 1.49 – 1.40 (m, 2H, Lys-δ), 1.70 – 1.61 (m, 1H, Lys-β'), 1.77 – 1.71 (m, 1H, Lys-β), 1.82 (s, 3H, N-Acetyl), 2.75 (dd, 1H, *J*=13.7, 10.7 Hz, Phe-β), 2.98 (apparent q, 2H, *J*=6.3 Hz, Lys-ε), 3.09 (dd, 1H, *J*=13.7, 3.5 Hz, Phe-β'), 3.62 and 3.66 (AB of ABX pattern, 2H, J_{AB}=16.5, J_{AX}=5.8, J_{BX}=5.7 Hz, Gly-α), 4.24 (apparent p, 1H, *J*=7.0 Hz, Ala-α), 4.35 (apparent q, 1H, *J*=7.7 Hz, Lys-α), 4.43 (d, 2H, *J*=5.3 Hz, alloc), 4.56 (ddd, 1H, *J*=10.7, 8.6, 3.5 Hz, Phe-α), 5.14 (dd, 1H, *J*=10.6, 3.0 Hz, alloc), 5.25 (s, 2H, Bz), 5.88 (ddt, 1H, *J*=17.0, 10.6, 5.3 Hz, alloc), 7.18 – 7.12 (m, 1H, *p*-Ph), 7.29 – 7.18 (m, 5H, *o,m*-Ph and Lys-ε-NH), 7.42 (d, 2H, *J*=8.5 Hz, PABC-$H_{2,6}$), 7.60 – 7.53 (AA'XX' pattern, 2H, PNP-$H_{2,6}$), 7.67 (d, 2H, *J*=8.5 Hz, PABC-$H_{3,5}$), 8.00 (d, 1H, *J*=7.3 Hz, Ala-α-NH), 8.04 (X of ABX, 1H, J_{AX}=5.8, J_{BX}=5.7 Hz, Gly-α-NH), 8.22 (d, 1H, *J*=7.4 Hz, Phe-α-NH), 8.24 (d, 1H, *J*=6.2 Hz, Lys-α-NH), 8.36 – 8.28 (AA'XX' pattern, 2H, PNP-$H_{3,5}$), 10.05 (s, 1H, PABC-NH) ppm.

2.2.5 Synthesis of Ac-GaFK-PABC-Doxaz, phosphate salt.

Ac-GaFK(alloc)-PABC-Doxaz (10). An oven dried round bottom flask equipped with a magnetic stir bar was cooled under argon and charged with **9** (126.13 mg, 0.1161 mmoles), 1-hydroxybenzotriazole (23.61 mg, 1 equiv) and 500 µL dry DMSO (stored over 4Å molecular sieves for at least 3 days). To this, 1 equiv doxaz (85.68 mg) dissolved in 500 µL of similarly dried DMSO was added and the mixture was left to stir under argon in the dark and monitored by HPLC (Method 1) until complete, as evidenced by the disappearance of carbonate starting material (approximately 36 h). The reaction mixture was then diluted with an additional 2 mL of

DMSO. A 15 mL medium fritted sintered glass funnel was charged with 10 mL cold PBS, pH 7.4. The red reaction mixture was added dropwise and the resulting red precipitate was washed four times with 10 mL of PBS and then two washes with 10 mL of deionized water. The precipitate was washed from the filter with a mixture of 10:1 chloroform/methanol and concentrated by rotary evaporation. The majority of the crude red solid, which was a mixture containing a 46% yield of **10**, was moved forward without any additional purification. However, to fully purify **10** for characterization, the red solid was purified by preparative TLC, spotted in and eluted with 10:1 chloroform:methanol. The desired product (the major band) was excised, suspended and vortexted in the elution solvent, and centrifuged to remove the silica gel. The solvent was removed by rotary evaporation to produce solid, pure Ac-GaFK(alloc)-PABC-doxaz that was characterized by the following spectroscopic data with NMR assignments made from 1D ^{1}H NMR, homonuclear COSY, ROESY, HSQC, and HMBC spectra: ^{1}H NMR at 55 ^{o}C (500 MHz, $CDCl_3$) δ 1.20 (d, 3H, J = 7 Hz, a-Me), 1.31 (d, 3H, J = 5 Hz, 5'-Me), 1.32 (m, 2H, K-γ), 1.44 (m, 1H, K-δ), 1.50 (broad m, 1H, K-δ), 1.73 (m, 1H, K-β), 1.75 (m, 1H, 2□), 1.87 (m, 1H, K-β), 1.88 (s, 3H, Ac), 2.1 (dt, 1H, J = 14, 4 Hz, 8), 2.17 (broad m, 1H, 2'), 2.41 (d, 1H, J = 14, Hz, 8), 3.01 (d, 1H, J = 18 Hz, 10), 2.98 (dd, 1H, J = 9, 5 Hz, F-β), 3.09 (m, 2H, K-ε), 3.23 (m, 1H, F-β), 3.23 (d, 1H, J = 18 Hz, 10), 3.98 (dd, 1H, J = 5, 1 Hz, 4'), 4.03 (s, 3H, 4-OMe), 4.10 (m, 1H, a-α), 4.08-4.12 (m, 2H, 3' and 5'), 4.45 (dd, 1H, J = 9, 5, K-α), 4.49 (broad, 2H, 3'''), 4.55 (dd, 1H, J = 9, 6 Hz, F-α), 4.70 (s, 2H, 14), 4.90 (d, 1H, J = 4 Hz, OCH_2N), 4.96 (broad, 1H, OCH_2N), 5.06 and 5.8 (broad AB pattern, 2H, J = 11 Hz, Bn), 5.14 (d, 1H, J = 10 Hz, 1'''c ROESY), 5.23 (d, 1H, J=18 Hz, 1'''t ROESY), 5.26 (m, 1H, 7), 5.39 (t, 1H, J = 5 Hz, 1'), 5.85 (ddt, 1H J = 16, 10, 5 Hz, 2'''), 7.15 (m, 1H, F-p-Ph), 7.16 (m, 2H, F-o-Ph), 7.22 (m, 2H, F-m-

Ph), 7.26 (d, 2H, J = 8 Hz, 2'' ROESY), 7.37 (d, 1H, J = 8 Hz, 3), 7.56 (d, 2H, J = 8 Hz, 3''), 7.74 (t, 1H, J = 8 Hz, 2), 7.99 (d, 1H, J = 8 Hz, 1); ^{13}C NMR chemical shifts from HSQC δ 15.75 (5□-Me), 16.19 (a-Me), 22.25 (Ac), 22.54 (K-γ), 29.11 (K-δ), 29.27 (2'), 30.49 (K-β), 34.09 (10) 36.73 (F-β), 35.84 (8), 40.33 (K-ε), 42.79 (G-α), 49.83 (a-α), 53.68 (K-α), 55.16 (F-α), 56.59 (4-OMe), 65.05 (14), 65.33 (3' and 5'), 65.61 (3'''), 66.79 (Bn), 68.95 (7), 77.60 (4'), 78.83 (O-CH_2-N), 99.59 (1'), 117.29 (1'''), 118.97 (3), 119.76 (1), 120.11 (3''), 126.88 (p-Phe), 128.81 (o-Phe), 128.79 (2''), 128.52 (m-Phe), 132.79 (2'''), 135.54 ppm (2); some unprotonated carbons from HMBC δ 121.7 (4a), 133.8 (6a), 161.5 (4), 170.5 (K-α CO), 171.8 (Ac-CO), 170.8 (G-CO), 171.9 (F-CO), 173.7 (a-CO), 213.9 ppm (13); MS-ESI$^+$, observed MH^+ 1234.4832; calculated M 1233.4754.

Deprotection to Ac-GaFK-PABC-Doxaz, phosphate salt (2b). Compound **10** (5.3 mg, 0.0043 mmoles) was dissolved in 600 uL of 5:1 DCM:AcOH. To this, 1 equiv of tetrakis(triphenylphosphine) Pd^0 was added (4.96 mg). The reaction was left in the dark for 80 min, at which point the DCM was removed by rotary evaporation. The acidic solution was diluted with 6 mL 20 mM phosphate buffer, pH 4.6, and extracted 3 times with 6 – 7 mL of ethyl acetate to remove any triphenylphosphine oxide produced during the deprotection, spinning briefly at 1500 xg to produce a clean interface. The desired product was purified from the extracted aqueous solution by preparative HPLC on a C-18 Dyanmax 100 Å 25 cm semi-preparatory column (10 mm i.d.) run isocraticly with 50% acetonitrile, 50% 20 mM phosphate buffer, pH 4.6, at 3 mL/min The product eluted at 10 min. The eluent was lyophilized to yield a red solid consisting of a mixture of the final material and sodium phosphate in 95% yield, relative to the fraction of **9** in the crude starting material. The prodrug was dissolved away

from the majority of the sodium phosphate by 5 washes with 50 µL 9:1 DMSO:water, to yield an acidic water-DMSO solution of **2b**. Cold storage (> 3 weeks at -20 ºC) of **2b** in this form eventually resulted in multiple red products by HPLC, presumably due to a low level reactivity of DMSO with the small percentage of deprotonated Lys-ε-NH_3^+. Therefore, following removal of the majority of the phosphate salts, the DMSO was evaporated by speedvac (10^{-2} torr) and the pure final material dissolved in saline containing 10% PEG-400. To add to the stability of the product, 5 mM sodium phosphate, pH 4.6, was added to this solution. Cold storage of this formulation has shown good stability for at least 2 months. The final yield of the formulated final **2b**, was 78% yield, relative to fraction of **9** in the crude starting material. Ac-GaFK-PABC-doxaz was characterized by the following spectroscopic data with NMR assignments made from 1D ^{1}H NMR, homonuclear COSY, ROESY, HSQC, and HMBC spectra: ^{1}H NMR at 50 ºC (500 MHz, DMSO-d_6/D_2O phosphate pH 4) δ 1.01 (d, 3H, J = 7 Hz, a-Me), 1.17 (d, 3H, J = 7 Hz, 5'-Me), 1.24-1.42 (broad m, 2H, K-δ), 1.55 (p, J = 8 Hz, 2H, K-γ), 1.6-1.76 (broad m, 2H, K-β), 1.84 (m, 2H, 2'), 1.83 (s, 3H, Ac), 2.13 (dd, 1H, J = 14, 5 Hz, 8), 2.18 (dd, 1H, J = 14, 3 Hz, 8), 2.75 (m, 2H, K-ε), 2.89 and 2.91 (AB pattern, 2H, J = 18 Hz, 10), 2.79 (m, 1H, F-β), 3.04 (m, 1H, F-β), 3.97 (dd, 1H, J = 6, 2 Hz, 4'), 4.14 (q, J = 6 Hz, 1H, a-α), 3.93 (s, 3H, 4-OMe), 4.04 (q, J = 6 Hz, 1H, 3'), 4.24 (m, 1H, 5'), 4.26 (m, 1H, K-α), 4.42 (dd, 1H, J = 11, 2 Hz, F-α), 4.54 and 4.55 (AB pattern, J = 20 Hz, 2H, 14), 4.82 and 4.83 (AB pattern, 2H, J = 3 Hz, OCH_2N), 4.95 (dd, J = 5, 3 Hz, 1H, 7), 4.99 and 5.01 (AB pattern, 2H, J = 13 Hz, Bn), 5.22 (t, 1H, J = 4 Hz, 1'), 7.10 (broad m, 1H, F-p-Ph), 7.16 (broad m, 4H, F-o- and m-Ph), 7.25 (d, 2H, J = 7 Hz, 2'' ROESY), 7.37 (d, 1H, J = 8 Hz, 3), 7.51 (broad, 2H, 3''), 7.56 (m, 1H, 2), 7.84 (m, 2H, 1 and 3); ^{13}C NMR chemical shifts from HSQC δ 16.15 (5'-Me), 17.76 (a-Me), 22.50 (Ac), 26.57 (K-γ),

22.57 (K-δ), 29.27 (2'), 30.99 (K-β), 32.47 (10) 37.15 (F-β), 36.95 (8), 48.82 (K-ε), 42.37 (G-α), 48.86 (a-α), 49.7 (3'), 53.99 (K-α), 54.58 (F-α), 56.91 (4-OMe), 63.86 (14), 64.20 (5'), 66.40 (Bn), 69.85 (7), 77.45 (4'), 78.25 (O-CH_2-N), 99.49 (1'), 11.46 (1 and 3), 120.03 (3''), 129.37 (F-p- and o-Phe), 128.61 (2''), 128.52 (F-m-Phe), 135.54 ppm (2); some unprotonated carbons from HMBC δ 75.58 (9), 119.78 (12a), 135.18 (4a), 134.56 (6a), 161.39 (4), 161.42 (12), 171.73 (Ac-CO), 170.20 (G-CO), 171.9 (F-CO), 173.15 (a-CO), 214.12 ppm (13); MS-ESI^+, observed MH^+ 1150.4590; calculated M 1149.4454.

2.2.5 Synthesis of bis-tBoc-aFK-PABC-Doxaz (11).

Bis-tBoc-aFK-PABA and Bis-tBoc-aFK-PABA-PNP. The loading of Fmoc-PABA to resin, the SPPS and cleavage of bis-tBoc-aFK-PABA and the activation of the benzyl alcohol to the pNP carbonate ester were all performed with the same stoichiometry and solvent molarity as described in Sections 2.2.2 to 2.2.3.

Bis-tBoc-aFK-PABC-Doxaz (11). An oven dried round bottom flask equipped with a magnetic stir bar was cooled under argon and charged with bis-tBoc-aFK-PABA-pNP (9.62 mg, 0.0.011 mmoles), 1-hydroxybenzotriazole (1.67 mg, 1 equiv) and 300 µL dry DMSO (stored over 4Å molecular sieves for at least 3 days). To this, 1 equiv doxaz (6.04 mg) dissolved in 200 µL of similarly dried DMSO was added and the mixture was left to stir under argon in the dark and monitored by HPLC (Method 1) until complete, as evidenced by the disappearance of carbonate starting material (approximately 29 h). The reaction mixture was then diluted with an additional 2 mL of DMSO. A 15 mL medium fritted sintered glass funnel was charged with 10 mL cold PBS, pH 7.4. The red reaction mixture was added dropwise and the resulting red precipitate was washed four times with 10 mL of PBS and then two washes with 10 mL of deionized water. The

precipitate was washed from the filter with a mixture of 35:1 chloroform/methanol and concentrated by rotary evaporation. The majority of the crude red solid, which was a mixture containing a 62% yield of **11. T**he red solid was purified by radial silica chromatography eluted with 35:1 chloroform:methanol. The desired product (the major band) was collected. The solvent was removed by rotary evaporation to produce solid, pure bis-tBoc-aFK-PABC- doxaz was characterized by the following spectroscopic data with NMR assignments made from 1D ^{1}H NMR, and homonuclear COSYspectra: ^{1}H NMR at 50 ºC (500 MHz, DMSO-d_6) δ 0.95 (d, 3H, J = 7 Hz, a-Me), 1.17 (d, 3H, J = 7 Hz, 5'-Me), 1.38-1.44 (broad m, 2H, K-δ), 1.57-1.58 (p, 2H, K-γ), 1.6-1.76 (broad m, 2H, K-β), 1.84 (m, 2H, 2'), 2.13 (dd, 1H, J = 14, 5 Hz, 8), 2.18 (dd, 1H, J = 14, 3 Hz, 8), 2.79 (dd, J = 13.9, 10.1 Hz, 1H, F-β), 2.89 and 2.91 (AB pattern, 2H, J = 18 Hz, 10), 2.9 (m, 2H, K-ε), 3.11 (dd, J – 13.9, 3.8 Hz, 1H, F-β), 3.85 (dd, 1H, J = 6, 2 Hz, 4'), 3.95 (q, J = 6 Hz, 1H, a-α), 3.97 (s, 3H, 4-OMe), 4.07 (q, J = 6 Hz, 1H, 3'), 4.21 (m, 1H, 5'), 4.36 (m, 1H, K-α), 4.53 (dd, 1H, J = 11, 2 Hz, F-α), 4.6 and 4.64 (AB pattern, J = 20 Hz, 2H, 14), 4.82 and 4.83 (AB pattern, 2H, J = 3 Hz, OCH_2N), 4.95 (dd, J = 5, 3 Hz, 1H, 7), 5.22 (t, 1H, J = 4 Hz, 1'), 5.25 (s, 2H, Bn), 7.10 (broad m, 1H, F-p-Ph), 7.2 (broad m, 4H, F-o- and m-Ph), 7.25 (d, 2H, J = 7 Hz, 2), 7.43 (m, 2H, PABA), 7.52 (d, 1H, J = 8 Hz, 3), 7.69 (m, 2H, PABA), 8.11 (d, *J* = 8 Hz, 1H, a-NH), 8.16 (d, *J* = 7 Hz, 1H, K-NH), 8.21 (d, *J* = 7 Hz, 1H, F-NH), 9.31 (t, *J* = 5.7 Hz, 1H, K-ε-NH), 9.92 (s, 1H, anilide)

2.2.6 Synthesis of bis-TFA-GaFK-PABC-Doxaz(12).

The loading of Fmoc-PABA to resin, the SPPS and cleavage of bis-TFA-GaFK-PABA and the activation of the benzyl alcohol to the pNP carbonate ester were all performed by the same

procedures and with the same stoichiometry and solvent molarity as described in Sections 2.2.2 and 2.2.3.

Bis-TFA-GaFK(alloc)-PABC-Doxaz (12) An oven dried round bottom flask equipped with a magnetic stir bar was cooled under argon and charged with bis-TFA-GaFK-PABA-pNP (5.00 mg, 0.0.0057 mmoles), 1-hydroxybenzotriazole (0.867 mg, 1 equiv) and 225 µL dry DMSO (stored over 4Å molecular sieves for at least 3 days). To this, 1 equiv doxaz (3.14 mg) dissolved in 100 µL of similarly dried DMSO was added and the mixture was left to stir under argon in the dark and monitored by HPLC (Method 1) until complete, as evidenced by the disappearance of carbonate starting material (approximately 44 h). The reaction mixture was then diluted with an additional 2 mL of DMSO. A 15 mL medium fritted sintered glass funnel was charged with 10 mL cold PBS, pH 7.4. The red reaction mixture was added dropwise and the resulting red precipitate was washed four times with 10 mL of PBS and then two washes with 10 mL of deionized water. The precipitate was washed from the filter with a mixture of 30:1 chloroform/methanol and concentrated by rotary evaporation. The majority of the crude red solid, which was a mixture containing a 64% yield of **12. T**he red solid was purified by radial silica chromatography eluted with 30:1 chloroform:methanol. The desired product (the major band) was collected. The solvent was removed by rotary evaporation to produce solid, pure bis-TFA-GaFK-PABC-doxaz that was characterized by the following spectroscopic data with NMR assignments made from 1D ^{1}H NMR, homonuclear COSY, HSQC and HMBC spectra. 1D ^{1}H NMR at 55^{0}C (500 MHz, DMSO-d6) δ 0.99 (d, *J* = 7.0 Hz, 3H, 5'-Me), 1.24 (d, *J* = 6.6 Hz, 3H, a-Me), 1.27 – 1.44 (m, 2H, K-γ), 1.51 (p, *J* = 7.4 Hz, 2H, K-δ), 1.67 – 1.78 (m, 2H, K-β), 1.79 – 1.94 (m, 2H, 2'), 2.13 – 2.28 (m, 2H, 8), 2.77 (dd, *J* = 13.9, 10.1 Hz, 1H, F-β), 2.98 (tight AB,

2H, 10), 3.09 (dd, *J* = 13.9, 4.1 Hz, 1H, F-β), 3.17 (m, 2H, K-ε), 3.79 and 3.83 (AB of ABX pattern, 2H, J_{AB} =16, J_{AX}=J_{BX}=6, G-α), 3.94 – 3.98 (m, 1H, 4'), 3.99 (s, 3H, OMe), 4.07 (dt, *J* = 7.7, 5.8 Hz, 1H, 3'), 4.27 (q, *J* = 8 Hz, 1H, a-α), 4.30 – 4.42 (m, 1H, K-α, 1H, 5'), 4.50 – 4.63 (m, 1H, F-α, 2H, 14), 4.81 – 4.92 (m, 2H, OCH_2N), 4.97 – 5.14 (m, 2H, Bn, 1H, 7), 5.27 (t, *J* = 4.3 Hz, 1H, 1'), 7.08 – 7.18 (m, 1H, F-p-Ph), 7.17 – 7.24 (m, 4H, F-Ph), 7.29 (d, *J* = 8.2 Hz, 2H, PABA), 7.57 (d, *J* = 8.1 Hz, 2H, PABA), 7.64 (dd, *J* = 7.7, 2.0 Hz, 1H, 3'), 7.82 – 7.96 (m, 1H,1, 1H, 2), 8.06 (d, *J* = 7.7 Hz, 1H, a-NH), 8.13 (d, *J* = 7 Hz, 1H, K-NH), 8.14 (d, *J* = 7 Hz, 1H, F-NH), 9.28 (t, *J* = 5.7 Hz, 1H, K-ε-NH), 9.41 (s, 1H, G-NH), 9.82 (s, 1H, anilide).

2.2.7 Synthesis of bis-Ac-GaFK-PABC-Doxaz (13).

Bis-Ac-GaFK(alloc)-PABA and Bis-Ac-GaFK(alloc)-PABA-PNP The loading of Fmoc-PABA to resin, the SPPS and cleavage of bis-Ac-GaFK-PABA and the activation of the benzyl alcohol to the pNP carbonate ester were all performed by the same procedures and with the same stoichiometry and solvent molarity as described in Sections 2.2.2 and 2.2.3.

Bis-Ac-GaFK(alloc)-PABC-Doxaz (13) An oven dried round bottom flask equipped with a magnetic stir bar was cooled under argon and charged with bis-Ac-GaFK-PABA-pNP (6.41 mg, 0.0.0083 mmoles), 1-hydroxybenzotriazole (1.58 mg, 1 equiv) and 100 µL dry DMSO (stored over 4Å molecular sieves for at least 3 days). To this, 1 equiv doxaz (4.59 mg) dissolved in 100 µL of similarly dried DMSO was added and the mixture was left to stir under argon in the dark and monitored by HPLC (Method 1) until complete, as evidenced by the disappearance of carbonate starting material (approximately 27 h). The reaction mixture was then diluted with an additional 2 mL of DMSO. A 15 mL medium fritted sintered glass funnel was charged with 10 mL cold PBS, pH 7.4. The red reaction mixture was added dropwise and the resulting red

precipitate was washed four times with 10 mL of PBS and then two washes with 10 mL of deionized water. The precipitate was washed from the filter with a mixture of 30:1 chloroform/methanol and concentrated by rotary evaporation. The majority of the crude red solid, which was a mixture containing a 52% yield of **13. T**he red solid was purified by radial silica chromatography eluted with 30:1 chloroform:methanol. The desired product (the major band) was collected. The solvent was removed by rotary evaporation to produce solid, pure bis-Ac-GaFK-PABC-doxaz that was characterized by the following spectroscopic data with NMR assignments made from 1D ^{1}H NMR, homonuclear COSY, HSQC and HMBC spectra. 1D ^{1}H NMR at 55^{o}C (500 MHz, DMSO-d6) δ 1.00 (d, *J* = 7.0 Hz, 3H, 5'-Me), 1.24 (d, *J* = 6.6 Hz, 3H, a-Me), 1.26 – 1.36 (broad m, 2H, K-γ), 1.40 (m, 1H, K-δ), 1.65 (m, 1H, K-δ), 1.73 (, 1H, 2'), 1.77 (s, 3H, K-Ac), 1.83 (s, 3H, G-Ac), 1.84 – 1.91 (m, 1H, 2'), 2.14 – 2.26 (m, 2H, 8), 2.78 (dd, *J* = 13.9, 10.1 Hz, 1H, F-β), 2.99 (s, 2H, 10), 3.00 – 3.05 (m, 2H, K-ε), 3.09 (dd, *J* = 13.9, 4.1 Hz, 1H, F-β'), 3.62 and 3.66 (AB of ABX pattern, 2H, J_{AB} =17, J_{AX}=J_{BX}=6, G-α), 3.96 (dd, *J* = 5.9, 2.2 Hz, 1H, 4'), 4.00 (s, 3H, 4-OMe), 4.06 (dt, *J* = 7.6, 5.8 Hz, 1H, 3'), 4.23 (p, *J* = 7.0 Hz, 1H, 5'), 4.30 – 4.37 (m, 2H, a-α), 4.53 (dd, *J* = 9.8 Hz, 1H, F-α), 4.56 (dd, *J* = 5.9, 4.4 Hz, 3H), 4.50 – 4.59 (m, 3H), 4.71 (t, *J* = 5.9 Hz, 1H), 4.86 (d, *J* = 3.6 Hz, 1H, OCH_2N), 4.89 (d, *J* = 3.5 Hz, 1H, OCH_2N), 4.97-5.11 (m, 2H, Bn, 1H, 7), 5.27 (t, *J* = 4.2 Hz, 1H, 1'), 7.10 – 7.17 (m, 1H, p-F), 7.17 – 7.26 (m, 4H, F-Ph), 7.29 (d, *J* = 8.2 Hz, 2H, PABA), 7.58 (d, *J* = 8.2 Hz, 2H, PABA), 7.63 – 7.70 (m, 1H, K-NH), 7.86 – 7.97 (m, 1H, 3, 1H, G-NH, 1H, 2, a-NH, 1H), 8.00 (d, *J* = 7.8 Hz, 1H, 1), 8.07 (d, *J* = 8.2 Hz, 1H, F-NH), 9.77 (s, 1H, K-ε-NH), 10.09 (s, 1H, anilide), 13.25 (s, 1H, 6-OH), 14.03 (s, 1H, 11-OH).

2.2.8 In vitro assays (Performed by Dr. Ben Barthel)

IC_{50} Assays. Initial characterization of PAD was performed in MiaPaCa2 human pancreatic carcinoma and MCF-7 human breast cancer lines. The cells were seeded into 96-well plates at a density of 1000 cells/well and allowed to adhere overnight. The media was replaced with 90 µL of serum-free media containing one or more of plasmin (0.2 U/well), trypsin (0.2 U/well), cathepsin B (0.2 U/well), aprotinin (5 µM, Research Products International, Mt Prospect, IL), or Complete Mini protease inhibitors (1X according to package instructions, Roche Applied Science, Indianapolis, IN). PAD (10 µL) was added to the wells for final concentrations between 2000 nM and 1 nM and controls received only vehicle (either DMSO or saline with 10% PEG). The cells were treated with PAD and activator/inhibitor for 24 h, at which point the treatment media was replaced with complete media and the cells allowed to grow for 5 days or until the control wells reached 80% confluency, whichever was shorter. The cells were then fixed with 5% formalin in PBS for 10 min and stained with crystal violet (0.01% w/v in water) for 20 – 30 min. The plates were rinsed and air-dried and the stain redissolved either in a mixture of ethanol, water, and methanol (6:3:1) or in 2-propanol:water (1:1) with 2% sodium dodecylsulfate (SDS). Cell density was measured by absorbance at 582 nm. Percent optical density, relative to control wells, was fit to a variable slope sigmoidal dose-response curve by non-linear regression analysis in GraphPad Prism 5.0. These experiments indicated that pure DMSO formulations or saline/PEG/phosphate formulations of PAD resulted in identical growth inhibition.

Following initial tests in MiaPaCa-2 and MCF-7 cells, tests with PAD alone or with plasmin (0.2 U/well) were performed on an array of pancreatic cancer lines (BxPC3, L3.3, L3.5,

and L3.6PL), a small-cell lung cancer line (SHP77), and on an ovarian cancer line (NCI-RES/Adr), as well as a non-tumor derived cell line (HEK-293T). All experiments were performed identically as described above.

Cellular Uptake. MCF-7 or MiaPaCa-2 cells were plated into 6-well plates at a density of 250,000 cells/well and allowed to adhere overnight. The media was then replaced with serum free media and 0.5 μM PAD or 0.5 μM PAD + 0.2 U plasmin was added (final concentrations). The cells were incubated for up to 5 h, then trypsinized and analyzed for the presence of the anthracycline fluorophore by flow cytometry (FL3 channel). The mean fluorescence values were converted fold-over-background, in which background was defined as cells receiving no PAD.

2.3 Results and Discussion

In an attempt to synthesize a Doxaz prodrug targeted to plasmin, a strategy analogous to the de Groot *et al*. procedure was employed.[36] The Dox prodrug de Groot and co-workers synthesized had on average a 15 fold reduced cytotoxicity toward seven human tumor cell lines. This was attributed to the varying concentrations of uPA or plasmin expressed in the tumor lines. Incorporation of a second self-eliminating spacer exhibited improved activity.[37] Plasmin is a particularly attractive enzyme for prodrug therapy, and we hypothesized that with the elevated activity of Doxaz relative to Dox, prodrugs using similar targeting moieties tethered to Doxaz would exhibit better cytotoxic activity toward human cancer cell lines.

The desire to work toward scalable syntheses using commercially available materials seemed realistic based on the reagents used by de Groot. Synthesis of D-Ala-L-Phe-L-Lys-PABC-

Doxaz (aFKPABCDoxaz) was therefore attempted. The use of the unnatural isomer of alanine was designed to safeguard the prodrug from non-specific exopeptidases found in the body.[40-42] Originally the synthesis was hypothesized to be straightforward. This was not the case.

Synthesis of the three amino acid peptide was first done on an automatic peptide synthesizer, and cleavage from the resin was accomplished using standard trifluoroacetic acid (TFA) conditions. Addition of the *p*-aminobenzyl alcohol (PABA) spacer analogous to literature procedures[37] required the use of a coupling strategy in which the carboxy terminus of the peptide was activated with a chloroformate. This chloroformate was then displaced with p-aminobenzyl alcohol. The synthetic scheme reportedly[37] produced yields of 93% and is shown in Scheme 2.3.1. In our hands, difficulty in controlling the addition of the chloroformate to the carboxy terminus was observed, and side products were observed.

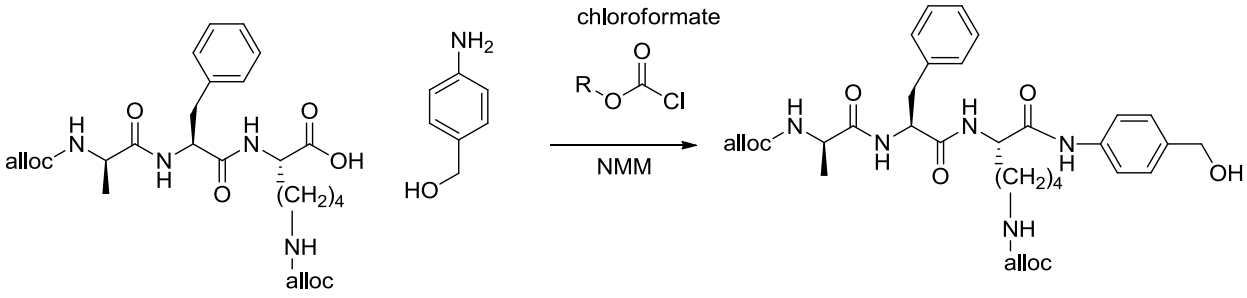

Scheme 2.3.1 Addition of *p*-aminobenzyl alcohol spacer to the bis alloc protected aFK peptide.

To circumvent this problem, the addition of PABA to the polystyrene resin was performed. To function harmoniously with the peptide synthesizer, Fmoc-PABA was synthesized as shown in Scheme 2.3.2. Use of a slight excess of the water soluble PABA allowed a rapid and scalable reaction of the hydrophobic Fmoc-PABA. Simple washing with water removed the excess starting materials and afforded the desired product in high yield and purity.

This synthesis has been performed on a 10 gram scale. Addition of the Fmoc-PABA to the resin using standard techniques was straightforward. Automated synthesis using standard Fmoc synthetic procedures originally resulted in very poor yields.

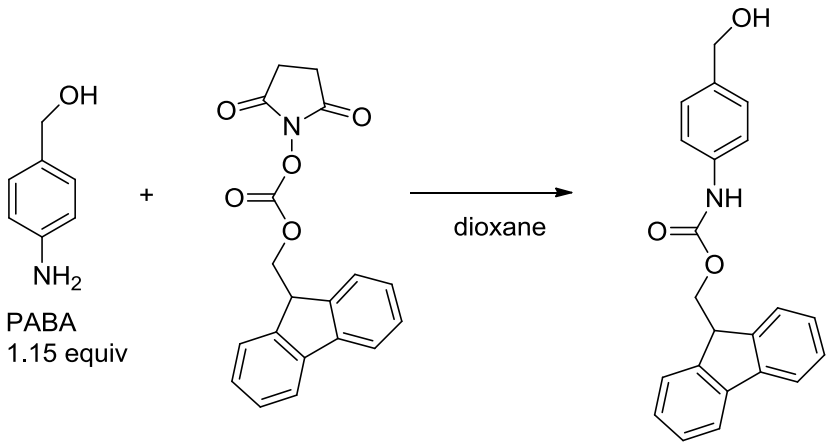

Scheme 2.3.2 Slight excess of PABA allows large scale synthesis of needed Fmoc-PABA.

It was concluded that the deprotection of the resin bound Fmoc-PABA went smoothly; however, the lower reactivity of the aniline nitrogen caused the poor yield. Relatively involved reprogramming of the peptide synthesizer allowed us to create a custom method in which the aniline nitrogen was allowed to react with the activated carboxy-terminus of the N-Fmoc-protected lysine for over sixteen hours with agitation cycles. The isolated peptide with the incorporated spacer was easily cleaved from the resin, and activated to the desired *p*-nitrophenyl mixed carbonate as shown in Scheme 2.3.3.

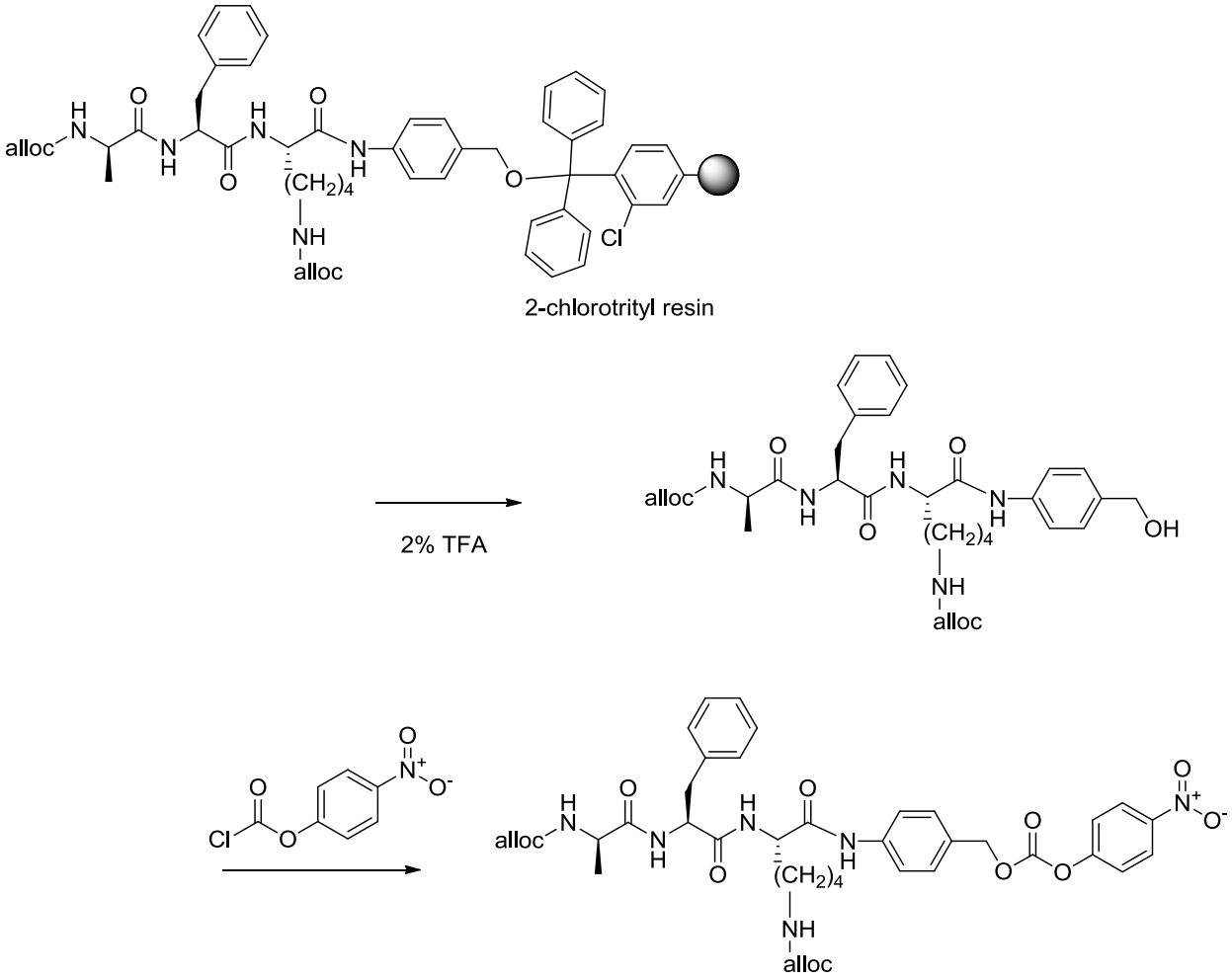

Scheme 2.3.3 Cleavage of peptide from resin and activation with *p*-nitrobenzyl chloroformate.

With the mixed carbonate in hand, the coupling of Doxazolidine was attempted using the conditions used by de Groot. It was thought that Doxazolidine would be a strong enough nucleophile to displace the stable *p*-nitrophenolate leaving group. Unfortunately, even the hindered nucleophilic nitrogen of triethylamine was able to react more quickly, and form an unwanted contaminant with the evolution of ethylene gas as shown in Scheme 2.3.4. Multiple modifications of the solvent system and reagents used were attempted. The side products from triethylamine (TEA) and a suitable substitute, diisopropylethylamine (DIEA) were difficult

to remove. Purification by radial silica gel chromatography afforded the desired product, but in yields less than 50%.

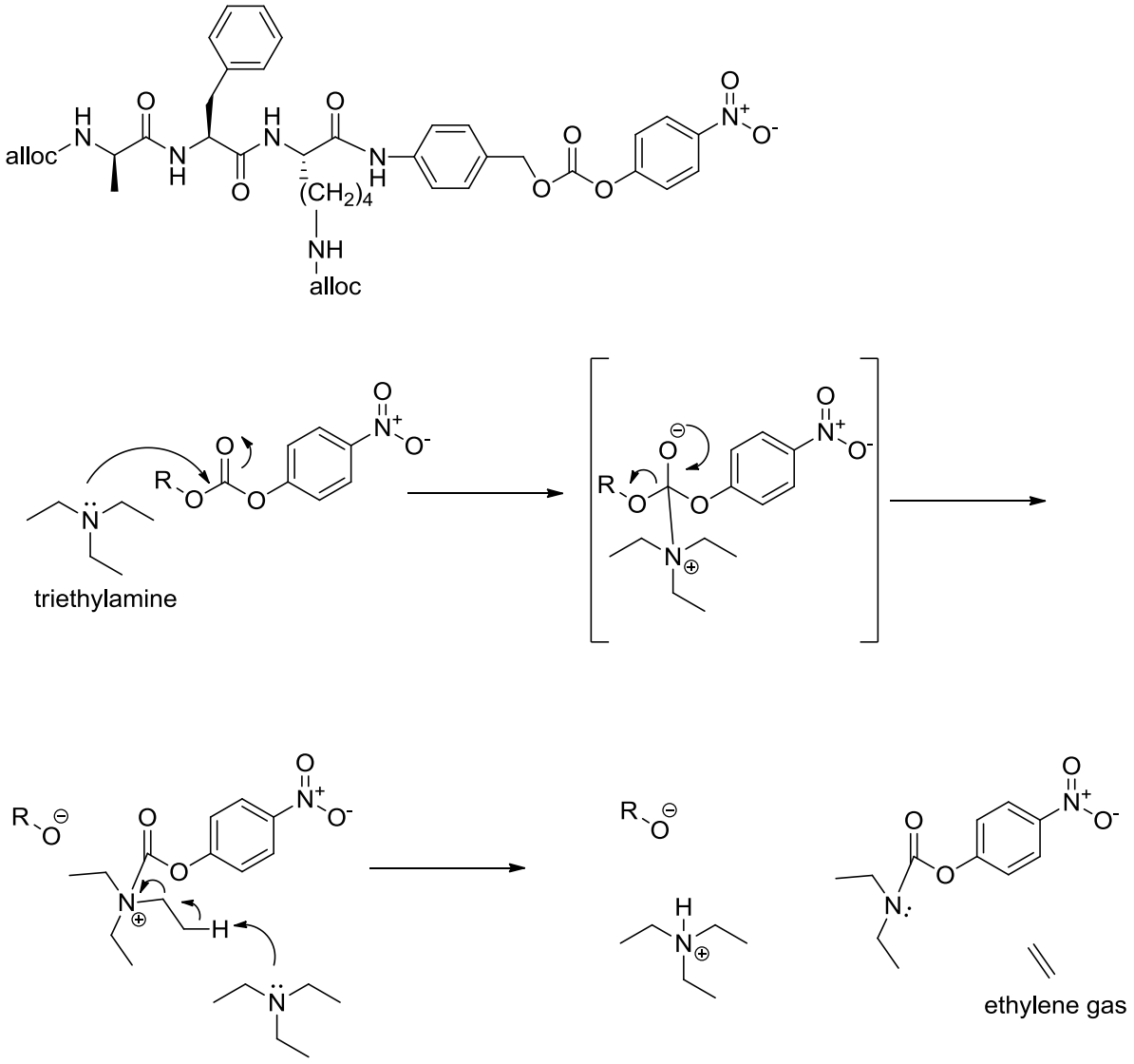

Scheme 2.3.4 Formation of an unwanted contaminant. Triethylamine can act as a better nucleophile than Doxaz, forming unwanted products.

The Pd^0 mediated deprotection shown in Scheme 2.3.5 using literature conditions[37] went poorly. In fact, NMR analysis of the final product seemed acceptable; however the drug showed little or no activity toward cells in culture. Purification by RP-HPLC afforded active

drug. It was hypothesized that the presence of Pd^0 was somehow inactivating the activating enzyme. This hypothesis was overshadowed by the observation that epimerization of the D-alanine was occurring. Closer inspection of NMR data showed 15% contamination of the epimer. The epimerization was traced to the acidification of the liberated Lys-ε-amino by HCl dissolved in ethyl acetate to afford the HCl salt of the final product.

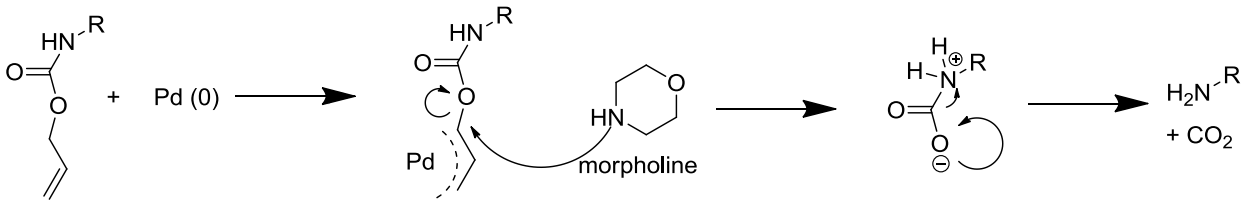

Scheme 2.3.5 Mechanism of alloc deprotection.

To address the epimerization, alternate amino acid protecting groups were used. The use of commercially available *tert*-butyloxycarbonyl (tBoc) protected amino acids afforded the final product shown in Figure 2.3.1. Multiple (>32) deprotection conditions were employed using standard solvents and reagents. The overwhelming conclusion was that the acidic nature of the conditions needed to remove tBoc caused the loss of the daunosamine sugar, resulting in the isolation of aglycone as the predominant product. The aglycone is shown in Figure 2.3.2.

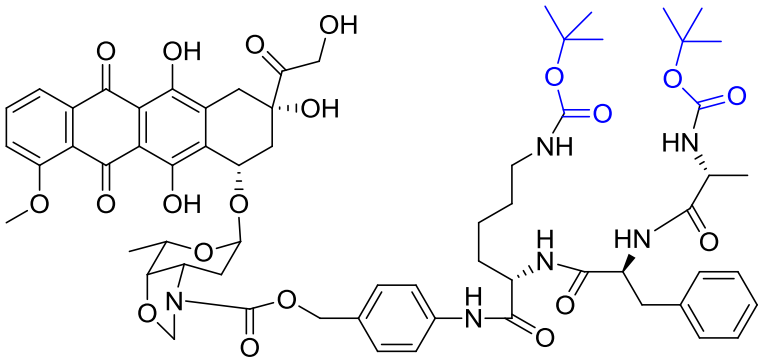

Figure 2.3.1 Structure of bis-tBoc-aFK-PABC-Doxaz.

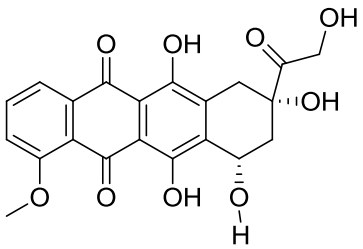

Figure 2.3.2 Structure of the aglycone after acid hydrolysis of the daunosamine sugar.

Armed with the knowledge surrounding the deprotection, we designed the so called fourth generation protease prodrug, Ac-GaFK(alloc)-PABC-Doxaz shown in Figure 2.3.3. The rationale was that the use of Glycine at the amino–terminus would both eliminate the possibility of epimerization, and remove the need for a second protected amino acid. The peptide would effectively be "capped". All syntheses went smoothly, and scalable methods were attempted. The discovery that the activated prodrugs could be precipitated from phosphobuffered saline at pH 7.4 led to the synthesis of protected products on the 100 mg scale. Unfortunately, the the final deprotection once again proved problematic. Use of catalytic Pd^0 was ineffective. Stoichiometric amounts of Pd^0 afforded an isolable product. This product was unfortunately unstable and not easily characterized. NMR conditions necessitated dissolution in d_6-DMSO and the heating of the product to above 50^{o}C. The vast knowledge pertaining to the stability and solubility of prodrugs of this type obtained throughout this project coupled with extensive experimentation led to acceptable deprotection conditions.

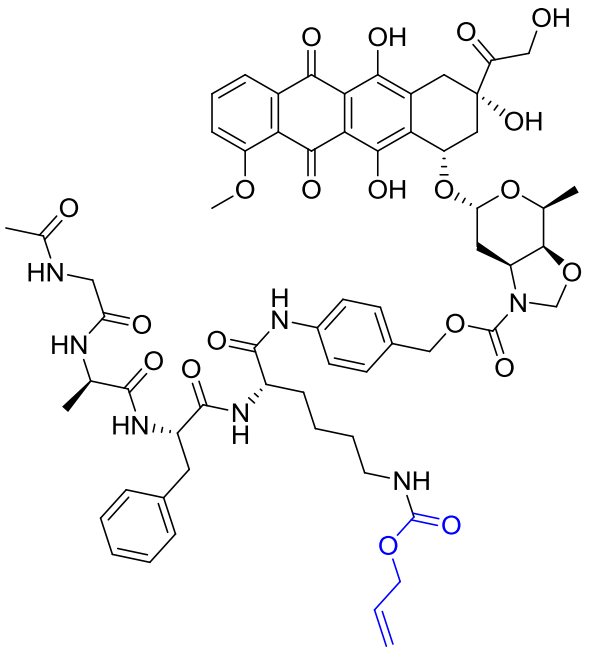

Figure 2.3.3 Structure of Ac-GaFK(alloc)-PABC-Doxaz.

Interestingly, the prodrugs were stable to, and soluble in, acetic acid. The use of a mixed solvent composed of five parts anhydrous dichloromethane and one part acetic acid easily dissolved the protected starting material, did not harm the molecule with excessive acidity, and immediately protonated the free Lys-ε-amine upon deprotection. Rotary evaporation of the dichloromethane and dissolution in preparative RP-HPLC eluent allowed direct injection of the crude reaction mixture onto the preparative RP-HPLC and subsequent purification. Although larger amounts than previously possible were isolated, it was observed by NMR that triphenylphosphine oxide, resulting from the tetrakis(triphenylphosphine)Pd^0 reagent, was contaminating the sample, even after purification. To address this, the crude reaction mixture upon removal of the dichloromethane, was diluted with 20 mM sodium phosphate buffer at pH 4.6. This is also the aqueous phase of the preparative RP-HPLC purification. Extraction of this aqueous acidic phase with ethyl acetate removed the triphenylphosphine oxide, and subsequent purification afforded the desired product as the

phosphate salt. The phosphate salt was more stable than the preceding salts. The final structure is shown in Figure 2.3.4.

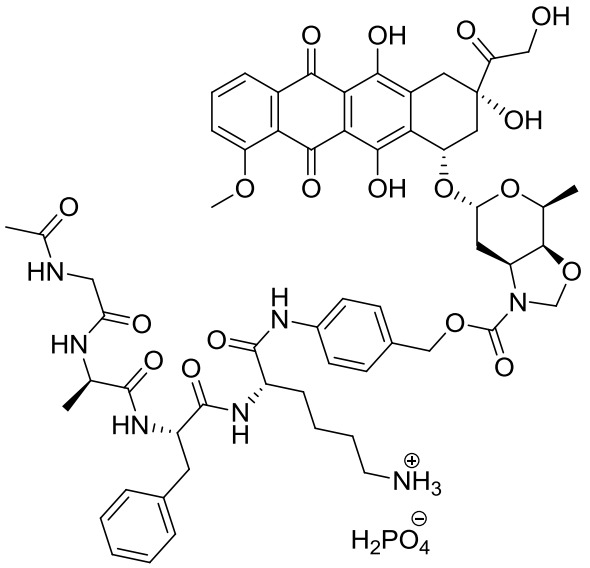

Figure 2.3.4 Ac-GaFK(H_2PO_4)-PABC-Doxaz. The final product is isolated as a phosphate salt.

Concurrently, the syntheses of bis-Ac-GaFK-PABC-Doxaz and bis-TFA-GaFK-PABC-Doxaz were being performed. Ironically, the use of TFA as a protecting group under basic deprotection conditions led to the epimerization of the D-Alanine. The use of exogenous enzymes such as porcine acylase to remove the acetyl and TFA protecting groups failed, but led to the idea that perhaps the body could facilitate the deprotection of the prodrug. A review of the literature[43-48] showed that histone deacetylases, or HDAC's encompass a large family, and are commonly overexpressed in cancer. In fact, HDAC's are considered targets themselves.[49] Interestingly, HDAC's have been shown to remove the TFA group from the Lysine-ε-amine.[48] The idea of a "double filter" quickly emerged. Perhaps even more selective targeting could be achieved by using the two groups. Cell experiments were therefore undertaken by Dr. Ben Barthel, and the results are summarized in Tables 2.3.1 and 2.3.2. A reminder to the reader is

that the more negative the number in an IC_{50} the better the response to the drug. Inspection of these results begs the question if they are statistically relevant. It did however lead us to examine other proteases, such as cathepsin B, as possible activators. This assisted in the design of prodrugs presented in Chapter 3. Further investigation is currently underway.

Drug	MiaPaCa-2	nM
Dox	-6.8±0.2	158
+ Plasmin	-6.7±0.3	200
Doxaz	-8.5±0.3	3
aFKPABC-Dox	-6.6±0.6	251
+ Plasmin	-6.1±0.1	316
aFKPABC-Doxaz	-6.9±0.3	126
+ Plasmin	-7.4±0.4	32
Bis-TFA-GaFK-PABC-Doxaz	-7.0±0.2	100
+ Plasmin	-7.4±0.3	40
+ Acylase	-6.9±0.2	126
+ Plasmin and Acylase	-6.8±0.2	158
Peptide	No Change	
+ Plasmin	No Change	
+ Acylase	No Change	
+ Plasmin and Acylase	-5.3±0.4	5012

Table 2.3.1 Comparison of prodrugs and drugs with and without added activating enzymes. MiaPaCa-2 are pancreatic cancer cells.

Drug	Cell Line	IC_{50}
Bis-TFA-GaFK-PABC-Doxaz	MCF-7	-6.8±0.3
+Plasmin		-7.18±0.1
Bis-TFA-GaFK-PABC-Doxaz	MiaPaCa	-6.8±0.1
+Plasmin		-6.9±0.1
Bis-Ac-GaFK-PABC-Doxaz	MCF-7	-6.3±0.3
+Plasmin		-6.7±0.1
Bis-Ac-GaFK-PABC-Doxaz	MiaPaCa	-6.3±0.1
+Plasmin		-6.4±0.1

Table 2.3.2 Comparison of prodrugs and drugs with and without added activating enzymes against two cell lines. MCF-7 are from a breast cancer line, and MiaPaCa are from a pancreatic cancer line.

With the improved synthetic methods, and increased enzymatic activity, Ac-GaFK-PABC-Doxaz became the tier one compound. Growth inhibition of a panel of cell lines by 24 h treatment with PAD and PAD with 0.2 U of human plasmin, represented by the IC_{50} in log M units was performed by Dr. Barthel. BxPC3, L3.3, L3.5, and L3.6PL are pancreatic cancer, SHP77 are small-cell lung cancer, and NCI-RES/Adr are ovarian cancer cells. The latter two lines are dox-resistant. HEK-293T cells are non-tumor derived human embryonic kidney cells. Values for individual cell lines are the mean ± standard error of at least 12 measurements. The values for cancer cells were averaged and are shown in the Cancer Cell Mean row ± the standard deviation. It is clear that plasmin is activating these prodrugs, as shown by Table 2.3.3. These promising results have prompted further study, and preliminary *in vivo* studies are currently underway.

	PAD Alone	PAD + Plasmin (0.2 U)
BxPC3	-6.0 ± 0.1	-7.4 ± 0.1
L3.3	-6.6 ± 0.1	-8.40 ± 0.07
L3.5	-6.65 ± 0.04	-8.58 ± 0.04
L3.6PL	-6.50 ± 0.08	-8.50 ± 0.04
SHP77 [a]	-5.80 ± 0.03	-7.53 ± 0.05
NCI-RES/Adr [a]	-6.04 ± 0.05	-7.93 ± 0.05
Cancer Cell Mean	-6.3 ± 0.3	-8.1 ± 0.5 [c]
HEK-293T [b]	-6.7 ± 0.1	-8.52 ± 0.04

Table 2.3.3 Activity of prodrugs agains eight cancer lines, with and without additional plasmin.

2.4 Conclusions

At the conception of this project, we thought the synthesis of a protease activated Doxaz prodrug would be straightforward. This was not the case. The pathway to this molecule has been difficult, yet the lessons learned have led to the capability to regularly synthesize the

final prodrug at a 50 mg scale, without the assistance of specialized equipment. Consultation with a local manufacturing facility has indicated that synthesis on the scale needed for larger species and human trials is possible. This prodrug could have wide utility against resistant and metastatic cancers. Our focus is on the underserved pancreatic cancer indication. As a preliminary step toward commercialization, this project was a success.

2.5 References

1. López-Otín, C.; Matrisian, L.M. Emerging roles of proteases in tumour suppression. *Nat. Rev. Cancer*. **2007**, 7, 800-808.

2. Gabriel, D.; Zuluaga, M.F.; van den Bergh, H.; *et al*. It is all about proteases: From drug delivery to in vivo imaging and photomedicine. *Curr. Med. Chem*. **2011**, 18, 1785–1805.

3. Pollard, J.W. Tumour-educated macrophages promote tumour progression and metastasis. *Nat. Rev. Cancer*. **2004**, 4, 71–78.

4. Coussens, L.M.; Werb, Z. Inflammation and cancer. *Nature*. **2002**, 420, 860–867.

5. Nyberg, P.; Salo, T.; Kalluri, R. Tumor microenvironment and angiogenesis. *Front. Biosci*. **2008**, 13, 6537-6553.

6. Borgoño, C.A.; Diamandis, E.P. The emerging roles of human tissue kallikreins in cancer. *Nat. Rev. Cancer*. **2004**, 4, 876–890.

7. Kalluri, R. Basement membranes: structure, assembly and role in tumour angiogenesis. Nat. Rev. Cancer. **2003**, 3, 422-433.

8. Sund, M.; Xie, L.; Kalluri, R. The contribution of vascular basement membranes and extracellular matrix to the mechanics of tumor angiogenesis. *Apmis*, **2004**, 112, 450- 462.

9. Bernik, M.B.; Kwaan, H.C. Plasminogen activator activity in cultures from human tissues. An immunological and histochemical study. *J. Clin. Invest.* **1969**, 48, 1740–1753.

10. Bernik, M.B.; Kwaan, H.C. Origin of fibrinolytic activity in cultures of the human kidney. *J. Lab. Clin. Med*. **1967**, 70, 650–661.

11. Blasi, F.; Carmeliet, P. uPAR: a versatile signalling orchestrator. *Nat. Rev. Mol. Cell. Biol.* **2002**, 3, 932–943.

12. Wall, M.E.; Wani, M.C.; Cook, C.E.; *et al.* Plant antitumor agents, I: the isolation and structure of camptothecin, a novel alkaloidal leukemia and tumor inhibitor from Camptotheca acuminate. *J. Am. Chem. Soc.* **1966**, 88, 3888-3890.

13. Hsiang, Y.H.; Hertzberg, R.; Hecht, S.; *et al*. Camptothecin induces protein-linked DNA breaks via mammalian DNA topoisomerase I. *J. Biol. Chem.* **1985**, 260, 14873-14878.

14. Rivory, L.P.; Bowles, M.R.; Robert, J.; *et al.* Conversion of irinotecan (CPT-11) to its active metabolite, 7-ethyl-10-hydroxycamptothecin (SN-38), by human liver carboxylesterase. *Biochem. Pharmacol*. **1996,** 52, 1103-1111.

15. Bencharit, S.; Morton, C.L.; Xue, Y.; *et al. St*ructural basis of heroin and cocaine metabolism by a promiscuous human drug-processing enzyme. *Nat. Struct. Biol.* **2003**, 10, 349-356.

16. Sanghani, S.P.; Quinney, S.K.; Fredenburg, T.B.; *et al.* Hydrolysis of irinotecan and its oxidative metabolites, 7-ethyl-10-[4-N-(5-aminopentanoic acid)-1-piperidino] carbonyloxycamptothecin and 7-ethyl-10-[4-(1-piperidino)-1-amino]-carbonyloxycamptothecin, by human carboxylesterases CES1A1, CES2, and a newly expressed carboxylesterase isoenzyme, CES3. *Drug. Metab. Dispos*. **2004**, 32, 505-511.

17. Durand, M.K.; Bødker, J.S.; Christensen, A.; *et al*. Plasminogen activator inhibitor-I and tumour growth, invasion, and metastasis. *Thromb. Haemost*. **2004**, 91, 438–449.

18. Mignatti, P.; Rifkin, DB. Biology and biochemistry of proteinases in tumor invasion. *Physiol. Rev.* **1993**, 73, 161–195.

19. Kwaan, HC. The plasminogen-plasmin system in malignancy. *Cancer. Metastasis. Rev*. **1992**, 11, 291–311.

20. Danø, K.; Andreasen, P.A.; Grøndahl –Hansen, J.; *et al.* Plasminogen activators, tissue degradation, and cancer. *Adv. Cancer. Res.* **1985**, 44, 139–266.

21. Kirchheimer, J.C.; Wojta, J.; Christ, G.; *et al*. Proliferation of a human epidermal tumor cell line stimulated by urokinase. *Faseb.J*. **1987**, 1, 125–128.

22. Kirchheimer, J.C.; Wojta, J.; Hienert, G.; *et al*. Effect of urokinase on the proliferation of primary cultures of human prostatic cells. *Thromb. Res*. **1987**, 48, 291–298.

23. Kwaan, H.C.; Wang, J.; Svoboda, K.; *et al*. Plasminogen activator inhibitor 1 may promote tumour growth through inhibition of apoptosis. *Br. J. Cancer*. **2000**, 82, 1702–1708.

24. Soff, G.A.; Sanderowitz, J.; Gately, S.; *et al*. Expression of plasminogen activator inhibitor type 1 by human prostate carcinoma cells inhibits primary tumor growth, tumorassociated angiogenesis, and metastasis to lung and liver in an athymic mouse model. *J. Clin. Invest.* **1995**, 96, 2593–2600.

25. Madsen, C.D.; Ferraris, G.M.; Andolfo, A.; *et al.* uPAR-induced cell adhesion and migration: vitronectin provides the key. *J. Cell. Biol.* **2007**, 177, 927–939.

26. Caiolfa, V.R.; Zamai, M.; Malengo, G.; *et al.* Monomer dimer dynamics and distribution of GPI-anchored uPAR are determined by cell surface protein assemblies. *J. Cell. Biol.* **2007**, 179, 1067–1082.

27. Cunningham, O.; Andolfo, A.; Santovito, M.L.; *et al.* Dimerization controls the lipid raft partitioning of uPAR/CD87 and regulates its biological functions. *EMBO. J.* **2003**, 22, 5994–6003.

28. Choi, K.Y.; Swierczewska, M.; Lee, S.; *et al.* Protease-Activated Drug Development. *Theranostics.* **2012**, 2, 156–178.

29. Cao, Y.; Cao, R.; Veitonmäki, N. Kringle structures and antiangiogenesis. *Curr. Med. Chem. Anticancer. Agents*. **2002**, 2, 667-681.

30. Albright, C.F.; Graciani, N.; Han, w.; *et al.* Matrix metalloproteinase-activated doxorubicin prodrugs inhibit HT1080 xenograft growth better than doxorubicin with less toxicity. *Mol. Cancer. Ther.* **2005**, 4, 751-760.

31. Kline, T.; Torgov, M.Y.; Mendelsohn, B.A.; *et al.* Novel antitumor prodrugs designed for activation by matrix metalloproteinases-2 and -9. *Mol. Pharm*. **2004**, 1, 9-22.

32. Kratz, F.; Drevs, J.; Bing, G.; *et al.* Development and in vitro efficacy of novel MMP2 and MMP9 specific doxorubicin albumin conjugates. *Bioorg. Med. Chem. Lett.* **2001**, 11, 2001-2006.

33. Dubowchik, G.M.; Mosure, K.; Knipe, J.O.; *et al.* Cathepsin B-sensitive dipeptide prodrugs. 2. Models of anticancer drugs paclitaxel (Taxol), mitomycin C and doxorubicin. *Bioorg. Med. Chem. Lett*. **1998**, 8, 3347-3352.

34. Warnecke, A.; Fichtner, I.; Sass, G.; *et al.* Synthesis, cleavage profile, and antitumor efficacy of an albumin-binding prodrug of methotrexate that is cleaved by plasmin and cathepsin B. *Arch Pharm (Weinheim).* **2007**, 340, 389-395.

35. Chakravarty, P.K.; Carl, P.L.; Weber, M.J.; *et al.* Plasmin-activated prodrugs for cancer chemotherapy. 2. Synthesis and biological activity of peptidyl derivatives of doxorubicin. *J. Med. Chem*. **1983**, 26, 638-644.

36. de Groot, F.M.; de Bart, A.C.; Verheijen, J.H.; *et al.* Synthesis and biological evaluation of novel prodrugs of anthracyclines for selective activation by the tumor-associated protease plasmin. *J. Med. Chem*. **1999**, 42, 5277-5283.

37. Devy, L.; de Groot, F.M.; Blacher, S.; *et al.* Plasmin-activated doxorubicin prodrugs containing a spacer reduce tumor growth and angiogenesis without systemic toxicity. *Faseb. J.* **2004**, 18, 565-567.

38. Post, G. C.; Barthel, B. L.; Burkhart, D. J.; Hagadorn, J. R.; Koch, T. H. Doxazolidine, a proposed active metabolite of doxorubicin that cross-links DNA. *J Med Chem*. **2005**, 48, 7648-57.

39. Gude, M.; Ryf, J.; White, P. An accurate method for quantitation of Fmoc-derivitized solid phase supports. *Letters in Peptide Science*. **2002**, 9, 203-206.

40. Low, T. L.; Goldstein, A. L. The chemistry and biology of thymosin. II. Amino acid sequence analysis of thymosin alpha1 and polypeptide beta1. *J. Biol. Chem.* **1979**, 254, 987-95.

41. Abiko, T.; Sekino, H. Synthesis of an immunologically active fragment analog of prothymosin alpha with enhanced enzymatic stability. *Chem Pharm Bull (Tokyo).* **1991**, 39, 752-756.

42. Nguyen, L. T.; Chau, J. K.; Perry, N. A.; de Boer, L.; Zaat, S. A.; Vogel, H. J. Serum stabilities of short tryptophan- and arginine-rich antimicrobial peptide analogs. *PLoS One.* **2010**, 5.

43. Huang, Y.; Tan, M.; Gosink, M. Wang, K.W.; Sun, Yi. Histone deacetylase 5 is not a p53 target gene, but its overexpression inhibits tumor cell growth and induces apoptosis. *Cancer Res.* **2002.** 62, 2913-2922.

44. Wilson, A.J.; Byun, D.S.; Nasser, S.; *et al.* HDAC4 Promotes growth of colon cancer cells via repression of p21. *Mol. Bio. Cell*. **2008**, 19, 4062-4075.

45. Gallinari, P.; Di Marco, S.; Jones, P.; Pallaoro, M.; Steinkühler, C. HDACs, histone deacetylation and gene transcription: from molecular biology to cancer therapeutics. *Cell Res*. **2007**, 17, 195-211.

46. Matsuoka, H.; Fujimura, T.; Hayashi, M.; *et al*. Disruption of HDAC4/N-CoR complex by histone deacetylase inhibitors leads to inhibition of IL-2 gene expression. *Biochem. Pharm*. **2007**, 74, 465-476.

47. Avvakumov, N. Cóté. The MYST family of histone acetyltransferases and their intimate links to cancer. *Oncogene*. **2007**, 26, 5395-5407.

48. Lahm, A.; Paolini, C.; Pallaoro, M.; *et al*. Unraveling the hidden catalytic activity of vertebrate classIIa histone deacetylases. *PNAS*. **2007**, 104, 17335-17340.

49. Dekker, G.J.; Haisma, H.J. Histone acetyl transferases as emerging drug targets. *Drug Discov. Today*. **2009**, 14, 942-948.

Chapter 3 Prodrugs Activated by Hypoxic Conditions

3.1 Introduction

3.1.1 The Role of Hypoxia in Cancer

The biology of tumors and their responses to therapy can be influenced by many factors, one of which is hypoxia. The highly abnormal nature of tumor vascularization and limitations to oxygen diffusion can lead to hypoxic conditions. The diffusion range of oxygen is up to ~200 μm and is dependent on the oxygen concentration in blood plasma in the vicinity of the tumor as well as unstable blood flow in tumor microvasculature[1]. Dewhirst *et al*. reviewed the eight dominant features of oxygen deficient transport[1]. Sparse arteriolar supply, inefficient orientation of microvessels, low vascular density, extreme variation in microvessel red blood cell flux (many tumor vessels do not carry red blood cells, but vessels bypassing the tumor, known as shunt vessels do), oxygen gradients caused by the limited arteriolar supply creating low pO_2 in tissue distant from the arteriolar supply, sluggish blood flow due to high blood viscosity of rigid hypoxic red blood cells, large diameter shunts directing blood away from the tumor, and finally the cyclic nature of the hypoxia exhibiting the inherent instability of the tumor environment, are all factors that can affect the oxygen diffusion range. Hypoxia also influences the genomic stability of tumor cells in many ways.

While hypoxic conditions are often associated with resistance to therapy through varying mechanisms, it is important to note that hypoxic conditions have also been observed to result in drug sensitivity.[2] A limited number of these sensitivities or resistances are shown in

Resistance			
Effect of hypoxia	Mode of Action	Therapies affected	Example
Resistance to apoptosis	Downregulation of BID and BAX	Multiple	Etoposide
Cell cycle arrest in G1 and G2	Repair before progression to S and M phase	Cycle selective drugs	5' fluorouracil
Extracellular acidification	Decreased uptake	Basic Drugs	Doxorubicin
Distance from vasculature	Reduced drug exposure	Drugs bound in tumor cells	Taxanes
Sensitivity			
Cell cycle arrest in S phase	Collapse of stalled replication forks	PARP inhibitors	Veliparib (ABT-888)
Supression of DNA repair	Downregulation of NER	Bulky DNA methylating agents	Many
Extracellular acidification	Increased intake	Acidic drugs	Chlorambucil

Table 3.1.1 Examples of hypoxic tumor sensitivity and resistance to therapeutics.

The genetic events triggered by hypoxia are many and varied and include expression of genes that suppress apoptosis[3], anabolic changes in metabolism[4], tumor angiogenisis[5], vasculogenis[6], suppression of immune reactivity, and transition of epithelial to mesenchymal cells.[7] Perhaps the two most important are generation of reactive oxygen species[8] and downregulation of DNA repair pathways.[9]

Hypoxia Inducible Factor 1 (HIF1) is perhaps the most important player, and has been referred to as the "master regulator of oxygen homeostasis"[10] HIF1 is a transcription factor responsible for the expression of many genes implicated in cell survival, migration, homeostasis, angiogenesis, therapeutic resistance and most importantly, anaerobic metabolism.[1] In addition, HIF1 has been shown to be regulated by growth factors,[11] oncogenes and free radicals.[8,12] The enzymatic conversion of superoxide (O_2^-) to hydrogen peroxide (H_2O_2) by superoxide dismutase (SOD) has been shown to produce elevated levels of H_2O_2 which in

turn can regulate the activity of HIF1. Another free radical, Nitric oxide (NO), has been observed at elevated concentrations in many cancers[13,14] due to the overexpression of nitric oxide synthases. The observation that ρ^o cells, chemically stripped of mitochondria cannot increase HIFα levels in response to hypoxia, thereby stabilizing HIF1 by Schumacker and Chandel led to the conclusion that reactive oxygen species formed by the mitochondria under hypoxia are ultimately partially responsible for the overexpression of hypoxia enzymes.[12,15] These enzymes are attractive targets for cancer prodrugs.

3.1.2 Cancer Therapeutics Activated by Hypoxic Conditions

Originally, the observation that some nitroimidazoles sensitized tumors to radiation began the investigation into hypoxia as a hallmark of cancer. Clinical trials of nitroimidazoles concluded that the drugs were ineffective at sufficiently sensitizing the cells due to their toxicity limiting the maximum tolerated dose.[16] These observations prompted the design of many prodrugs to exploit hypoxic conditions, with varying success. For example, β-glucoronide metabolites of an aniline nitrogen mustard in tumors with identified β-glucoronidase activity have been generally ineffective due to unpredictable tumor expression levels of the desired activating enzyme.[17] Other areas of investigation have been the bioreduction of chemical moieties under hypoxic conditions such as nitro groups, quinones, aromatic *N*-oxides, aliphatic *N*-oxides and transition metals.

Our group has been particularly interested in the reduction of nitro aryl groups. A group of two-electron reductases capable of bypassing the oxygen-sensitive free radical intermediate through the transfer of a hydride from NAD(P)H have been shown to reduce quinones, nitro compounds and aromatic *N*-oxides.[2] Two enzymes of particular interest are NAD(P)H

dehydrogenase [quinone] 1 (NQO1); also known as DT diaphorase and NAD(P)H dehydrogenase [quinone] 2 (NQO2). Both of these enzymes have been shown to reduce CB1954 (tretazicar) to its active metabolite[18] (see Figure 3.1.1), with preference for NQO2.[19-21] Although NQO1 is a less effective activator, the similarity to exogenous *E. coli* nitroreductase has prompted investigation into the latter as a useful Gene Directed Enzyme Prodrug Therapy (GDEPT) agent.[22]

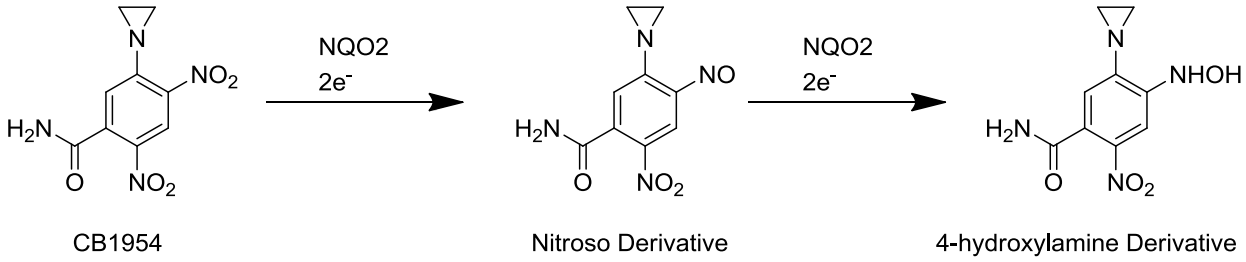

Figure 3.1.1 Proposed activation of CB1954 by NQO2.

NQO2 is of special interest because it is expressed at high levels in several human cancer cell lines.[23] The discovery that CB1954 was a substrate for NQO2 opened the possibility of its use as a conventional prodrug, obviating the need for the DEPT strategies. CB1954 is currently under clinical investigation.[24] NQO2 is also advantageous due to the observation that the exogenous *E. coli* nitroreductase (NTR) used in the DEPT strategies can reduce both nitro groups, therefore rendering half of the therapeutic ineffective, while human NQO2 catalyzes the reduction at the 4 position only.[25,26]

While NQ01 and NQ02 expression has been a driving factor for the advancement of some therapies, another prodrug, PR104, has recently begun phase 1 clinical trials for the breast cancer indication.[27] PR104 is a nitrogen mustard prodrug that sequentially reacts with

phosphatases then reductases in hypoxic tissue to form first, PR-104A and then the active metabolites Pr-104M and PR104H (See Figure 3.1.2). One reductase that has been shown to activate PR-104 is AKR1C3,[28] and the wide expression of this reductase in hepatocellular carcinomas and non-small cell lung cancers has led to the investigation of this prodrug in acute myeloid leukemia (AML).[29]

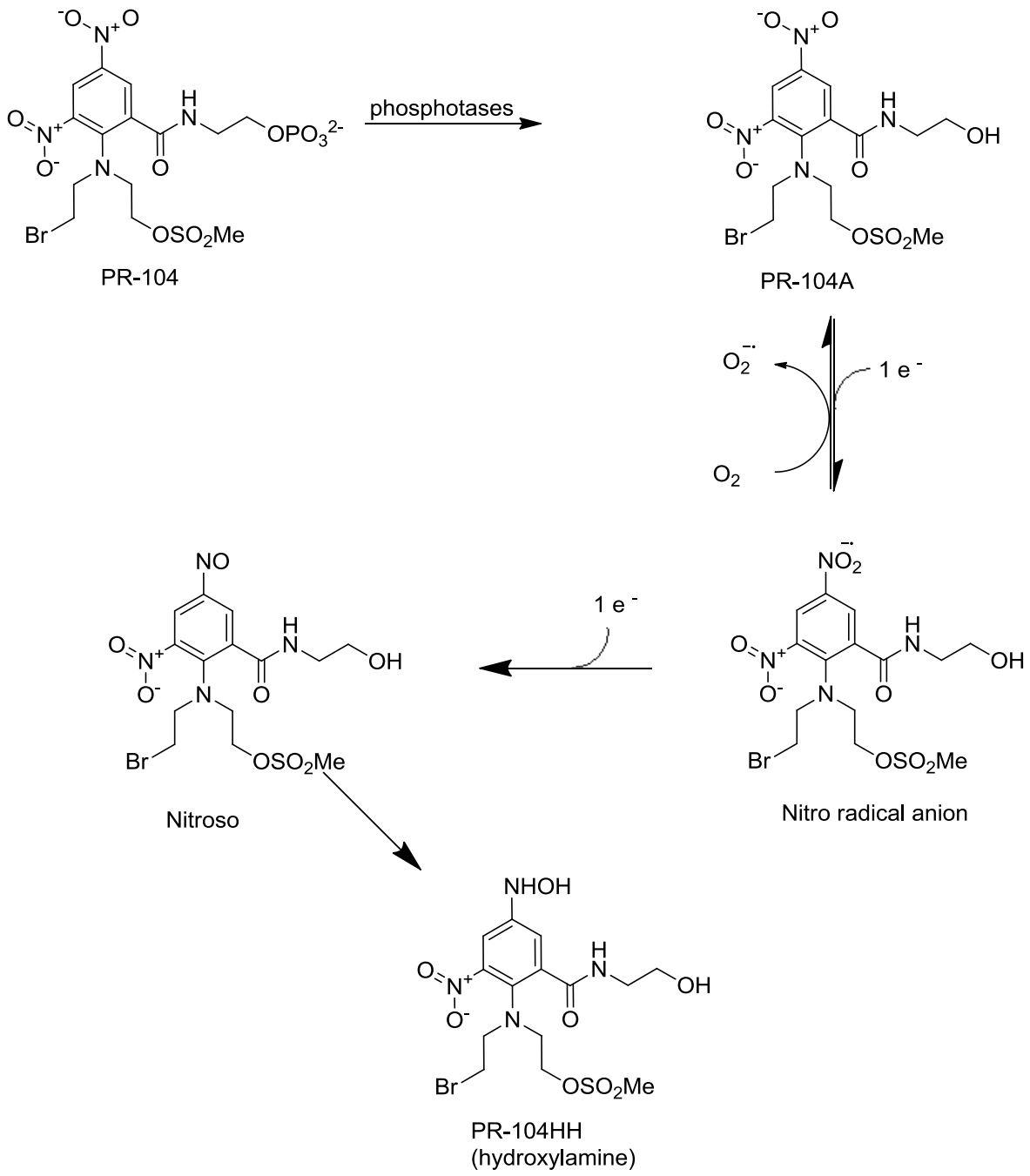

Figure 3.1.2 Proposed activation pathway of PR104H from prodrug PR104[28].

PR-104A can also be activated under hypoxia by other members of the diflavin reductase family, NADPH-dependent diflavin oxidoreductase 1 (NDOR1) and methionine

synthase reductase (MTRR).[30] Other flavoproteins capable of one-electron prodrug activation include NADH-cytochrome *b*5 reductases,[31] ferredoxin reductase (FDXR),[32] xanthine oxidase[33] and xanthine dehydrogenase, which is also capable of two-electron reduction.[34] However, investigation into the relative activity of these and other reductases in hypoxic regions of human tumors is still needed.

Another interesting class of hypoxia activated compounds containing reducible nitro aryl groups are prodrugs containing *p*-nitrobenzyl carbamate triggers. Members of this class of prodrugs have been shown to be activated by xanthine oxidase (XO) and NADH:cytochrome P450 reductase (NPR) under hypoxic conditions, but not in air,[35] demonstrating the utility of this trigger. One such example is β-aminopropionitrile (BAPN), an inhibitor of lysyl oxidase (LOX). LOX overexpression in hypoxic tumour cells has recently been determined and, at the same time, LOX has been proven to play a key role in the promotion of the metastatic process of several solid tumours.[36] The extremely simple BAPN molecule itself cannot be used as a therapeutic due to unselective biological interactions and its role in lathyrism, a neurological disease affecting humans and livestock correlating to the over ingestion of legumes high in BAPN.[37,38] A prodrug of BAPN, pro-BAPN has been designed and shown to go through bioreductive activation, and after 1,6-elimination of the quinone methide and loss of CO_2 produces BAPN under hypoxic tumor conditions *in vitro*[39] (See Figure 3.1.3). Giglia *et al*. used the same *p*-nitrobenzyl trigger to create an interesting imaging agent capable of being activated in hypoxic tissue.[40] This bioreductive pharmacophore can activate the corresponding technetium and rhenium complexes to selectively image hypoxic tumor tissues. These compounds are shown in Figure 3.1.4.

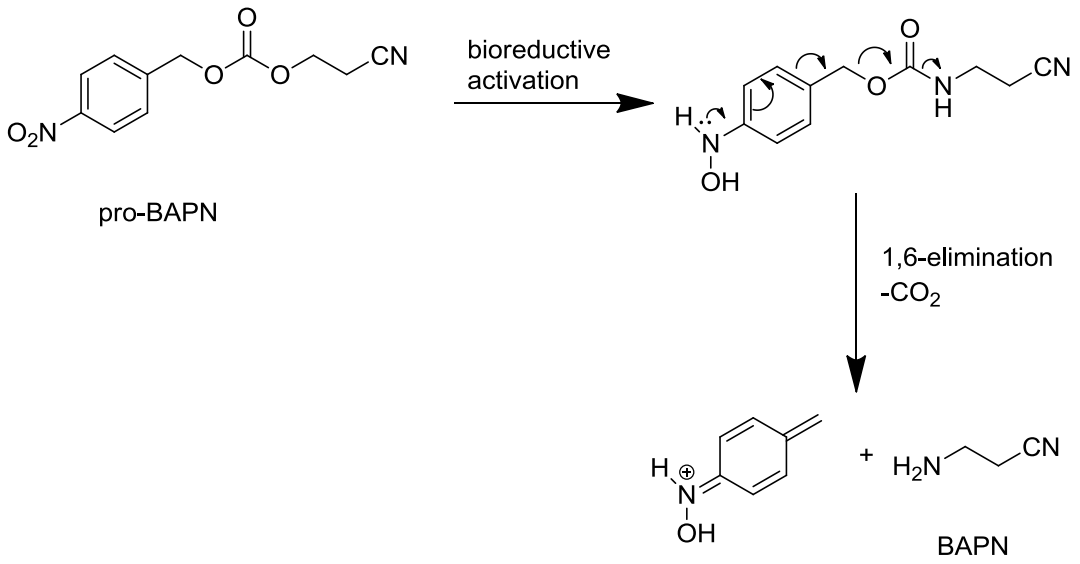

Figure 3.1.3 Reduction and 1,6-elimination of pro-BAPN to release the active BAPN.

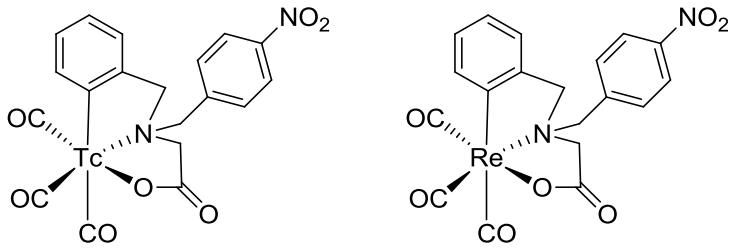

Figure 3.1.4 Imaging agents activated in hypoxic tissues. Reduction of the nitro group allos 1,6-elimination of the quinon methide, activating the imaging agent.

The interest in *p*-nitrobenzyl prodrugs activated by exogenous enzymes, often coupled to antibodies has also been explored. Antibody Directed Enzyme Prodrug Therapy (ADEPT) will not be discussed in detail here, but briefly, an exogenous enzyme is coupled to a cancer specific antibody, and administered to the patient or test animal. Subsequently, a prodrug with a moiety activated by the exogenous enzyme is then administered, and theoretically, the antibody/enzyme conjugate would be localized to the tumor, and the prodrug activated at the tumor site. Mauger *et al*. created just such prodrugs, with *p*-nitrobenzyl triggers, to be activated by *E. Coli* nitroreductase (NTR)[41]. The nitrobenzyl moiety was added to actinomycin D

(AMD), mitomycin C, and doxorubicin, as well as a nitrogen mustard compound, 4-[bis(2-chloroethyl)amino]aniline, and these prodrugs are depicted in Figure 3.1.5. The overall conclusion was that the prodrugs were less cytotoxic than their parent drug to normal tissues and cells, and NTR activated all the prodrugs except the doxorubicin prodrug.

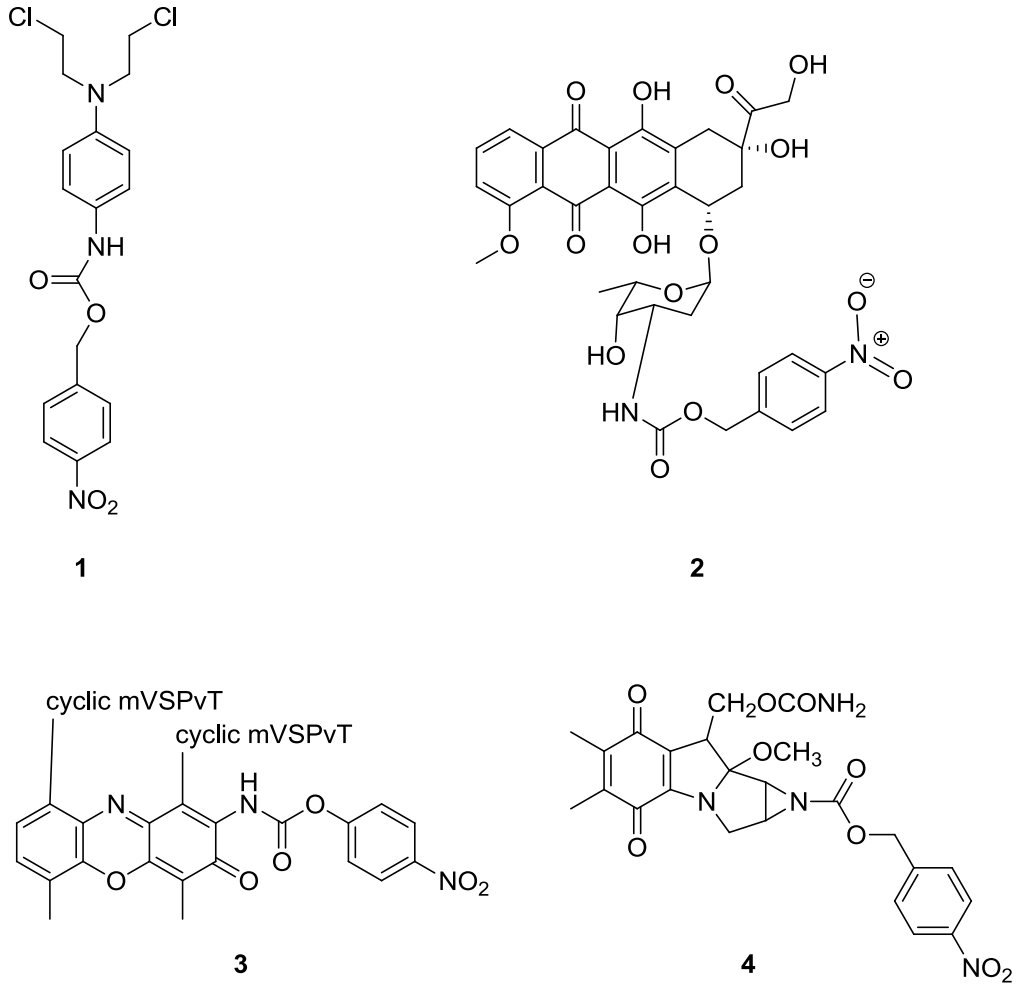

Figure 3.1.5 *p*-Nitrobenzyl prodrugs of: 4-[bis(2-chloroethyl)amino]aniline 1**; doxorubicin** 2**; actinomycin D** 3**; and mytomycin C** 4**.**

Hay *et al*. investigated several molecules with the *p*-nitrobenzyl moiety, but of particular interest was the addition of a self immolative Katzenellenbogen spacer to the doxorubicin prodrug in a study focused on Gene Directed Enzyme Prodrug Therapy (GDEPT).[42] This prodrug

is depicted in Figure 3.1.6. Hay and colleagues observed that this prodrug was not toxic to hamster ovary cells in culture, and *in vivo*, the MTD of the prodrug was 40 times higher than that of doxorubicin alone. The prodrug was also activated in nitroreductase transfected cells in culture, but showed little efficacy, explained by poor tumor penetration, *in vivo*.

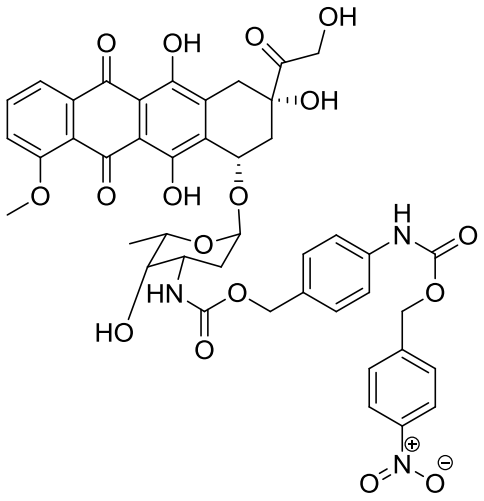

Figure 3.1.6 *p*-Nitrobenzyl doxorubicin containing a self immolative Katzenellenbogen spacer.

3.1.3 Development of a Doxaz Prodrug Activated by Hypoxia

Using nitro-aromatic prodrugs as templates, carbamate prodrugs of Doxaz were designed to be activated by two-electron reducing enzymes overexpressed in tumor associated hypoxic conditions. The design contains a *p*-nitrobenzyl moiety, and, in one case, a self eliminating Katzenellenbogen spacer as described previously. This chapter describes the design, synthesis, and characterization of the *p*-nitrobenzyl carbamate Doxaz prodrugs.

3.2 Experimental Methods

3.2.1 General Remarks

Doxorubicin hydrochloride clinical samples (formulated with lactose) were a gift from FeRx (Aurora, CO). NMR solvents were purchased from Cambridge Isotope Laboratories, Inc.

(Andover, MA). All other chemicals were purchased from Aldrich (Milwalkee, WI). Analytical HPLC was performed on a Hewlet-Packard/Agilent 1050/1100 hybrid instrument equipped with a 1050 autoinjector, a 1100 UV-vis diode array detector, and a 1046A fluorescence detector. Chromatography was performed using an Agilent Zorbax 4.6 mm i.d. x 15 cm, 5 µm reverse-phase octadecylsilane (ODS) column, eluting with a gradient of room temperature acetonitrile/20 mM sodium phosphate buffer, pH 4.6 (buffer ramped down from 80% to 20% over 10 min, held isocratic until 14.5 min, then returned to 80% by 16 min) at 1.0 mL/min. The presence of anthracycline-containing molecules was monitored by absorbance at 280 and 480 nm. NMR spectra were taken using a Varian Unity 500 MHz spectrometer (Palo Alto, CA). Electrospray mass spectra were measured on a Sciex API III+ (Toronto, Canada) or ABI Pulsar QqT high resolution instrument (Foster City, CA) equipped with an ion spray source and run at atmospheric pressure. Preparative radial chromatography was performed using a Chromatotron 7924T (T-Squared Technology, Inc., San Bruno, CA) equipped with a FMI Lab Pump (Fluid Metering, Inc., Oyster Bay, NY).

3.2.2 Synthesis of Doxaz

Doxaz was synthesized as previously described (Section 2.2.2)

3.2.3 Synthesis of PNBDoxaz

p-Nitrobenzyl chloroformate (5.05 mg, 23.3 µmol) was added to a solution of Doxaz (13.0 mg, 23 µmol) in 10.0 mL of DCM followed immediately by pyridine (1.89 µl, 23.3 µmol). The reaction mixture was stirred for 90 min at room temperature. The reaction mixture was washed once with 15.0 mL of brine, and dried over sodium sulfate. Evaporation of the solvent afforded PNBDoxaz (15.74mg, 21.4 µmol) as a pale red solid in 92% yield, and 95% purity as

evidenced by HPLC. ^{1}H NMR assignments made using 1D ^{1}H NMR and homonuclear COSY. ^{1}H NMR (500 MHz, Chloroform-d) δ 1.30 (d, *J* = 6.6 Hz, 3H, 5'-Me), 1.77 (td, *J* = 13.2, 4.2 Hz, 1H, 2'), 1.82 (d, *J* = 8.0 Hz, 1H, 4'-OH), 1.90 (dd, *J* = 13.5, 5.1 Hz, 1H, 2'), 2.18 (dd, *J* = 14.7, 4.1 Hz, 1H, 8), 2.34 (d, *J* = 14.7 Hz, 1H, 8), 2.99 (t, *J* = 5.0 Hz, 1H, 14-OH), 3.04 (d, *J* = 18.8 Hz, 1H, 10), 3.29 (d, *J* = 18.8 Hz, 1H, 10), 3.67 (d, *J* = 7.3 Hz, 1H, 4'), 3.84-3.93 (m, 1H, 3'), 4.09 (s, 3H, 4-OMe), 4.14 (t, *J* = 6.7 Hz, 1H, 5'), 4.49 (s, 1H, 9-OH), 4.75 (dd, *J* = 5.0, 2.3 Hz, 2H, 14), 4.90 (d, *J* = 3.8 Hz, 1H,), 4.95 (d, *J* = 3.8 Hz, 1H, OCH_2N), 5.05 – 5.16 (m, 2H, Bn), 5.17 – 5.26 (m, 1H, NHCO), 5.30 (s, 1H, 7), 5.51 (d, *J* = 4.1 Hz, 1H, 1'), 7.41 (d, *J* = 8.6, Hz, 1H, 3), 7.46 (m, 2H, PNB), 7.80 (dd, *J* = 8.4, 7.7 Hz, 1H, 2), 8.06 (m, 2H, PNB), 8.19 (d, *J* = 8.5 Hz, 2H, 1). Calculated (MH^+) m/z 734.1959. Found 734.1957.

3.2.4 Synthesis of PNBPABAPNP

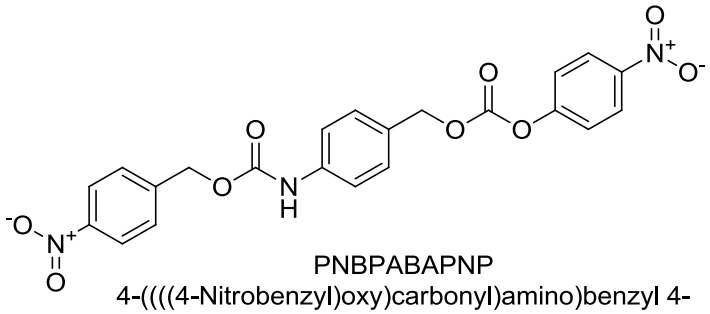

Figure 3.2.4.1 PNBPABAPNP

Under an argon atmosphere, a solution of p-nitrobenzyl chloroformate (200.0 mg, 0.928 mmol) in 20 mL freshly distilled THF was added dropwise over 60 min to a solution of *p*-aminobenzyl alcohol (114.3 mg, 0.928 mmol) and pyridine (149.50 µl, 1.856 mmol) in 20 mL freshly distilled THF. To this reaction mixture, a solution of p-nitrophenyl chloroformate (187.0 mg, 0.928 mmol) in 20 mL freshly distilled THF was added dropwise over 60 min. The reaction

mixture was left to stir for 16 h at room temperature under static argon, whereupon an off white precipitate formed. Vacuum filtration through a medium fritted glass funnel afforded PABAPNBPNP (342.6 mg, 0.733 mmol) in 79% yield and 90% purity as evidenced by HPLC, and was used without further purification. ^{1}H NMR in $(CD_3)_2SO$ was in agreement with published assignments[42].

3.2.5 Synthesis of PNBPABADoxaz.

To a solution of Doxaz (44.6 mg, 80.25 μmol) and HOBT (12.3 mg, 80.25 μmol) in 0.6 mL of anhydrous DMSO, PNBPABAPNP (25.0 mg, 53.48 μmol) and the reaction vessel purged with argon. The reaction mixture was left to react under static argon and monitored by HPLC until the peak corresponding to the PNBPABAPNP disappeared, usually around three days. The reaction mixture was then diluted with 1.0 mL of DMSO, and then added dropwise to 10 mL of PBS buffer, pH 7.4 affording a red precipitate. The precipitate was isolated by vacuum filtration using a medium fritted funnel, and purified by radial chromatography with 30:1 chloroform/methanol eluent. The final product was obtained in 45% yield and 91% purity as evidenced by HPLC. ^{1}H NMR assignments made using 1D ^{1}H NMR and homonuclear COSY. ^{1}H NMR (400 MHz, Chloroform-d) δ 1.29 (d, *J* = 6.6 Hz, 3H, 5'-Me), 1.77 (broad m, 1H, 2'), 2.08 (overlapping d, *J* = 14.7 Hz, 1H, 8; J = 4.2 Hz, 1H, 2'), 2.37 (d, *J* = 14.8 Hz, 1H, 8), 2.97 (d, *J* = 18.8 Hz, 1H, 10), 3.17 (dd, *J* = 19.1, 2.0 Hz, 1H, 10), 3.98 (d, *J* = 7.3 Hz, 1H, 4'), 3.99 (s, 3H, 4-OMe), 4.04 – 4.16 (m, 1H, 3'; 1H, 5'), 4.65 (s, 2H, 14), 4.91 (d, *J* = 3.8 Hz, 1H, OCH_2N), 4.95 (d, *J* = 3.8 Hz, 1H, OCH_2N), 5.17 – 5.19 (m, 2H, Bn), 5.20 – 5.27 (m, 2H, 7), 5.37 (t, *J* = 5.3 Hz, 1H, 1'), 7.22 – 7.27 (m, 1H, PNB), 7.34 (d, *J* = 8.5 Hz, 2H, PABA), 7.64 (tt, *J* = 7.7, 1.8 Hz, 2H, PNB), 7.71 (t, *J* =

8.1 Hz, 1H, 2), 7.91 – 7.98 (m, 2H, PABA), 8.06 – 8.19 (m, 2H, 1), 8.42 – 8.50 (m, 1H, PNB). Calculated (MH^+) m/z 883.2436. Found 883.2431.

3.3 Results and Discussion

3.3.1 Synthesis of Doxaz PNB

Doxaz was synthesized on a 500 mg scale as described previously. The oxazolidine nitrogen in this case was sufficiently reactive to form the carbamate with *p*-nitrobenzyl chloroformate in 92% yield and 95% yield, using pyridine as a catalyst. Compared to other coupling reactions with Doxaz, this coupling was incredibly straightforward as was the workup. As with the compounds previously described, the Doxaz carbamates did not produce adequate NMR spectra at ambient temperature, presumably due to the Doxaz daunosamine sugar flip from chair to twist boat.[43] The synthetic pathway is shown in Scheme 3.3.1

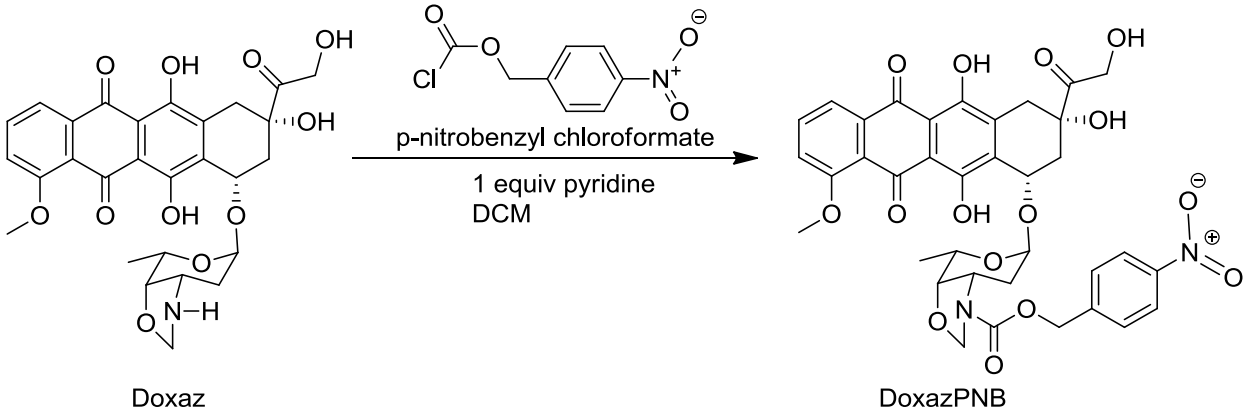

Scheme 3.3.1 Synthesis of Doxaz PNB.

3.3.2 Synthesis of DoxazPABAPNB

3.3.2.1 Synthesis of PNBPABAPNP or 4-nitrobenzyl (4-((((4-nitrophenoxy)carbonyl)oxy)methyl)phenyl)carbamate

Hay *et al*.[42] utilized a *tert*-butyldimethylsilyl ester protected *p*-aminobenzyl alcohol (PABA) and p-nitrobenzyl chlorformate (PNB chloroformate) to produce a carbamate with a protected alcohol that was then deprotected to produce a free benzyl alcohol which was subsequently reacted with *p*-nitrophenyl chloroformate (PNP chloroformate) to yield a mixed carbonate as depicted in Scheme 3.3.2.1.1. Also shown in the scheme are the representative yields for each step, which culminate in a yield of 8% over three steps. Commercialization of the Doxaz technology being in the forefront of our minds in tandem with the knowledge that at our current state of experience with the coupling of Doxaz to a mixed *p*-nitrophenyl carbonate results in large losses in the ultimate or penultimate step of any Doxaz prodrug synthetic pathway, the overall yield of 8% to the final product, 4-nitrobenzyl (4-((((4-nitrophenoxy)carbonyl)oxy)methyl)phenyl)carbamate (PNBPABAPNP) was unacceptable.

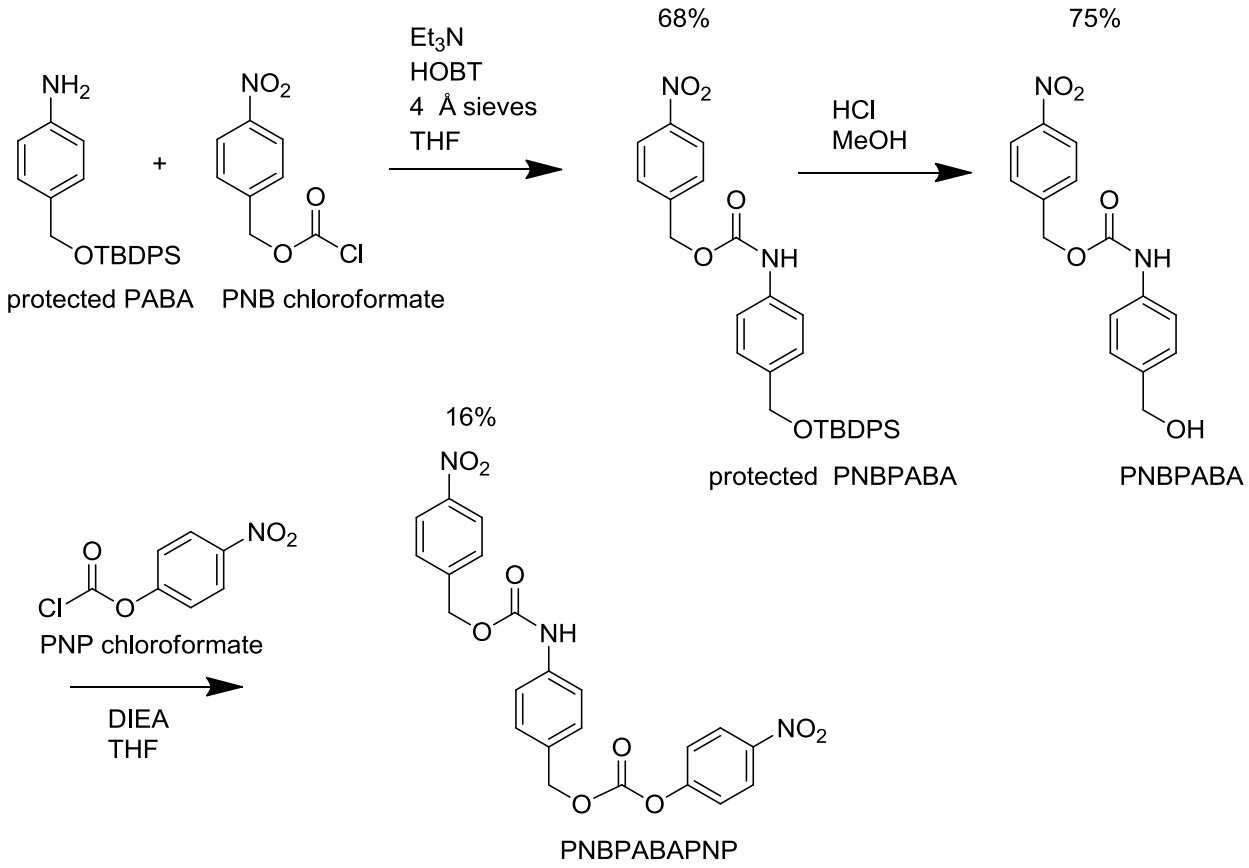

Scheme 3.3.2.1.1 **PNBPABAPNP synthetic scheme.** Hay *et al*. synthetic scheme for preparation of 4-nitrobenzyl (4-((((4-nitrophenoxy)carbonyl)oxy)methyl)phenyl)carbamate.

In an attempt to improve this yield, previous experience with *p*-aminobenzyl alcohol and chloroformates was drawn upon. Firstly, efforts were put forward to eliminate the protection-deprotection steps and the use of triethylamine or diisopropylethyl amine. It had been observed that these bases can react with the chloroformates or mixed carbonates, forming products that were difficult to remove and decreasing the yield of the desired product. An example of this reaction is shown in Scheme 3.3.2.1.2. The hypothesis that controlled addition PABA to *p*-nitrobenzyl chloroformate would create a solution phase scenario in which the PABA was in excess, and the more reactive aniline nitrogen (relative to the benzyl alcohol) would react first, and this was indeed the case. Analysis of the reaction progression by HPLC revealed

that this first step went in less than one hour and incredibly cleanly. Isolation of the product was straightforward, however, again considering large scale production, the exploration of a one-pot synthesis followed. Many iterations were attempted, but the simple slow addition of PNP chloroformate to the reaction mixture in the presence of pyridine afforded the best product yield and purity. The fortuitous precipitation of the hydrophobic product from anhydrous THF afforded an overall yield of 79%, a nearly ten fold improvement over the literature procedure,[42] and a potentially scalable sequence.

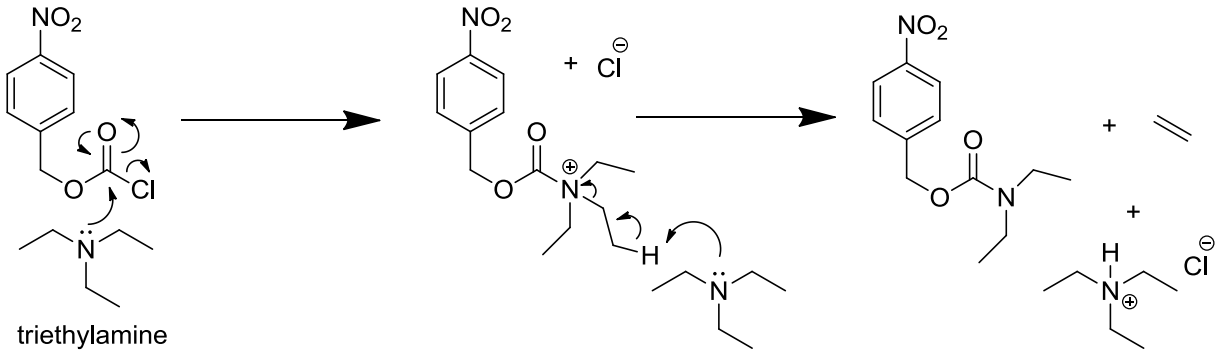

Scheme 3.3.2.1.2 Reaction of base with chloroformate or mixed carbonate. Triethylamine can act as a nucleophile and form unwanted products.

3.3.2.2 Synthesis of DoxazPABAPNB

The coupling of PNP mixed carbonates to Doxaz has historically been problematic. In certain cases, a small excess of the PNP mixed carbonate has proven successful, however, this was not the case with PNBPABAPNP. We hypothesized that the PNBPABAPNP was "pi-stacking" with the doxazolidine, affecting the reactivity. Catalysis with HOBT improved yields from 15% to 26%; however, use of excess Doxaz, previously contrary to our experience, afforded a yield of 46%. The reaction mixture in DMSO was diluted and then added dropwise to a buffer solution, and the highly hydrophobic prodrug precipitated. The excess Doxaz was quickly

hydrolyzed upon workup to Dox, and washed away with the aqueous filtrate. Although the yield in the final step was low, precipitation of the intermediates and the final product were favorable for commercial scale up. The overall synthetic scheme is presented in Scheme 3.3.2.2.1.

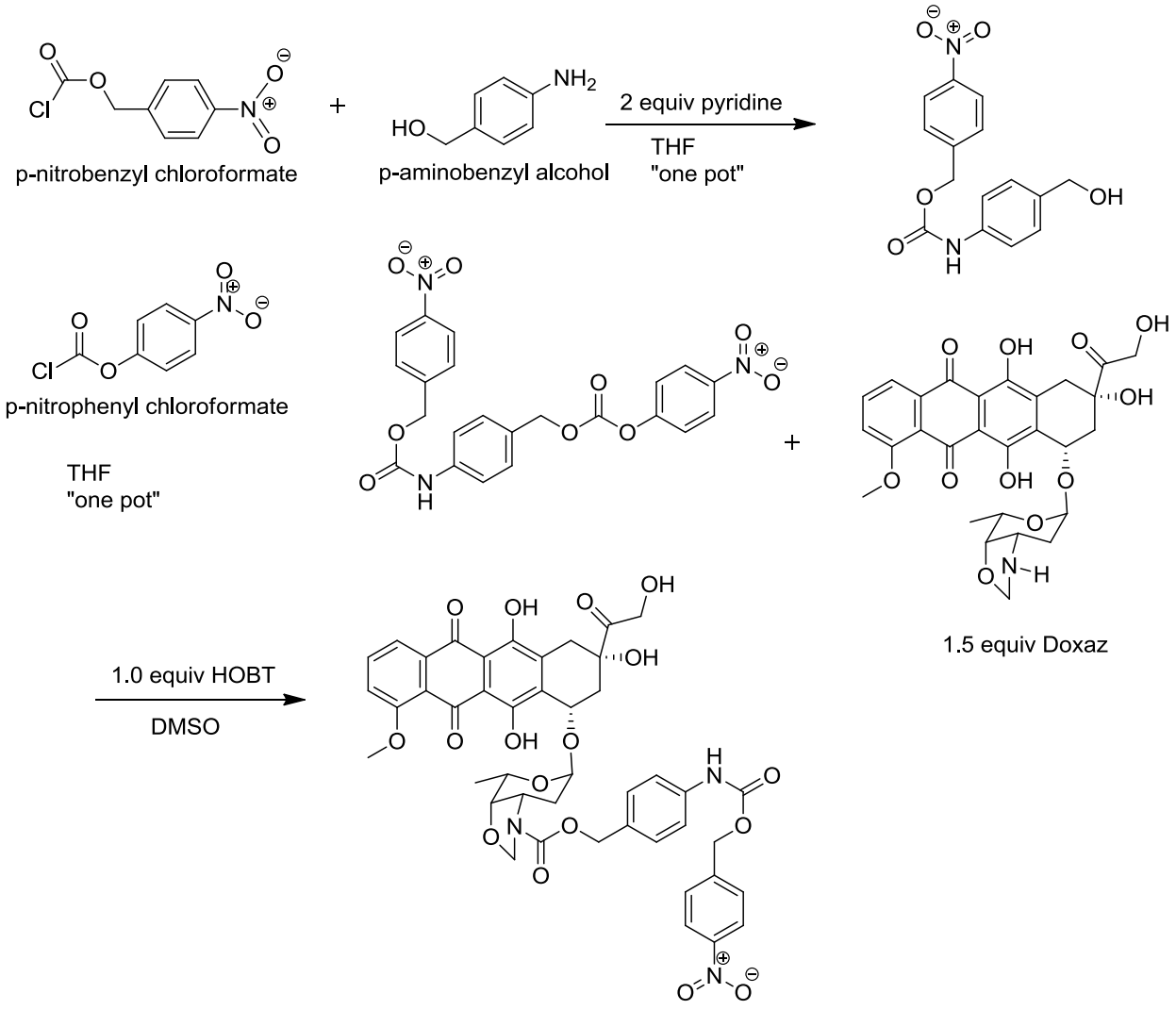

Scheme 3.3.2.2.1 Complete synthetic pathway to DoxazPABAPNB

3.4 Conclusions

The purpose of this project was to demonstrate that simple, scalable prodrugs of Doxaz could be synthesized. In this respect the project was a success. The exploration of alternate reaction pathways is critical to the success of any Doxaz commercialization endeavor. Because specialized cell culture equipment is required for creating and ultimately testing hypoxic tumor cell lines, no *in vitro* analyses were performed. The Koch group is currently seeking collaborative partners to examine DoxazPNB and DoxazPABAPNB. Determining which hypoxic cell lines are sensitive to these prodrugs will be followed by exploration of the potential enzymes responsible for activation.

3.5 References

1. Dewhirst, M. W.; Cao, Y; Moeller, B. Cycling hypoxia and free radicals regulate angiogenesis and radiotherapy response. *Nature. Rev. Cancer.* **2008,** 8, 425–437.

2. Wilson, W.R; Hay, M.P. Targeting hypoxia in cancer therapy. *Nature. Rev. Cancer.* 11, 4, 393-410.

3. Erler, J.T.; Cawthorne, C.J.; Williams, K.J.; *et al.* Hypoxia-mediated down-regulation of Bid and Bax in tumors occurs via hypoxia-inducible factor 1-dependent and -independent mechanisms and contributes to drug resistance. *Mol. Cell. Biol.* **2004**, 24, 2875–2889.

4. Cairns, R. A., Harris, I. S.; Mak, T. W. Regulation of cancer cell metabolism. *Nature Rev. Cancer.* **2011**, 11, 85–95.

5. Wang, Y.; Ohh, M. Oxygen-mediated endocytosis in cancer. *J. Cell. Mol. Med.* **2010**, 14, 496–503.

6. Kioi, M.; Vogel, H.; Schultz, G.; *et al.* Inhibition of vasculogenesis, but not angiogenesis, prevents the recurrence of glioblastoma after irradiation in mice. *J. Clin. Invest.* **2010,** 120, 695–705.

7. Hill, R.P.; Marie-Egyptienne, D.T.; Hedley, D.W. Cancer stem cells, hypoxia and metastasis. *Semin. Radiat. Oncol.* **2009**, 19, 106–111.

8. Guzy, R.D.; Hoyos, B.; Robin, E.; *et al.* Mitochondrial complex III is required for hypoxia-induced ROS production and cellular oxygen sensing. *Cell. Metab.* **2005**, 1, 401–408.

9. Bristow, R.G.; Hill, R.P. Hypoxia, DNA repair and genetic instability. *Nat. Rev. Cancer.* **2008,** 8, 180–192.

10. Semenza, G.L. Targeting HIF-1 for cancer therapy. *Nature Rev. Cancer*. **2003**, 3, 721–732.

11. Li, F.; Sonveaux, P.; Rabbani, Z.N.; *et al.* Regulation of HIF-1α stability through S-nitrosylation. *Mol. Cell.* **2007**, 26, 63–74.

12. Chandel, N.S.; McClintock, D.S.; Feliciano, C.E.; *et al.* Reactive oxygen species generated at mitochondrial complex III stabilize hypoxia-inducible factor-1α during hypoxia: a mechanism of O2 sensing. *J. Biol. Chem.* **2000**, 275, 25130–25138.

13. Tozer, G.M.; Everett, S.A. Nitric oxide in tumor biology and cancer therapy. Part 2: Therapeutic implications. *Clin. Oncol. (R. Coll. Radiol).* **1997**, 9, 357–364.

14. Tozer, G.M.; Everett, S.A. Nitric oxide in tumour biology and cancer therapy. Part 1: Physiological aspects. *Clin. Oncol. (R. Coll. Radiol).* **1997,** 9, 282–293.

15. Bell, E.L.; Klimova, T.A.; Eisenbart, J.: *et al.* The Qo site of the mitochondrial complex III is required for the transduction of hypoxic signaling via reactive oxygen species production. *J. Cell Biol.* **2007**, 177, 1029–1036.

16. Brown, J. M. Clinical trials of radiosensitizers: what should we expect? *Int. J. Radiat. Oncol. Biol. Phys.* **1984,** 10, 425–420.

17. Connors, T.A.; Whisson, M.E. Cure of mice bearing advanced plasma cell tumours with aniline mustard: the relationship between glucuronidase activity and tumour sensitivity. *Nature.* **1966,** 210, 866–867.

18. Knox, R.J.; Boland, M.P.; Friedlos F.; *et al.* The nitroreductase enzyme in Walker cells that activates 5-(aziridin-1-yl)-2,4-dinitro-benzamide (CB 1954) to 5-(aziridin-1-yl)-4-hydroxylamino-2-nitrobenzamide is a form of NAD(P)H dehydrogenase (quinone) (EC 1.6.99.2). *Biochem. Pharmacol.* **1988**, 37, 4671–4677.

19. Long, D.J.; Jaiswal, A.K. NRH: quinone oxidoreductase2 (NQO2) *Chemino-Biol. Interact.* **2000**, *129*, 99-112.

20. Skelly, J.V.; Knox, R.J.; Jenkins, T.C. Aerobic nitroreduction by flavoproteins: enzyme structure, mechanism and role in cancer chemotherapy. *Mini. Rev. Med. Chem.* **2001**, *1*, 293-306.

21. Bianchet, M.A.; Faig, M.; Amzel, L.M. Structure and mechanism of NAD(P)H: quinone accpetor oxidoreductases (NQO). *Methods. Enzymol.* **2004**, *382*, 144-174.

22. Niculescu-Duvaz, I.; Cooper, R.G.; Stribbling, S.M.; *et al.* Recent developments in genedirected enzyme prodrug therapy (GDEPT) for cancer. *Curr. Opin. Mol. Ther.* **1999**, *4*, 480-486.

23. Knox, R.J.; Jenkins, T.C.; Hobbs, S.M.; *et al.* Bioactivation of 5-(Aziridine-1-yl)-2,4-dinitrobenzamide (CB1954) by human NADPH Quinone Oxidoreductase 2: A Novel Cosubstrate-mediated Antitumor Prodrug Therapy. *Cancer. Res.* **2000**, *60*, 4179-4186.

24. Knox, J.R.; Burke, P.J.; Chen, S.; *et al.* CB 1954: from the Walker tumor to NQO2 and VDEPT. *Curr. Pharm. Des.* **2003**, *9*, 2091-2104.

25. AbuKhader, M.; Heap, J.; De Matteis, C.; *et al.* Binding of the anticancer prodrug CB1954 to the activating enzyme NQO2 revealed by the crystal structure of their complex. *J. Med. Chem*. **2005**, 48, 7714-7719.

26. Patterson, A.V.; Ferry, D.M.; Edmunds, S.J.; *et al.* Mechanism of action and preclinical antitumor activity of the novel hypoxia-activated DNA cross-linking agent PR-104. *Clin. Cancer. Res*. **2007**, 13, 3922-3932.

27. McKeage, M.J.; Gu, Y.; Wilson, W.R.; Hill, A.; Amies, K.; Melink, T.J.; Jameson, M.B. McKeage et al. *BMC Cancer* **2011**, 11, 432-446.

28. Guise, C.P.; Abbattista, M.R.; Singleton, R.S.; *et al.* The bioreductive prodrug PR-104A is activated under aerobic conditions by human aldo-keto reductase 1C3. *Cancer. Res.* **2010,** 70, 1573–1584.

29. Birtwistle, J.; Hayden, R.E.; Khanim, F.L.; *et al.* The aldo-keto reductase AKR1C3 contributes to 7,12-dimethylbenz(a) anthracene-3,4-dihydrodiol mediated oxidative DNA damage in myeloid cells: implications for leukemogenesis. *Mutat. Res.* **2009**, 662, 67–74.

30. Guise, C.P. *et al.* Identification of human oxidoreductases involved in the hypoxia-dependent activation of bioreductive prodrugs. *Proc. Am. Assoc. Cancer. Res.* **2010**, 51, Abstract 453.

31. Hodnick, W.F.; Sartorelli, A. C. Reductive activation of mitomycin C by NADH:cytochrome *b*5 reductase. *Cancer. Res.* **1993**, 53, 4907–4912.

32. Miskiniene, V.; Dickancaite, E.; Nemeikaite, A.; *et al.* Nitroaromatic betulin derivatives as redox cycling agents. *Biochem. Mol. Biol. Int.* **1997**, 42, 391–397.

33. Yan, C.; Kepa, J.K.; Siegel, D.; *et al.* Dissecting the role of multiple reductases in bioactivation and cytotoxicity of the antitumor agent 2, 5-diaziridinyl-3-(hydroxymethyl)-6-methyl-1,4-benzo quinone (RH1). *Mol. Pharmacol.* **2008**, 74, 1657–1665.

34. Kutcher, W.W.; McCalla, D.R. Aerobic reduction of 5-nitro-2-furaldehyde semicarbazone by rat liver xanthine dehydrogenase. *Biochem. Pharmacol.* **1984**, 33, 799–805.

35. Seow, H.A.; Penketh, P.G.; Shyam, K.; *et al.* A.C. 1,2-Bis(methylsulfonyl)-1-(2-chloroethyl)-2-[[1-(4-nitrophenyl)ethoxy]carbonyl]hydrazine: an anticancer agent targeting hypoxic cells. *Proc. Natl. Acad. Sci*. *USA*. **2005**, 102, 9282-9287.

36. Erler, J.T.; Giaccia, A.J. Lysyl oxidase mediates hypoxic control of metastasis. *Cancer Res*. **2006**, 66, 10238–10241.

37. Dawson, D.A.; Rinaldi, A.C.; Pöch, G. Biochemical and toxicological evaluation of agent-cofactor reactivity as a mechanism of action for osteolathyrism. *Toxicology*. **2002**, 177, 267–284.

38. Bachhuber, T.E.; Lalich, J.J.; Angevine, D.M.; Schilling, E.D.; Strong, F.M. Lathyrus factor activity of beta-aminopropionitrile and related compounds. *Proc. Soc. Exp. Biol. Med*. **1955**, 89, 294–297.

39. Granchi, C.; Funaioli, T.; Erler, J.T.; *et al.* Bioreductively activated lysyl oxidase inhibitors against hypoxic tumours. *Chem. Med. Chem*. **2009**, 4, 1590–1594.

40. Giglio, J.; Patsis, G.; Pirmettis, I.; *et al.* Preparation and characterization of technetium and rhenium tricarbonyl complexes bearing the 4-nitrobenzyl moiety as potential bioreductive diagnostic radiopharmaceuticals. In vitro and in vivo studies. *Eur. J. Med. Chem.* **2008**, 43, 741-748.

41. Mauger, A.B.; Burke, P.J, Somani, H.H.; *et al*. Self-Immolative prodrugs: Candidates for Antibody-Directed Enzyme Prodrug Therapy in Conjunction with a Nitroreductase Enzyme. *J. Med. Chem.* **1994**, 37, 3452-3458.

42. Hay, M.P.; Wilson, W.R.; Denny, W.A. Nitroarylmethylcarbamate prodrugs of doxorubicin for use with nitroreductase gene-directed enzyme prodrug therapy. *Bioorg. Med. Chem*. **2005**, 13, 4043–4055.

43. Post, G.P.; Barthel, B.L.; Koch, T.H.; *et al.* Doxazolidine, a proposed active metabolite of Doxorubicin that cross-links DNA. *J. Med. Chem*. **2005**, 48, 7648-7657.

Chapter 4 Prodrug Albumin Conjugates

4.1 Introduction

The previously described prodrug technologies employ active targeting strategies, exploiting the overexpression of endogenous enzymes in certain cancer types to activate prodrugs. Passive targeting of cancer by exploitation of the enhanced permeability and retention effect (EPR) has gained some attention, and therapeutics aimed at diabetes, hepatitis C, rheumatoid arthritis and cancer using albumin as a drug carrier are currently in clinical trials, and two agents for treating diabetes and one agent for treating solid tumors have gained market approval from the Food and Drug Administration (FDA).[1]

The study of the most abundant protein in blood, albumin, has been extensive, yet albumin has not been exploited for use in drug delivery until recently. An article by Dr. Felix Kratz of the Tumor Biology Center, Division of Macromolecular Prodrugs in Freiburg, Germany in 2008 prompted many researchers to begin exploring the possibility of albumin as a candidate for drug delivery.[2] Interestingly, the utility of albumin had been overlooked by Kratz himself during his early work in 1989.[3] While investigating transferrin-mediated drug delivery, Kratz tested the efficacy of an acid-sensitive doxorubicin-transferrin conjugate in the MDA-MB-435 melanoma model.[4] The negative control chosen was a doxorubicin-albumin conjugate. There was no observed difference in efficacy between the two drug conjugates in a panel of tumor cell lines, nor in a breast cancer model *in vivo*.[4] Under the assumption that albumin had no beneficial delivery effect, it was concluded that the amount of transferrin receptors on the target cells was insufficient to create a therapeutic advantage for a common anticancer agent such as doxorubicin. Professor Maeda's work on the enhanced permeability and retention

effect (EPR), aimed at demonstrating the accumulation of an experimental antibody has shown clearly that albumin (and the test article) accumulates in the tumor area.[5,6] The work by Kratz, coupled with the subsequent research by Maeda *et al*. makes it apparent that albumin is as effective as transferrin at delivering drug to the target site.

Albumin is the most abundant protein in the body, with approximately 500 grams being distributed between the blood, lymphatic system, extracellular and intracellular compartments. In fact, albumin itself is a very profitable drug with annual sales upwards of $1.3 B worldwide in 2010.[1] Of the 4% of whole blood that is protein, albumin comprises 55%, and is primarily used as a blood substitute for malnourished or cachexic cancer patients. As a therapeutic, albumin has been used to carry drugs or peptide and antibody based prodrugs as covalent conjugates/complexes or in nanoparticles.

To illustrate the utility of albumin as a drug delivery vehicle, an inspection of prevalent diseases shows that there were 285 million cases of types 1 and 2 diabetes, which shockingly is 6.5% of the world population. As a comparison, cancer accounts for approximately 12 million cases per year. An insulin detemir, Levemir® is an albumin binding porcine insulin drug. A lysine at the B9 position of porcine insulin is modified with a fatty acid that is capable of binding albumin.[7] Insulin detemir in circulation is 98% albumin-bound, however the complex slowly dissociates, allowing long lasting administration of insulin.[8] Only the free insulin is available to interact with the insulin receptor and the insulin bound to albumin offers a distinct advantage to other administrations such as glargine (Sanofi-Aventis) and NPH insulin (Novo Nordisk) that commonly form crystalline deposits.[9] Scientists at Novo Nordisk attached a glucagon-like 1

peptide (GLP-1) to albumin to treat diabetes and market the product under the tradename Victoza®. The biologically active forms of GLP-1 are formed in the pancreas, and stimulate insulin secretion;[10] however, naturally formed GLP-1 has a very short half-life of 1.5-2 min due to degradation by ubiquitous enzymes. When bound to albumin, the half-life of GLP-1 is extended to 11-15 min, allowing one daily administration.

Treatment of another prevalent disease, hepatitis C, which affects 180 million people worldwide,[11] has also benefited from albumin delivery. Interferon-α-2B (INFα-2b) weighing approximately 19 kDa has effective antiviral qualities, yet a short half-life in humans of 2-3 hours. The short half-life requires that daily injections be administered. The currently marketed drug, Pegasys® is a pegylated version of INFα-2b and has a molecular weight of 40 kDa. Pegasys® is the current standard of care.[11] Albinterferon-α-2b is an albumin bound version of INFα-2b and has entered phase III clinical trials in direct comparison to Pegasys®. It was found that Albinterferon-α-2b could be administered subcutaneously once every four weeks and invokes a comparable response to Pegasys®.[11-13] Albumin binding drugs, fusion compounds such as antibodies, imaging agents and nitric oxide carriers amongst others are currently in many phases of development, and have recently been reviewed.[1]

Abraxane® is the first approved use of a nanoparticle albumin bound (nab) technology, exploiting the association of paclitaxel with albumin, to treat solid tumors. The nab technology increases solubility of lipophilic drugs by forming colloidal suspensions of albumin and, in Abraxane®, paclitaxel under high pressure.[14] The hydrophobic portions of albumin associate with drug, while the negative regions of albumin form the hydrophilic outer surface of the

nanoparticle. Particles on average of 130 nm are formed, but quickly dissolve into smaller complexes of around 10 nm upon injection. These smaller particles are small enough to avoid the blockage of capillaries.[15] Abraxane® has an advantage over the commercially available paclitaxel which is formulated with polyoxyethylated castor oil (Cremophor EL®), with an ethanol vehicle and a competitor compound, Docetaxel, which is formulated in polysorbate 80 (Tween 80®) with an ethanol diluent. Both drugs are further diluted with normal saline or 5% dextrose solution for administration.[16,17] Cremophor EL can cause acute hypersensitivity reaction,[18] severe, life-threatening reactions with dyspnea and hypotension in 1.5-3% of patients,[19] neutropenia[20] and peripheral neuropathy.[21] Although Abraxane® has shown improved administration dynamics relative to approved drugs, the significant treatment limiting toxicities such as fatigue, myalgia, myelosuppression, fluid retention neuropathy and hypersensitivity[22] have not produced an improved therapeutic index. Administering higher drug doses in breast cancer patients has produced increased toxicity without clinically meaningful benefits.[23] Other tumor indications including non-small cell lung carcinoma (NSCLS), pancreatic cancer, melanoma, and head and neck cancer, some in combination with approved therapies, is ongoing.[24-26]

An interesting development from the preclinical and clinical studies surrounding Abraxane® is the insight gained into the mode of albumin-bound drug delivery. As indicated before, upon injection, Abraxane® forms albumin-bound paclitaxel complexes comparable to the size of free albumin. The albumin-bound paclitaxel complexes accumulate in the tumor through the enhanced permeability and retention (EPR) effect. Tumor uptake can be further explained by an albumin transport pathway mediated by glycoprotein gp60, a 60 kDa protein

also known as albondin. Albondin is located on the surface of endothelial cells and has been shown to play a role in the tumor uptake of Abraxane® and release of paclitaxel.[26.27] Aldonin also assists in the even distribution of the prodrug throughout the tumor.[28] Circulating albumin and Abraxane® can bind gp60 in the nanomolar range[26] which induces gp60 clustering and transcytosis, transporting gp60 bound albumin or gp60 bound albumin-paclitaxel conjugates in caveolae. The formation of caveolae encapsulates vessel fluid, and additional Abraxane® and albumin. The caveolae transport the particles through the endothelium and releases paclitaxel in the subendothelial space.[26] The albumin-paclitaxel conjugate then binds with SPARC (Secreted Protein, Acidic and Rich in Cysteine), a 43 kDa matricellular glycoprotein with significant homology to gp60.[29] SPARC plays an important role in modulating cell migration and extracellular matrix proliferation, and SPARC overexpression correlates to tumor invasion and metastasis.[25,30] SPARC expression correlated to improved Abraxane® response when compared to Taxol®/Cromphore EL, and is therefore thought to play an important role in the efficacy of Abraxane®.[26]

The ease with which a drug can be attached and selectively cleaved from albumin is of great interest for albumin-bound therapeutics. Kratz demonstrated that the thiol in the exposed cysteine-34 of albumin quickly reacts with maleimide of a doxorubicin derivative DOXOEMCH to form a (6-maleimidocaproyl)hydrazone albumin-doxorubicin conjugate.[31] The structure of DOXOEMCH is presented in Figure 4.1.1. Intravenous administration of DOXOEMCH is followed by in situ coupling to circulating albumin. The (6-maleimidecaproyl)hydrazone is sensitive to the acidic microenvironment of the tumor and releases the chemotherapeutic in close proximity of the tumor. DOXOEMCH showed high

plasma stability in its album-bound form, and was put forward as a clinical candidate. Renamed INNO-206, the albumin-binding doxorubicin prodrug exhibited a favorable toxicity profile and reduced cardiotoxicity.[32,33] INNO-206 completed a phase 1 study enrolling patients with breast, small cell lung cancer and sarcoma in which the acid sensitive chemotherapeutic exhibited a good safety profile.[34] The Phase Ib study focused on sarcoma, and a Phase II study for gastric cancer is ongoing. Interestingly, the localization of INNO-206 through the EPR effect and the diffusion-mediated delivery of clinically available doxorubicin prompted Kratz to perform a combined therapy evaluation in an ovarian A2780 xenograft model.[35] The combined therapy reacted synergistically, and complete remissions in the xenograft model were observed.

Concurrently, studies combining DOXOEMCH and polyglycerol dendrimers with free thiols or amines afforded conjugates with varying particle size and Dox loading. The resulting particles were water soluble and of optimal size for EPR passive targeting. Also, the hydrazone linkage was effectively cleaved in acidic conditions. In ovarian cancer xenograft models, the dendritic conjugates exhibited less body weight change when compared to dox, suggesting better tolerability. Statistically significant antitumor effects compared to both vehicle control and doxorubicin were observed and remissions lasting 30 days were seen in mice receiving the dendritic conjugates.[36]

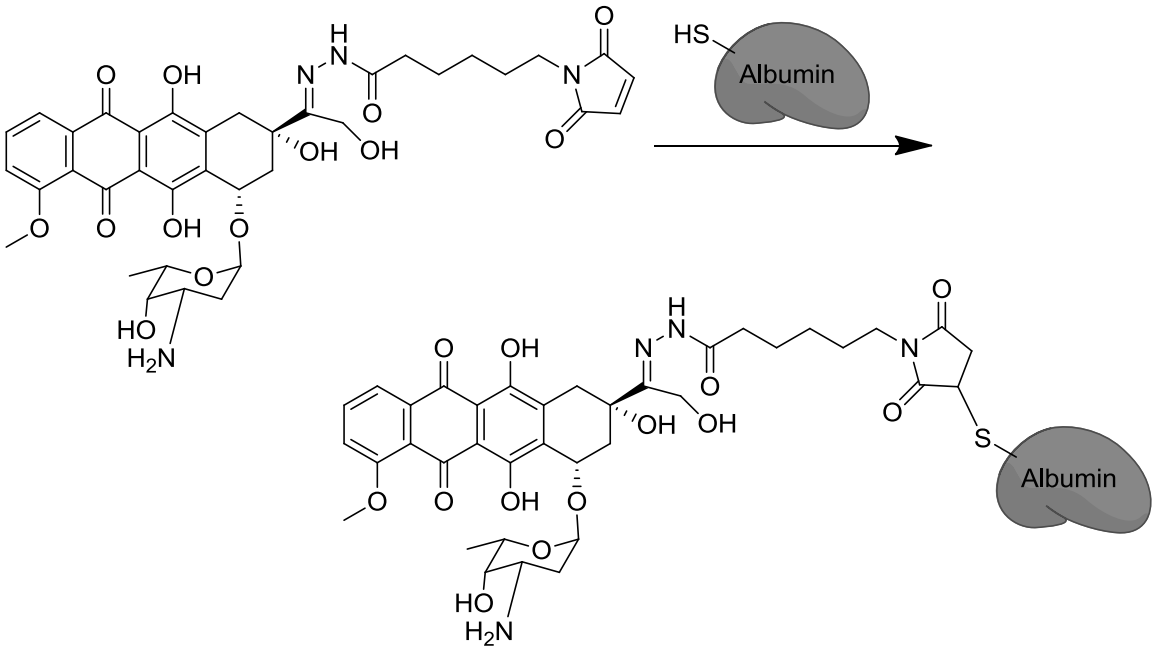

Figure 4.1.1 DOXOEMCH The albumin-binding acid sensitive doxorubicin conjugate known as DOXOEMCH

While multiple methods of passive targeting using several drugs aimed at differing diseases are at varying stages of preclinical and clinical development, researchers have also explored the use of combination targeting. Albumin binding prodrugs with active targeting moieties appear in the literature, with varying results. While these prodrugs with "double filters" have not progressed as far, they are of incredible interest. Most noticeably are prodrugs of doxorubicin that incorporate both passive targeting with albumin binding maleimides and active targeting with enzymatically cleaved triggers.

One example of a doxorubicin prodrug with both active and passive targeting is an albumin-binding prodrug containing a peptide sequence selectively cleaved by gelatinase A, a matrix metalloproteinase (MMP) that plays a critical role in the degradation of membranes and the extracellular matrix.[37-39] Gelatinase A specifically known as MMP-2, has been shown to play

a critical role in tumor progression, angiogenesis and metastasis.[40] Melanoma patients have historically responded marginally to chemotherapy due to non-selective therapeutic agents[41] and the correlation between overexpression of MMP-2 in melanoma and tumor progression has been demonstrated in preclinical and clinical investigations.[42-44] A prodrug of doxorubicin containing the MMP-2 substrate peptide sequence Gly-Pro-Leu-Gly-Ile-Ala-Gly-Gln and an albumin binding moiety was synthesized.[45] A maleimidotriethylenglycol group functioned as the albumin binding moiety, and the incorporation of the triethyleneglycol increased the water solubility of the molecule overall.[45] A schematic representation of the prodrug is provided in Figure 4.1.2. The prodrug was tested against A375 melanoma expressing high amounts of MMP-2 and showed superior efficacy to doxorubicin both *in vitro* and *in vivo*. Nude mice in a A375 melanoma model showed a maximum tolerability dose (MTD) for the prodrug four times higher than that for free doxorubicin.[45] The optimal dose of doxorubicin in *in vivo* experiments was found to be 2 doses of 13.3 µmol/kg each and produced a moderate inhibition in tumor growth that was comparable with the therapeutic results of the prodrug with 2 doses of 13.3 µmol/kg each. Due to the tolerability of the prodrug, administration of three doses at 39.9µmol/kg produced a good antitumor effect with mice showing remissions of up to 40 days in length.[45]

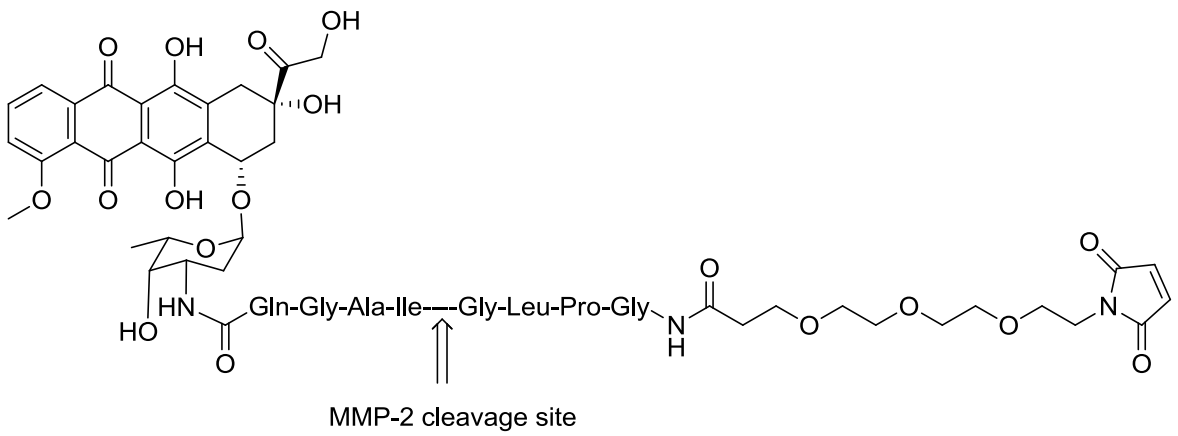

Figure 4.1.2 Albumin-binding prodrug of doxorubicin with a MMP-2 cleavage site.

As discussed above, and in Chapter 2, targeting enzymes (especially proteases) involved in tissue remodeling are attractive when producing prodrugs. A very interesting prodrug aimed at extracellular and intracellular proteases while utilizing the passive targeting of an albumin-binding moiety is EMC-Phe-Lys-PABC-Doxorubicn (EMCFKDox) first reported by Kratz *et al*. in 2009.[46] As mentioned previously, the cysteine protease cathepsin B is principally located in the endosomal/lysosomal compatment[47], but there is evidence that cathepsin B expression correlates with angiogenesis and promotes the remodeling of the extracellular matrix to permit neovascularization.[48,49] Analogous to the MMP-2 prodrug described above, EMCFKDox incorporates a maleimide moiety for passive targeting through albumin-binding and a short peptide sequence recognizable by cathepsin B (Phe-Lys). EMCFKDox also contains the 1,6-self-immolative spacer utilized in prodrugs described in Chapters 2 and 3, and is shown in Figure 4.1.3. This prodrug exhibited effective binding to, and cleavage from albumin in tumor homogenates at pH 5.0.[46] Interestingly, EMCFKDox was approximately 6 times less toxic to human tumor cell lines MDA-MB-231 LN (breast carcinoma and AsPCI LN (pancreatic carcinoma) than doxorubicin, but was significantly more active *in vivo* compared to doxorubicin

in an equitoxic comparison. Comparison of dox at its optimal conditions of 2 doses at 8 mg/kg and the prodrug at three doses of 24 mg/kg, in a nude mouse model (MDA-MB 435) showed clear antitumor response for the prodrug, and tumor progression in the dox treated mice. In fact, the tumors in dox treated mice increased by a factor of approximately 11, whereas the prodrug treatment resulted in an increase by a factor of three.[46]

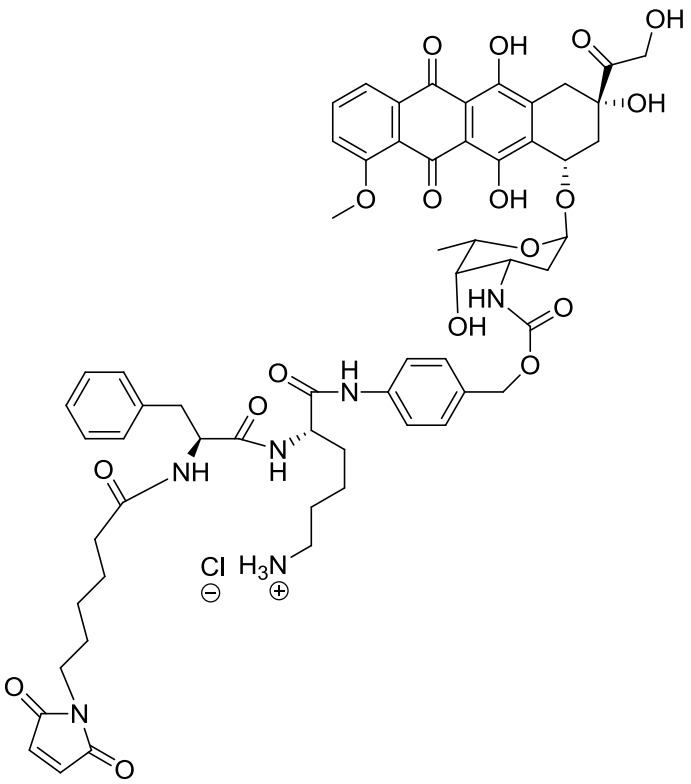

Figure 4.1.3 Albumin-binding doxorubicin prodrug with a cathepsin B peptide trigger.

Previously, the Koch group synthesized targeted prodrugs of the highly active doxorubicin derived chemotherapeutic, Doxazolidine (Doxaz).[50-54] Doxaz has been shown to be a 100-10,000 times more active chemotherapeutic than Dox. A targeted prodrug of Doxazolidine known as pentyl-PABC-Doxaz (PPDoxaz) aimed at carboxylesterases CES1 and CES2 has previously been evaluated.[50-52] PPDoxaz exploits the overexpression of CES2, as do marketed therapeutics Irinotecan and capecitabine (Xeloda). Irinotecan and capecitabine both

contain alkyl carbamates, and are transformed to their respective active metabolites SN-38 and 5-flurouracil (5-FU) by CES1 and/or CES2 as shown in Figure 4.1.4. PPDoxaz is similar to capecitabine. Capecitabine was first approved in 1998 as treatment for metastatic colorectal cancer, and has since been approved for other indications and combination therapies.[55-57] The search for prodrugs of doxazolidine with commercial potential has been challenged by manufacturing and synthetic difficulties. The successful synthesis of a scalable prodrug with both active and passive (albumin mediated) targeting has been recently accomplished in the Koch lab, and due to intellectual property concerns, will not be discussed. However, *in vitro* and *in vivo* testing has shown promise. The second generation molecule, protected under previous patents, is herein described.

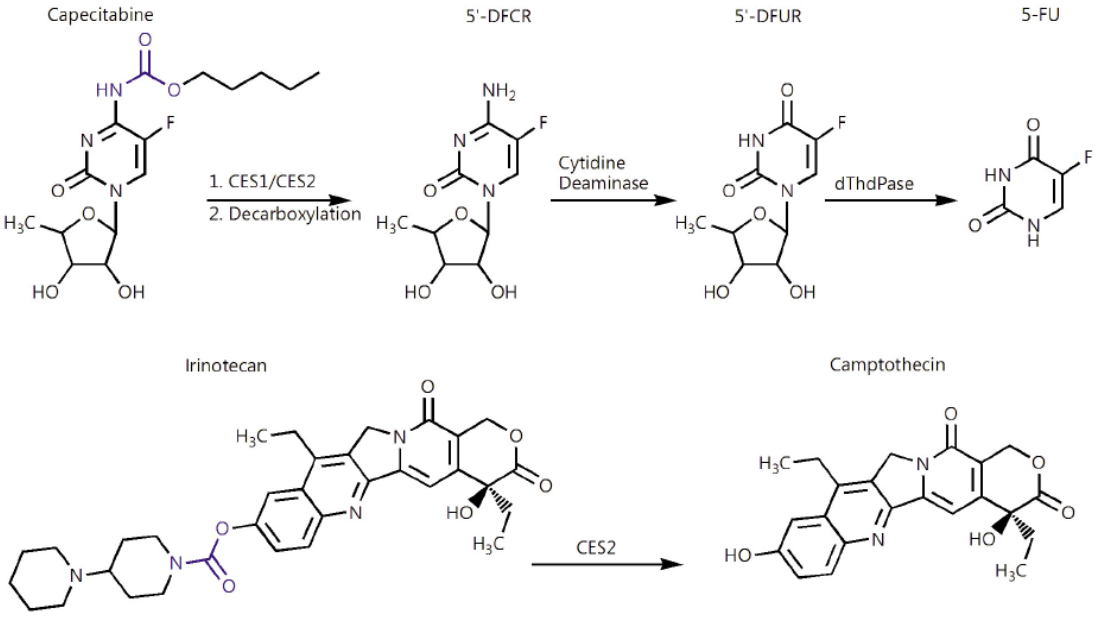

Figure 4.1.4 Alkyl carbamte drugs Capecitabine and Irinotecan and their enzymatic activation.

Analogously, the synthesis of a doxazolidine prodrug (EMCFKDoxaz) containing both active and passive (albumin mediated) targeting utilizing a protease trigger (activated by cathepsin B) is also described. EMCFKDoxaz was hypothesized to be a scalable drug with straightforward manufacturing. Contrary to original thought, the synthesis presented significant challenges, but allowed for exploration of varying synthetic schemes. The structure of the proposed prodrug EMCFKDoxaz is shown in Figure 4.1.5.

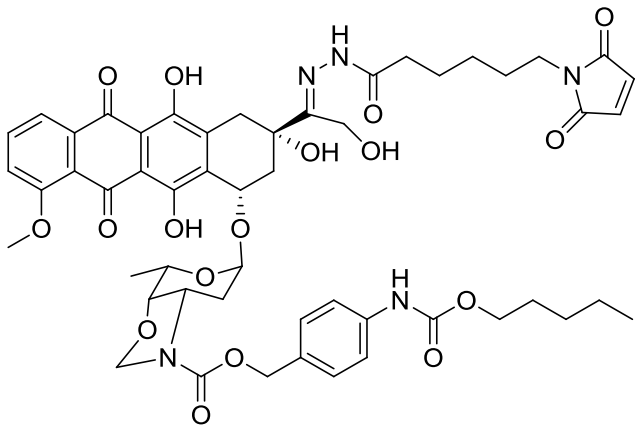

Figure 4.1.5 Structures of albumin-binding, enzymatically activated prodrugs of doxaz.

4.2 Experimental Methods

4.2.1 General Remarks

Clinical samples of doxorubicin hydrochloride formulated with lactose were gifted by FeRx (Aurora, CO). Unless otherwise noted, all reagents and amino acids for solid-phase peptide synthesis were purchased from Nova Biosciences (La Jolla, CA) and other chemicals and reagents were acquired from Aldrich (Milwaukee, WI). Analytical HPLC was performed on Agilent 1050/1100 hybrid instruments equipped with a 1050 series autoinjector, an 1100 series UV/visible diode-array detector, and a 1046A fluorescence detector. An Agilent Zorbax octadecylsilyl (C18) reverse phase column (4.6 mm i.d. x 150 mm, 5 µm) was used for

chromatography. Unless specifically indicated, elution was performed at 1 mL/min and room temperature with gradients of acetonitrile and 20 mM sodium phosphate buffer, pH 4.6, containing 0.02% sodium azide. Method 1 had acetonitrile percentages of: 20% from 0 to 1.5 min, 30% at 5 min, 80% from 15 to 20 min, 20% at 24 min. Method 2 consisted of acetonitrile percentages: 20% to 40% from 0 – 5 min, 50% from 8 – 9 min, and 20% at 11 min. The presence of anthracycline-containing molecules was monitored by absorbance at 480 nm and retention times are noted individually. All NMR spectra were taken at 400 or 500 MHz on a Varian Unity INOVA spectrometer (Palo Alto, CA) or a Bruker-Avance III 300 MHz spectrometer (Billerica, MA) in deuterated solvents from Cambridge Isotope Laboratories, Inc (Andover, MA). Chemical shifts are reported in δ values of ppm and were standardized by the residual solvent peak in MestReNova NMR software (Mestrelab Research, Santiago de Compostela, Spain). UV-vis spectroscopy was performed on a Hewlett-Packard /Agilent 8452A diode array instrument. Electrospray mass spectra were obtained with a Perkin-Elmer Sciex API III^+ (Waltham, MA) or ABI Pulsar QqT high resolution instrument (Foster City, CA), equipped with an ion-spray source at atmospheric pressure. Purification by radial chromatography purification was done with a Harrison Research Model 7924T Chromatotron (Palo Alto, CA). Photo deprotection was performed using a Rayonet Reactor (Southern New England Ultraviolet Co.). Shown below is the reference system for ^1H NMR assignments.

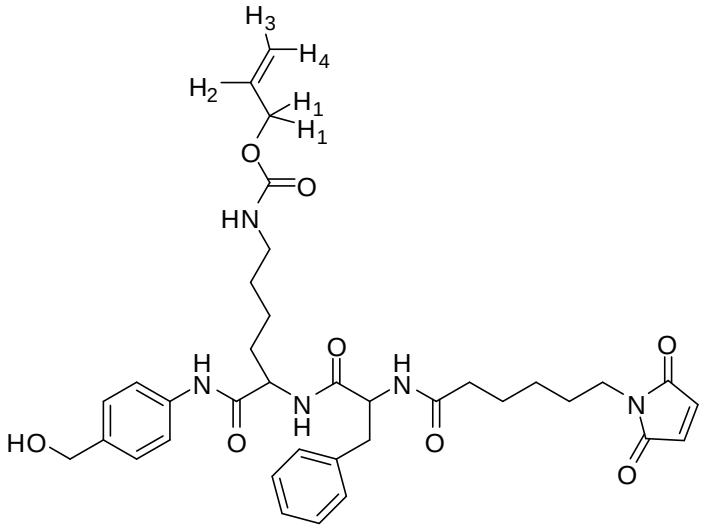

4.2.2 Doxorubicin Free Base from Clinical Samples.

Lyophilized pellets of expired clinical samples of doxorubicin HCl (20 – 50 mg) containing 100 – 250 mg lactose monohydrate (Bedford Laboratories, Bedford, OH) were dissolved in methanol to a final concentration of 2 mg/mL and combined in a separatory funnel. The methanol solution was diluted with 100 mM sodium phosphate buffer, pH 8.5, for a final concentration of 0.4 mg/mL dox HCl as a mixture of precipitated and solubilized material. The free base of Dox was extracted from the solution by two washes with equal volumes of chloroform, leaving almost no red color in the aqueous fraction. The chloroform was dried with anhydrous sodium sulfate, filtered, and removed by rotary evaporation to yield a red solid. The solid was dried thoroughly under high vacuum (10^{-2} torr) for at least 2.5 h to yield pure dox free base in a final yield of 98%, as indicated by optical density at 480 nm and a molar extinction coefficient of 11,500 M^{-1} cm^{-1} in 75% DMSO/25% water.

4.2.3 Synthesis of Doxazolidine (Doxaz)

Dox free base was dissolved to a final concentration of 5 – 10 mg/mL in deuteriochloroform and 1.1 – 2 equiv. of prilled paraformaldehyde (Aldrich, Milwaukee, WI) was added. The reaction mixture was monitored by ^{1}H NMR, with complete consumption of Dox occurring after 2 – 3 days, as evidenced by the appearance of the Doxaz methylene AX pattern at 4.31 and 4.68 ppm and doxf AX pattern at 4.21 and 4.73 ppm in the ^{1}H NMR spectrum. Loss of Dox was evident by the dox-specific aromatic triplet pattern for the proton at the 2-position, which appears at 7.81 ppm (as compared to 7.78 for Doxaz and 7.70 for Doxf). The amount of paraformaldehyde added determines the Doxaz/doxoform ratio, since Doxaz reacts with an additional equiv of formaldehyde to form Doxf. Complete assignments of the ^{1}H NMR spectra for Doxaz and Doxf have been published.[58] The reaction mixture was then filtered and the deuteriochloroform removed by rotary evaporation. The Doxaz/Doxf mixture was used without further purification, since Doxf readily hydrolyzes to produce tow equiv of Doxaz.

4.2.4 Synthesis of Fmoc-p-aminobenzyl alcohol (Fmoc-PABA)

N-(Fluorenylmethyloxycarbonyloxy)-succinimide (N-Fmoc-N-hydroxysuccinimide, 6.0 g, 17.8 mmol) in p-dioxane (60 mL) was added dropwise to p-aminobenzyl alcohol (PABA, 2.5 g, 20.5 mmol) in p-dioxane (30 mL). After 48 h of stirring, 90 mL of deionized H_20 was added and the desired product immediately precipitated. The product was isolated by filtration, and washed 4 times with deionized H_20 (60 mL). Fmoc-PABA (5.9 g, 95%) was isolated that showed the following spectral properties: ^{1}H NMR ($CDCl_3$): δ 4.26 (t, 1H, J = 7 Hz, Fmoc-CH), 4.53 (d, 2H, J = 7 Hz, Fmoc-CH_2), 4.63 (s, 2H, PABA-CH_2), 6.62 (bs, 1H, NH), 7.30 (t, 2H, J = 7 Hz, Fmoc), 7.34 (d, 2H, J = 7 Hz, PABA), 7.36 (b, 2H, PABA), 7.40 (t, 2H, J = 7 Hz, Fmoc), 7.60 (d, 2H, J = 7 Hz,

Fmoc), 7.77 ppm (d, 2H, J = 7 Hz, Fmoc); ESI-MS, observed m/z = 384.1014; calculated m/z for ($M + K^+$) = 384.0996.

4.2.5 Loading of Fmoc-PABA to 2-Chlorotrityl Resin

Fmoc-PABA (2 equiv) was added to 1.0 g of 2-chlorotrityl polystyrene resin in 10 mL dry THF followed by 4 equiv of dry pyridine. The solution was stirred and heated at 60 ºC in an oil bath for 16 h under argon. The solution was filtered through a coarse sintered glass frit, and the resin was washed with DCM/MeOH/DIEA 17:2:1 mL (3x), followed by DCM 10 mL (2x), DMF 10 mL (2x), DCM 10 mL (3x). The resin was dried under high vacuum (10^{-2} Torr) overnight and then checked for loading level according to previous published methods.[59]

4.2.6 Solid Phase Peptide Synthesis

The peptide was synthesized by the solid phase method using Fmoc strategy starting with preloaded Fmoc-PABA. The peptide was prepared on a 0.25 mmol scale by single amino acid couplings using a 4-fold excess of N-acetyl-Gly and the Fmoc-protected amino acids D-Ala (Chem-Impex, International, Wood Dale, IL), L-Phe, and L-Lys-alloc. Activation was done with 2-(1H-benzotriazole-1-yl)-1,1,3,3-tetramethyluronium hexafluoro-phosphate (HBTU)/N-hydroxy-benzotriazole (HOBT) and the synthesis was performed on an ABI 433A peptide synthesizer (Applied Biosystems, Carlsbad, CA). Owing to the poor nucleophilicity of the aniline nitrogen of PABA, the coupling of the first amino acid, Fmoc-Lys(alloc, Nvoc or azide), required an extended coupling time by modifying the software instructions to vortex the reaction for 60 sec, then allow it to sit for 10 min. This cycle was repeated 88 times. Fmoc groups were removed by sequential treatment (3x) with 20% piperidine/DMF. 6-maleimidocaproic acid (EMCA) was loaded as a standard amino acid, and all other amino acid couplings followed standard

conditions, to yield EMC-L-Phe-L-Lys(alloc, Nvoc or azide)-PABA (EMCFK(alloc Nvoc or azide)-PABA) coupled to the polystyrene resin.

4.2.7 Cleavage of EMCFK(alloc Nvoc or azide)-PABA from the Resin

The resin was placed into a medium-grain fritted funnel and washed twice with DCM (20 mL). Pyridine/MeOH (10% v/v, 20 mL) was added to the receiving flask to protect the peptide after cleavage. TFA/DCM (2% v/v, 10 mL) was then added and swirled for 1 min. The mixture was then gently vacuum filtered, without allowing the resin to proceed to dryness. This step was repeated 3 times followed by a 20 mL DCM wash. The filtrate contained the peptide and pyridine/TFA salt, and the solvent was rotary-evaporated to ~10% of the original volume. Approximately 40 mL of deionized water was added to the flask. Upon swirling, the peptide began to precipitate. The solution was allowed to cool in an ice bath for at least 10 min. The precipitate was collected on a fritted funnel and washed with deionized water 10 mL (3x), followed by ether, 10 mL (2x). The isolated amount of product and NMR assignments are presented in Table 4.2.7.1. ^{1}H NMR assignments for EMCFK(alloc)-PABA as the most illustrative representative of the group is provided. ^{1}H NMR assignments were made using 1D ^{1}H NMR and homonuclear COSY. ^{1}H NMR (500 MHz, DMSO-d6) δ 1.03 (q, *J* = 7.9 Hz, 2H, K-γ), 1.37 (dp, *J* = 22.9, 7.5 Hz, 6H, C, D, E), 1.66 (m, 2H, K-β), 2.00 (t, *J* = 7.3 Hz, 2H, B), 2.72 (dd, *J* = 13.9, 10.3 Hz, 1H, F-β), 2.96 (q, *J* = 6.5 Hz, 2H, K-ε), 3.02 (dd, *J* = 13.8, 4.1 Hz, 1H, F-β), 3.31 (t, *J* = 7.2 Hz, 2H, A), 4.36 (q, *J* = 7.8 Hz, 1H, K-α), 4.43 (m, 2H, Bn; 2H, alloc H_1), 4.56 (td, *J* = 9.7, 4.1 Hz, 1H, F-α), 5.11 (t, *J* = 5.7 Hz, 1H, Bn-OH), 5.14 (dt, *J* = 10.6, 1.6 Hz, 1H, alloc-H_3), 5.24 (dq, *J* = 17.2, 1.8 Hz, 1H, alloc-H_4), 5.87 (ddd, *J* = 22.4, 10.5, 5.3 Hz, 1H, alloc-H_2), 7.00 (s, 2H, maleimide), 7.13 – 7.17

(m, 1H, K-ε-NH), 7.18 – 7.31 (m, 5H, F; 2H, PABA), 7.50 – 7.59 (m, 2H, PABA), 8.01 (d, *J* = 8.4 Hz, 1H, F-NH), 8.14 (d, *J* = 7.7 Hz, 1H, K-NH), 9.95 (s, 1H, anilide).

	EMCFK(alloc)-PABA	EMCFK(Nvoc)-PABA	EMCFK(azide)-PABA
Amount isolated (mg)	153.26	191.10	64.86
Amount isolated (mmoles)	0.227	0.230	0.105
Yield	91%	92%	42%

Table 4.2.7.1 Experimental Details of mixed carbonates.

4.2.8 Activation to EMCFK(alloc)-PABA-pNP Carbonate Ester

An oven dried round bottom flask equipped with a magnetic stir bar was cooled under argon and charged with 4.0 mL of tetrahydrofuran (distilled from sodium metal and benzophenone) and EMCFK(alloc)PABA (53.43 mg, 0.079 mmol). To the stirring heterogeneous mixture, 1.1 equiv p-nitrophenyl chloroformate (17.5 mg, 0.087 mmol) was added followed immediately by 1.1 equiv pyridine (7.03 µL). Over the course of 20 min, all solids went into solution, after which the reaction progress was monitored by RP-HPLC (Method 1) until complete, as evidenced by the disappearance of starting material (eluting at 17.0 min), which typically required overnight reaction. The reaction mixture was then diluted with 50 mL of ethyl acetate and washed once with 50 mL deionized water, followed by extractions with 50 mL of saturated sodium bicarbonate until the aqueous layer no longer turned yellow (typically 5 extractions). The organic layer was dried over sodium sulfate and concentrated by rotary evaporation to yield 59.85 mg of a pale yellow solid that was used without further purification, with a final yield of 90%. EMCFK(alloc)-PABA-pNP was characterized by the following

spectroscopic data with NMR assignments made from 1D ^{1}H NMR and homonuclear COSY. ^{1}H NMR (500 MHz, DMSO-d6) δ 1.03 (q, *J* = 8.0 Hz, 2H, K-γ), 1.37 (dp, *J* = 14.9, 7.4 Hz, 6H, C, D, E), 1.67 (m, 2H, K-β), 2.00 (t, *J* = 7.4 Hz, 2H, B), 2.72 (dd, *J* = 13.8, 10.3 Hz, 1H, F-β), 2.96 (t, *J* = 6.5 Hz, 2H, K-ε), 3.02 (dd, *J* = 13.8, 4.1 Hz, 1H, F-β), 3.31 (t, *J* = 7.2 Hz, 2H, A), 4.37 (m, 1H, K-α), 4.42 (dd, *J* = 4.3, 2.9 Hz, 2H, alloc-H_1), 4.56 (td, *J* = 9.4, 9.0, 4.0 Hz, 1H, F-α), 5.13 (dd, J_1=J_2 = 1.4 Hz, 1H, alloc-H_3), 5.24 (dq, *J* = 17.3, 1.6 Hz, 1H, alloc-H_4), 5.24 (s, 2H, Bn), 5.87 (ddd, *J* = 22.3, 10.5, 5.4 Hz, 1H, alloc-H_2), 7.00 (s, 2H, maleimide), 7.12 – 7.29 (m, 5H, F), 7.42 (m, 2H, PABA), 7.52 – 7.60 (m, 2HpNP), 7.61 – 7.71 (m, 2H, PABA), 8.01 (d, *J* = 8.3 Hz, 1H, F-NH), 8.18 (d, *J* = 7.8 Hz, 1H, K-NH), 8.23 – 8.39 (m, 2H, pNP), 10.11 (s, 1H, anilide).

4.2.9 Activation to EMCFK(Nvoc)-PABA-pNP Carbonate Ester

An oven dried round bottom flask equipped with a magnetic stir bar was cooled under argon and charged with 4.0 mL of tetrahydrofuran (distilled from sodium metal and benzophenone) and EMCFK(Nvoc)PABA (67.20 mg, 0.081 mmol). To the stirring heterogeneous mixture, 1.1 equiv p-nitrophenyl chloroformate (17.9 mg, 0.089 mmol) was added followed immediately by 1.1 equiv pyridine (7.04 µL). Over the course of 50 min, all solids went into solution, after which the reaction progress was monitored by RP-HPLC (Method 1) until complete, as evidenced by the disappearance of starting material (eluting at 15.8 min), which typically required overnight reaction. The reaction mixture was then diluted with 50 mL of ethyl acetate and washed once with 50 mL deionized water, followed by extractions with 50 mL of saturated sodium bicarbonate until the aqueous layer no longer turned yellow (typically 5 extractions). The organic layer was dried over sodium sulfate and concentrated by rotary

evaporation to yield 70.9 mg of a pale yellow solid that was used without further purification, with a final yield of 88%. EMCFK(Nvoc)-PABA-pNP slowly degraded over time, even at lower temperatures, and in the solid phase, and was therefore not characterized by NMR.

4.2.10 Activation to EMCFK(azide)-PABA-pNP Carbonate Ester

An oven dried round bottom flask equipped with a magnetic stir bar was cooled under argon and charged with 1.0 mL of tetrahydrofuran (distilled from sodium metal and benzophenone) and EMCFK(azide)PABA (15.56 mg, 0.025 mmol). To the stirring heterogeneous mixture, 1.1 equiv p-nitrophenyl chloroformate (5.59 mg, 0.028 mmol) was added followed immediately by 1.1 equiv pyridine (2.26 µL). Over the course of 20 min, all solids went into solution, after which the reaction progress was monitored by RP-HPLC (Method 1) until complete, as evidenced by the disappearance of starting material (eluting at 15.4 min), which typically required overnight reaction. The reaction mixture was then diluted with 50 mL of ethyl acetate and washed once with 50 mL deionized water, followed by extractions with 50 mL of saturated sodium bicarbonate until the aqueous layer no longer turned yellow (typically 5 extractions). The organic layer was dried over sodium sulfate and concentrated by rotary evaporation to yield 10.24 mg of a pale yellow solid that was impure by HPLC, with a final yield by extrapolation from the HPLC chromatogram of 52%. Due to the high amounts of impurities, EMCFK(azide)-PABA-pNP was not characterized by NMR.

4.2.11 Synthesis of EMCFK(alloc)-PABC-Doxaz

An oven dried round bottom flask equipped with a magnetic stir bar was cooled under argon and charged with EMCFK(alloc)-PABC-pNP (59.85 mg, 0.0711 mmol), 1-hydroxybenzotriazole (10.89 mg, 1 equiv) and 500 µL dry DMSO (stored over 4Å molecular

sieves for at least 3 days). To this, 1 equiv doxaz (39.54 mg) dissolved in 500 µL of similarly dried DMSO was added and the mixture was left to stir under argon in the dark and monitored by HPLC (Method 1) until complete, as evidenced by the disappearance of carbonate starting material (approximately 36 h). The reaction mixture was then diluted with an additional 2 mL of DMSO. A 15 mL medium fritted sintered glass funnel was charged with 10 mL cold PBS, pH 7.4. The red reaction mixture was added dropwise and the resulting red precipitate was washed four times with 10 mL of PBS and then two washes with 10 mL of deionized water. The precipitate was washed from the filter with a mixture of 10:1 chloroform/methanol and concentrated by rotary evaporation. The majority of the crude red solid, which was a mixture containing a 40% yield of EMCFK(alloc)-PABC-Doxaz, was moved forward without any additional purification. However, to fully purify EMCFK(alloc)-PABC-Doxaz for characterization, the red solid was purified by preparative silica gel TLC, spotted in and eluted with 10:1 chloroform:methanol. The desired product (the major band) was excised, suspended and vortexted in the elution solvent, and centrifuged to remove the silica gel. The solvent was removed by rotary evaporation to produce solid, pure EMCFK(alloc)-PABC-Doxaz that was characterized by ^{1}H NMR assignments made using 1D ^{1}H NMR and homonuclear COSY. ^{1}H NMR (500 MHz, DMSO-d6) δ 1.00 (d, *J* = 7.0 Hz, 3H, 5'-Me), 1.03 (q, *J* = 8.0 Hz, 2H, K-γ), 1.37 (dp, *J* = 14.9, 7.4 Hz, 6H, C, D, E), 1.67 (m, 2H, K-β), 1.73 (m, 1H, 2'), 1.84 – 1.91 (m, 1H, 2'), 2.00 (t, *J* = 7.4 Hz, 2H, B), 2.14 – 2.26 (m, 2H, 8), 2.72 (dd, *J* = 13.8, 10.3 Hz, 1H, F-β), 2.96 (t, *J* = 6.5 Hz, 2H, K-ε), 2.99 (s, 2H, 10), 3.02 (dd, *J* = 13.8, 4.1 Hz, 1H, F-β), 3.31 (t, *J* = 7.2 Hz, 2H, A), 3.96 (dd, *J* = 5.9, 2.2 Hz, 1H, 4'), 4.06 (dt, *J* = 7.6, 5.8 Hz, 1H, 3'), 4.10 (s, 3H, 4-OMe), 4.23 (p, *J* = 7.0 Hz, 1H, 5'), 4.37 (m, 1H, K-α), 4.42 (dd, *J* = 4.3, 2.9 Hz, 2H, alloc-H_1), 4.56 (td, *J* = 9.4, 9.0, 4.0 Hz, 1H, F-

α), 4.75 (dd, *J* = 5.0, 2.3 Hz, 2H, 14), 4.86 (d, *J* = 3.6 Hz, 1H, OCH_2N), 4.89 (d, *J* = 3.5 Hz, 1H, OCH_2N), 4.97-5.11 (m, 2H, Bn, 1H, 7), 5.13 (dd, *J* = 1.4 Hz, 1H, alloc-H_3), 5.24 (dq, *J* = 17.3, 1.6 Hz, 1H, alloc-H_4), 5.24 (s, 2H, Bn), 5.87 (ddd, *J* = 22.3, 10.5, 5.4 Hz, 1H, alloc-H_2), 5.27 (t, *J* = 4.2 Hz, 1H, 1'), 6.65 (s, 2H, maleimide), 7.12 – 7.29 (m, 5H, F), 7.42 (m, 2H, PABA), 7.61 – 7.71 (m, 2H, PABA), 7.86 – 7.97 (m, 1H, 3, 1H, 2), 8.00 (d, *J* = 7.8 Hz, 1H, 1), 8.01 (d, *J* = 8.3 Hz, 1H, F-NH), 8.18 (d, *J* = 7.8 Hz, 1H, K-NH), 10.11 (s, 1H, anilide) 13.25 (s, 1H, 6-OH), 14.03 (s, 1H, 11-OH).

4.2.12 Synthesis of EMCFK(Nvoc)-PABC-Doxaz

An oven dried round bottom flask equipped with a magnetic stir bar was cooled under argon and charged with EMCFK(Nvoc)-PABC-pNP (24.75 mg, 0.0249 mmol), 1-hydroxybenzotriazole (3.80 mg, 1 equiv) and 600 µL dry DMSO (stored over 4Å molecular sieves for at least 3 days). To this, 1 equiv doxaz (13.80 mg) dissolved in 600 µL of similarly dried DMSO was added and the mixture was left to stir under argon in the dark and monitored by HPLC (Method 1) until complete, as evidenced by the disappearance of carbonate starting material (approximately 36 h). The reaction mixture was then diluted with an additional 2 mL of DMSO. A 15 mL medium fritted sintered glass funnel was charged with 10 mL cold PBS, pH 7.4. The red reaction mixture was added dropwise and the resulting red precipitate was washed four times with 10 mL of PBS and then two washes with 10 mL of deionized water. The precipitate was washed from the filter with a mixture of 10:1 chloroform/methanol and concentrated by rotary evaporation. The majority of the crude red solid, which was a mixture containing a 52% yield of EMCFK(alloc)-PABC-Doxaz, was moved forward without any additional purification. However, to fully purify EMCFK(alloc)-PABC-Doxaz for characterization, the red solid was purified by preparative silica gel TLC, spotted in and eluted with 10:1

chloroform:methanol. The desired product (the major band) was excised, suspended and vortexted in the elution solvent, and centrifuged to remove the silica gel. The solvent was removed by rotary evaporation to produce solid, pure EMCFK(alloc)-PABC-Doxaz that was immediately used without characterization to preclude degradation.

4.2.13 Synthesis of EMCFK(PO_4)-PABC-Doxaz from EMCFK(Nvoc)-PABC-Doxaz

An oven dried convex pyrex vessel was cooled under argon and charged with EMCFK(Nvoc)-PABC-Doxaz (15.26 mg, 0.0127 mmol) and 1.0 mL of methylene chloride and 200 µL of glacial acetic acid. The vessel was sealed, located 0.5 cm awar from a single black lamp and irradiated at 310-400 nm (principal emission at 350 nm) for 45 min. The reaction was diluted with 500 µL of glacial acetic acid, and the methylene chloride removed by rotary evaporation. The reaction mixture was further diluted with 500 µL of the HPLC initial conditions solvent system of 80% aq. Phosphate buffer and 20% acetonitrile. Purification by RP-HPLC yielded 72% (11.61 mg, 0.0091 mmol) of EMCFK(PO_4)-PABC-Doxaz which was characteriezed by ^{1}H NMR assignments made using 1D ^{1}H NMR and homonuclear COSY. ^{1}H NMR (500 MHz, DMSO-d6) δ 0.97 (d, *J* = 7.2 Hz, 3H, 5'-Me), 1.05 (q, *J* = 8.1 Hz, 2H, K-γ), 1.34 (dp, *J* = 15.0, 7.2 Hz, 6H, C, D, E), 1.64 (m, 2H, K-β), 1.71 (m, 1H, 2'), 1.82 – 1.89 (m, 1H, 2'), 2.02 (t, *J* = 7.2 Hz, 2H, B), 2.10 – 2.22 (m, 2H, 8), 2.75 (dd, *J* = 13.8, 10.3 Hz, 1H, F-β), 2.94 (t, *J* = 6.5 Hz, 2H, K-ε), 3.01 (s, 2H, 10), 3.05 (dd, *J* = 14.0, 4.1 Hz, 1H, F-β), 3.31 (t, *J* = 7.2 Hz, 2H, A), 3.96 (dd, *J* = 6.0, 2.4 Hz, 1H, 4'), 4.00 (s, 3H, 4-OMe), 4.06 (dt, *J* = 7.5, 5.7 Hz, 1H, 3'), 4.27 (p, *J* = 7.0 Hz, 1H, 5'), 4.38 (m, 1H, K-α), 4.54 (td, *J* = 9.5, 9.0, 4.2 Hz, 1H, F-α), 4.77 (dd, *J* = 5.0, 2.3 Hz, 2H, 14), 4.87 (d, *J* = 3.5 Hz, 1H, OCH_2N), 4.89 (d, *J* = 3.5 Hz, 1H, OCH_2N), 4.94-5.01 (m, 2H, Bn), 5.02-

5.10(m, 1H, 7), 5.24 (s, 2H, Bn), 5.36 (t, *J* = 4.3 Hz, 1H, 1'), 7.00 (s, 2H, maleimide), 7.20 – 7.37 (m, 5H, F), 7.51 (m, 2H, PABA), 7.63 (m, 2H, PABA), 7.83 – 7.92 (m, 1H, 3, 1H, 2), 8.04 (d, *J* = 7.7 Hz, 1H, 1), 8.03 (d, *J* = 8.4 Hz, 1H, F-NH), 8.25 (d, *J* = 7.8 Hz, 1H, K-NH), 10.11 (s, 1H, anilide).

4.3 Results and Discussion

4.3.1 Synthesis of EMCFKPABCDoxaz (EMC-FK-Doxaz)

In an attempt to explore routes to a commercially scalable process to EMC-FK-Doxaz, the historically most problematic synthetic aspect was altered in three ways. The problematic deprotection of the lysine in the final step was addressed by using the allyloxycarbonyl (alloc), ortho-nitroveratryloxycarbonyl (Nvoc) and the azide protecting groups on the ε-amino of L-lysine. The 9-fluoroxycarbonyl (Fmoc) protected versions of each lysine are shown in Figure 4.3.1.1. A general synthetic scheme for the desired prodrug is shown in Scheme 4.3.1.1.

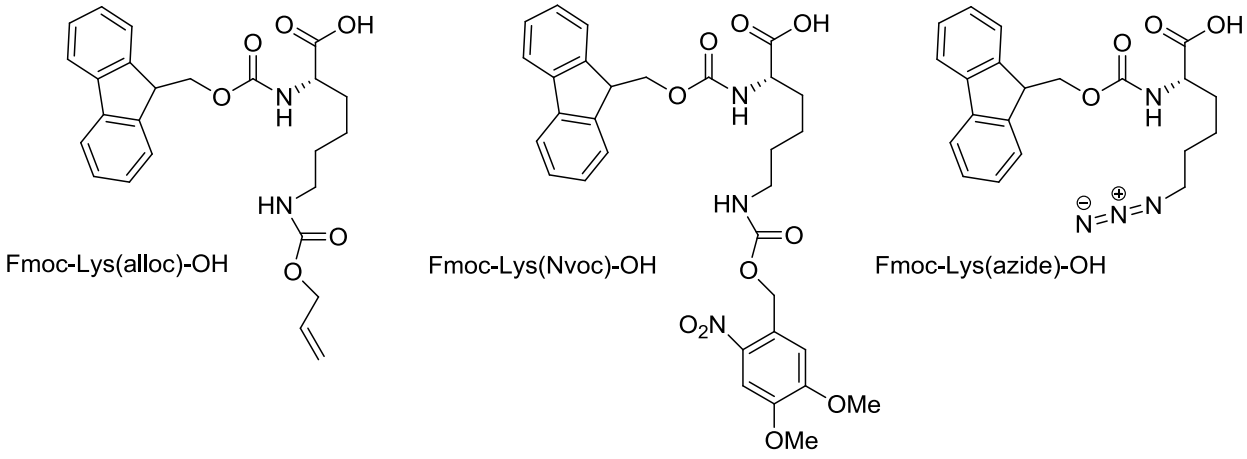

Figure 4.3.2.1 Fmoc and ε-amino protected lysines used

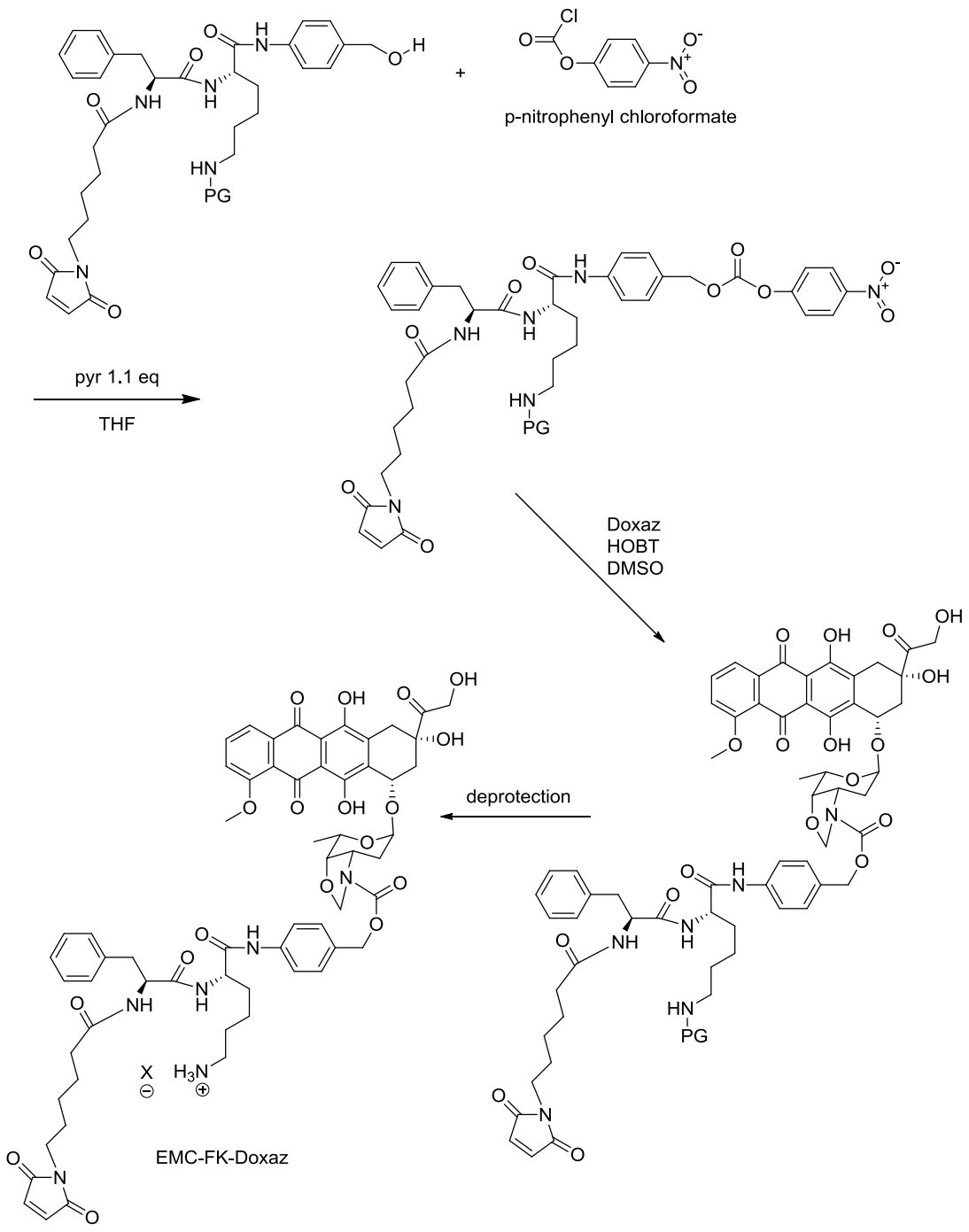

Scheme 4.3.1. 1 General scheme for the synthesis of EMCFKPABCDoxaz (EMC-FK-Doxaz).

4.3.1.1 EMCFK(alloc)PABCDoxaz

Synthesis of the maleimide-peptide-spacer was accomplished using established solid phase peptide synthetic techniques. Standard Fmoc deprotection methodology, and the loading of 6-maleimidocaproic acid as an amino acid allowed facile synthesis on a robotic peptide synthesizer. Cleavage from resin using TFA, and subsequent precipitation of the maleimide-peptide-spacer conjugate from water went smoothly, and in 91% yield. Interestingly, the activation of the benzyl alcohol with *p*-nitrophenylchloroformate (pNP-chloroformate) under varying conditions with this molecule, led to advancements in other syntheses previously described. Effort was expended on the investigation of various solvent systems and reagent stoichiometry in an attempt to create a clean, scalable reaction. It was learned that the use of a mixed anhydrous solvent system of tetrahydrofuran (THF) and methylene chloride in varying ratios, while effective at solvating the reagents, especially the peptide conjugate, impeded the reactions progress. With mixed solvent systems, and varying amounts of pyridine and pNP-chloroformate, yields of 40 – 76% were obtained. We also observed that formation of the stable and difficult to remove bis-*p*-nitrophenyl carbonate, was prevalent in the mixed solvent systems. The observation that the final products, however impure, were seemingly quite soluble in THF, as was pNP-chloroformate, led to the heterogeneous reaction described in section 4.2. The addition of pNP-chloroformate and pyridine to a suspension of EMCFK(alloc)PABA in anhydrous THF, quickly led to the solvated product.

As previously described, the coupling of Doxaz to the mixed carbonate continues to be inefficient due to the poor reactivity of the oxazolidine nitrogen; however, reaction conditions

and yields were on par with previous observations. There was some concern that Michael addition to the maleimide could occur; however, if this did occur, it did not change the overall yield based on previous experience.

Deprotection of the alloc protecting group with tetrakistriphenlphosphine Pd(0) was attempted in THF, methylene chloride, chloroform and mixtures in varying ratios to no avail. Use of catalytic to stoichiometric amounts of palladium presented a reaction that could only partially proceed, or form multiple side products, and possibly polymerize based on HPLC observations. We hypothesized that the ε-amino of lysine, once deprotected, would react quickly by 1,4-addition to the maleimide. The large amount of observed products made this a difficult hypothesis to prove, and the aim of the project was to find a scalable reaction, so this method was quickly abandoned. Use of N-iodosuccinimide and trifluoroacetic acid as described in Chapter 2 was also attempted, leading once again to multiple products that were not characterized.

4.3.1.2 EMCFK(Nvoc)PABCDoxaz

The use of *ortho*-nitroveratryloxycarbonyl (Nvoc) was next explored. The manufacturing utility of a photocleavable amino acid protecting group was not clear. Fmoc-Lys(Nvoc)-OH was used for SPPS. It had previously been shown that the Nvoc group was compatible with the maleimide.[60] Photodeprotection can be achieved using ultraviolet irradiation at $\lambda > 280$ nm and occurs through a p-nitrobenzyl photocleavage reaction as outlined in See Scheme 4.3.1.2.1. Fmoc-Lys(Nvoc)-OH was not commercially available, and a commercial shortage of Nvoc chloroformate coupled with the desire to create a safe scalable method led to an improved synthetic procedure. Elimination of gaseous phosgene by using triphosgene was first

attempted in dioxane. This led to formation of large amounts of the bis-Nvoc carbonate. A simple switch to anhydrous THF and stepwise addition of the benzyl alcohol to a phosgene solution led to quantitative formation of the Nvoc chloroformate after off-gassing of the unreacted phosgene and the newly formed HCl gas. See Scheme 4.3.1.2.2. Large scale production in this manner would require careful handling due to the production of the highly toxic HCl and phosgene gasses.

The literature procedure for the addition of the Nvoc chloroformate to Fmoc-Lys(OH) in mixed solvent system of dioxane/acetonitrile/water in the presence of sodium carbonate[60] was problematic in our hands. Formation of multiple viscous products that exhibited no solubility in standard solvents was observed. It was hypothesized that under these conditions, reaction of the lysine carboxylic acid with the Nvoc chloroformate occurred more quickly than reaction at the lysine ε-amino, and once the mixed carbonate was formed, the lysine ε-amino could displace the 2-nitro-4,5-dimethoxybenzyl alcohol forming a complex mixture of polymers of varying length. Based on the observations that Nvoc chloroformate was easily formed, and highly soluble in THF, and the problematic deprotonation of the lysine carboxylic acid under basic conditions, a heterogeneous reaction was attempted. The rationale was that unlike the Nvoc chloroformate the ε-amino protonated HCl salt of Fmoc lysine (Fmoc-Lys(HCl)-OH) would only be very partially soluble in THF. The small equilibrated amount of the free ε-amino lysine would react quickly with the Nvoc chloroformate, and remain solvated. This would push the equilibrium toward the desired, and now solvated product. Initially this procedure seemed to have only a small statistical chance for success, but based on previous success with heterogeneous solutions in THF, it was attempted, and in fact was highly successful.

With Fmoc-Lys(Nvoc)-OH in hand, SPPS of the desired maleimide-peptide-spacer conjugate and activation to the EMCFK(Nvoc)-pNP carbonate went smoothly and analogously to the procedures described in section 4.3.1.1 for EMCFK(alloc)-pNP. Coupling to Doxaz also proceeded similarly to previous procedures, and afforded yields of 55% as expected. Deprotection by ultraviolet irradiation in acetonitrile/water solvent systems were ineffective. Dissolution of the protected Doxaz conjugate in five parts methylene chloride and one part acetic acid yielded one major product as observed by HPLC after ultraviolet irradiation at 270 nm for 45 min. Purification by either preparative TLC or preparative HPLC produced the desired product in 74% yield as calculated by optical density.

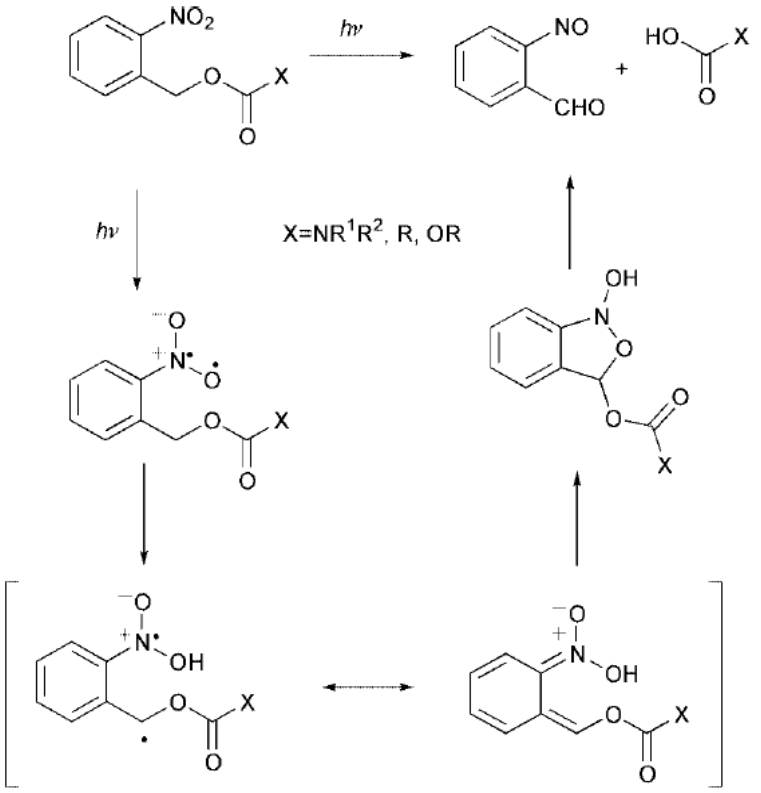

Scheme 4.3.1.2. 1 Proposed mechanism for p-nitrobenzyl photodeprotection of the Nvoc group.

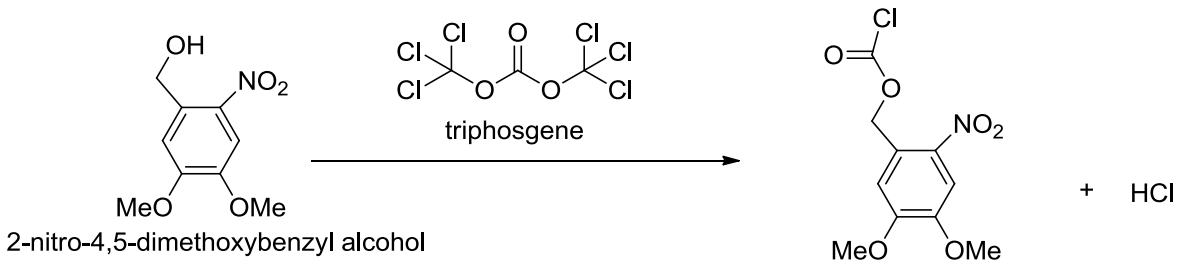

Scheme 4.3.1.2.2 Formation of Nvoc chloroformate using triphosgene.

4.3.1.3 EMCFK(azide)PABCDoxaz

In an attempt to explore alternate protecting strategies for Doxaz prodrugs containing lysine, Fmoc-Lys(azide)-OH was employed. This reagent recently became commercially available, but at an exorbitantly high cost. The final reaction of the azide to primary amine is through the use of a Staudinger reaction using triphenylphosphine. The mechanism for the Staudinger deprotection is shown in Scheme 4.3.1.3.1. As can be seen, triphenylphosphine oxide is a byproduct of the reaction. Triphenylphosphine oxide is notoriously difficult to remove; however, the chemoselective reaction was attractive for our needs. Peptide synthesis using standard Fmoc procedures was performed, and unexpectedly, the yield of final peptide was very low at 42%. Activation using similar methods as above, only yielded 52% of a very impure product. Many byproducts were observed by HPLC. Additionally, peptide stored at -20 ^{o}C was also showing degradation over time. We hypothesized that the azide was reacting, even in the solid phase, with the maleimide. Instability upon storage has been observed by manufacturers of azide-peg4-maleimide molecules used for click and bioconjugate chemistries. These manufactures now sell these molecules as a kit that can assemble *in situ*. With a high price, low yields and unpredictable reactivity, the azide protecting group on lysine was

determined to be ineffective for the projects goal of scalable, high yielding chemistries, and further investigation was not warranted.

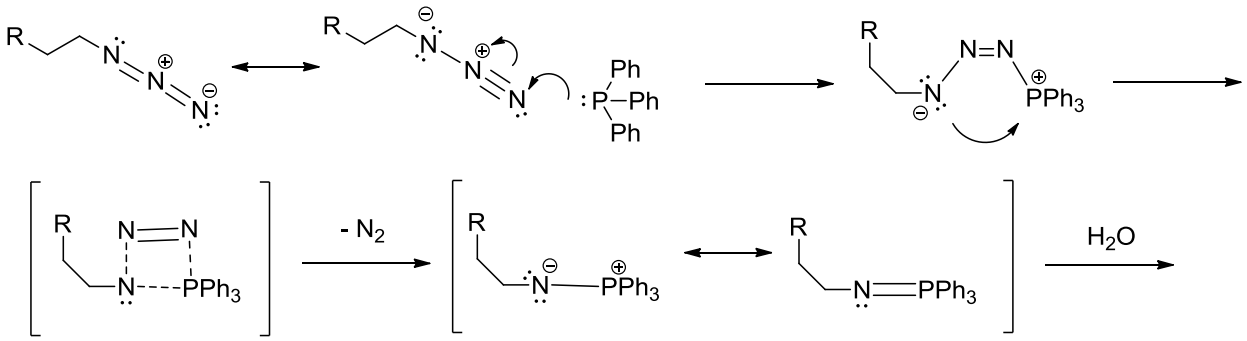

Scheme 4.3.1.3.1 Mechanism of Staudinger deprotection of azide protected Lysine.

4.4 Conclusions

The purpose of this project was to demonstrate that simple, scalable prodrugs of Doxaz of the type EMC-PAD-Doxaz could be synthesized. In this respect the project was a success. The exploration of alternate reaction pathways is critical to the success of any Doxaz commercialization endeavor. EMCPPDoxaz will be tested in more *in vivo* models soon, and funding for a second species of animal is being explored. The Koch group is currently seeking collaborative partners and funding to examine EMCFKPABCDoxaz. *In vitro* experiments are ongoing at the time of this writing.

4.5 References

1. Elsadek, B.; Kratz, F. Impact of albumin on drug delivery — New applications on the horizon. *J. Control. Release*. **2012**, 157, 4–28.

2. Kratz, F. Albumin as a drug carrier: design of prodrugs, drug conjugates and nanoparticles. *J. Control. Release*. **2008**, 132, 171–183.

3. Park, K. Albumin: A versatile carrier for drug delivery. *J. Control. Release*. **2012**, 157, 3. (Epub 2011.

4. Kratz, F.; Roth, T.; Fichiner, I.; *et al.* In vitro and in vivo efficacy of acid-sensitive transferrin and albumin doxorubicin conjugates in a human xenograft panel and in the MDA-MB-435 mamma carcinoma model, *J. Drug. Target*. **2000**, 8, 305–318.

5. Maeda, H.; Ueda, M.; Morinaga, T.; *et al.* Conjugation of poly(styrene-comaleic acid) derivatives to the antitumor protein neocarzinostatin: pronounced improvements in pharmacological properties. *J. Med. Chem*. **1985**, 28, 455–461.

6. Matsumura, Y.; Maeda, H. A new concept for macromolecular therapeutics in cancer chemotherapy: mechanism of tumoritropic accumulation of proteins and the antitumor agent smancs. *Cancer. Res*. **1986**, 46, 6387–6392.

7. Lindholm, A. New insulins in the treatment of diabetes mellitus. *Best. Pract. Res. Clin. Gastroenterol*. **2002**, 16, 475-492.

8. Hamilton-Wessler, M.; Ader, M.; Dea, M.; *et al*. Mechansim of protracted metabolic effects of fatty acid acylated insulin, NN304, in dogs: retention of NN304 by albumin. *Diabetologia.* **1999**, 42, 1254-1263.

9. Standl, E. Insulin analogues - state of the art. *Horm. Res*. **2002**, 57, Suppl 1:40-45.

10. Wootten, D.; Savage, E.E.; Valant, C.; *et al.* Allosteric modulation of endogenous metabolites as an avenue for drug discovery. *Mol. Pharmacol*. **2012**, May 10. [Epub ahead of print].

11. Flisiak, R.; Flisiak, I. Albinterferon-alpha 2b: a new treatment option for hepatitis C. *Expert. Opin. Biol. Ther.* **2010**, 10, 1509–1515.

12. Nelson, D.R.; Benhamou, Y.; Chuang, W.L.; *et al.* Albinterferon Alfa-2b was not inferior to pegylated interferon-alpha in a randomized trial of patients with chronic hepatitis C virus genotype 2 or 3. *Gastroenterology*. **2010**, 139, 1267–1276.

13. Zeuzem, S.; Sulkowski, M.S.; Lawitz, E.J.; *et al.* Albinterferon Alfa-2b was not inferior to pegylated interferon-alpha in a randomized trial of patients with chronic hepatitis C virus genotype 1. *Gastroenterology.* **2010**, 139, 1257–1266.

14. Gradishar WJ. Albumin-bound paclitaxel: a next-generation taxane. *Expert Opin Pharmacother*. **2006**. 7, 1041-1053.

15. Cortes J.; Saura C. Nanopartcle albumin-bound (nab™)-paclitaxel: improving efficacy and tolerability by targeted drug delivery in metastatic breast cancer. *Eur. J. Cancer. Suppl*. **2010**, 8, 1-10.

16. Taxotere (docetaxel) Injection Concentrate [Package Insert]. Aventis Pharmaceutical Products, Inc.; Bridgewater, NJ: 2003.

17. Taxol (paclitaxel) Injection [Package Insert]. Brystol-Meyers Squibb Co.; Princeton, NJ: 2003.

18. Weiss, R.B.; Donehower, R.C.; Wiernik, P.H.; *et al*. Hypersensitivity reactions from taxol. *J. Clin. Oncol.* **1990**, 8, 1263-1268.

19. ten Tije, A.J.; Verweij, J.; Loos, W.J.; *et al.* Pharmacological effects of formulation vehicles: implications for cancer chemotherapy. *Clin. Pharmacokinet*. **2003**, 42, 665-685.

20. Authier, N.; Gillet, J.P.; Fialip, J.; *et al*. Assessment of neurotoxicity following repeated cremophor/ethanol injections in rats. *Neurotox. Res.* **2001**, 3, 301-306.

21. Postma, T.J.; Vermorken, J.B.; Liefting, A.J.M.; *et al*. Paclitaxel-induced neuropathy. *Ann. Oncol*. **2004**, 6, 484-494.

22. Gelderblom, H.; Verweij, J.; Nooter, K.; *et al*. Cremophor EL: the drawbacks and advantages of vehicle selection for drug formulation. *Eur. J. Cancer*. **2001**, 37, 1590-1598.

23. Winer, E.P.; Berry, D.A.; Woolf, S.; *et al*. Failure of higher-dose paclitaxel toimprove outcome in patients with metastatic breast cancer: cancer and leukemia group B trial 9342. J. Clin. Oncol. **2004**, 22, 2061-2068.

24. Gradishar, W.J.; Krasnojon, D.; Cheporov, S.; *et al.* Significantly longer progression-free survival with nab-paclitaxel compared with docetaxel as first-line therapy for metastatic breast cancer. *J. Clin*. *Oncol*. **2009**, 27, 3611–3619.

25. Hawkins, M.J.; Soon-Shiong, P.; Desai, N. Protein nanoparticles as drug carriers in clinical medicine. *Adv. Drug. Deliv. Rev.* **2008**, 60, 876–885.

26. Desai, N.; Trieu, V.; Damascelli, B.: *et al.* SPARC expression correlates with tumor response to albumin-bound paclitaxel in head and neck cancer patients. *Transl. Oncol.* **2009**, 2, 59–64.

26. Tiruppathi, C.; Song, W.; Bergenfeldt, M.; *et al.* Gp60 activation mediates albumin transcytosis in endothelial cells by tyrosine kinase-dependent pathway. *J. Biol. Chem*. **1997**, 272, 25968–25975.

27. Schnitzer, J.E. gp60 is an albumin-binding glycoprotein expressed by continuous endothelium involved in albumin transcytosis. *Am. J. Physiol*. **1992**, 262, (1 Pt 2) H246–H254.

28. Wang, Z.; Tiruppathi, C.; Minshall, R.D.; *et al.* Size and dynamics of caveolae studied using nanoparticles in living endothelial cells. *ACS. Nano*. **2009**, 3, 4110–4116.

29. Sage, H.; Johnson, C.; Bornstein, P. Characterization of a novel serum albuminbinding glycoprotein secreted by endothelial cells in culture. *J. Biol. Chem.* **1984**, 259, 3993–4007.

30. Podhajcer, O.L.; Benedetti, L.G.; Girotti, M.R.; *et al.* The role of the matricellular protein SPARC in the dynamic interaction between the tumor and the host. *Cancer. Metastasis. Rev*. **2008**, 27, 691–705.

31. Kratz, F.; Müller-Driver, R.; Hofmann.; *et al.* A novel macromolecular prodrug concept exploiting endogenous serum albumin as a drug carrier for cancer chemotherapy. *J. Med. Chem*. **2000**, 43, 1253–1256.

32. Kratz, F.; Warnecke, K.; Scheuermann, C.; *et al.* Probing the cysteine-34 position of endogenous serum albumin with thiol-binding doxorubicin derivatives. Improved efficacy of an acid-sensitive doxorubicin derivative with specific albumin-binding properties compared to that of the parent compound. *J. Med. Chem*. **2002**, 45, 5523–5533.

33. Graeser, R.; Esser, N.; Unger, H.; *et al.* INNO-206, the (6-maleimidocaproyl hydrazone derivative of doxorubicin), shows superior antitumor efficacy compared to doxorubicin in different tumor xenograft models and in an orthotopic pancreas carcinoma model. *Invest. New. Drugs.* **2010**, 28, 14–19. Epub 2009, Jan 8.

34. Unger, C.; Häring, B.; Medinger, M.; *et al.* Phase I and pharmacokinetic study of the (6-maleimidocaproyl) hydrazone derivative of doxorubicin. *Clin. Cancer. Res*. **2007**, 13, 4858–4866.

35. Kratz, F.; Fichtner, I.; Graeser, R. Combination therapy with the albumin-binding prodrug of doxorubicin (INNO-206) and doxorubicin achieves complete remissions and improves tolerability in an ovarian A2780 xenograft model. *Invest. New. Drugs*. **2011**, [Epub ahead of print].

36. Calderón, M.; Welker, P.; Licha,K.; *et al.* Development of efficient acid cleavable multifunctional prodrugs derived from dendritic polyglycerol with a poly(ethylene glycol) shell. *J. Control. Release*. **2011**, 151, 295–301.

37. Hofmann, U.B.; Westphal, J.R.; van Muijen, G.N.P.; *et al.* Matrix metalloproteinases in human melanoma. *J. Investig. Dermatol.* **2000**, 115, 337–344.

38. Curran, S.; Murray, G.I. Matrix metalloproteinases in tumour invasion and metastasis. *J. Pathol.* **1999**, 189, 300–308.

39. Chambers, A.F.; Matrisian, L. M. Changing views of the role of matrix metalloproteinases in metastasis*. J. Natl. Cancer. Inst*. **1997**, 89, 1260–1270.

40. Hofmann, U.B.; Westphal, J.R.; Waas, E.T.; *et al.* Matrix metalloproteinases in human melanoma cell lines and xenografts: increased expression of activated matrix metalloproteinase-2 (MMP-2) correlates with melanoma progression. *Br. J. Cancer*. **1999**, 81, 774–782.

41. Sun, W.; Schuchter, L.M. Metastatic melanoma. *Curr. Treat. Options. Oncol*. **2001**, 2, 193–202.

42. Kurschat, P.; Zigrino, P.; Nischt, R.; *et al.* Tissue inhibitor of matrix metalloproteinase-2 regulates matrix metalloproteinase-2 activation by modulation of membrane-type 1 matrix metalloproteinaseactivity in high and low invasive melanoma cell lines. *J. Biol. Chem*. **1999**, 274, 21056–21062.

43. Fiebig, H.H.; Klostermeyer, A.; Schüler, J.B.; *et al.* Characterization of matrix metalloproteinases in 47 human tumor xenografts show high expression of MMP-2 in melanomas and sarcomas. *Proc. Am*. *Assoc. Cancer. Res*. **1999**, 40, 463.

44. Väisänen, A.; Tuominen, H.; Kallioinen, M.; *et al.* Matrix metalloproteinase-2 (72 kD type IV collagenase) expression occurs in the early stage of human melanocytic tumour progression and may have prognostic value. *J. Pathol*. **1996**, 180, 283–289.

45. Mansour, A.M.; Drevs, J.; Esser, N.; *et al.* A New Approach for the Treatment of Malignant Melanoma: Enhanced Antitumor Efficacy of an Albumin-binding Doxorubicin Prodrug That Is Cleaved by Matrix Metalloproteinase 2. *Cancer. Res*. **2003**, 63, 4062-4066.

46. Abu Ajaj, K.; Graeser, R.; Fichtner, I.; *et al.* In vitro and in vivo study of an albumin-binding prodrug of doxorubicin that is cleaved by cathepsin B. *Cancer. Chemother. Pharmacol*. **2009**, 64, 413–418.

47. Turk, B.; Turk, D.; Turk, V. Lysosomal cysteine proteases: more than scavengers. *Biochim*. *Biophys. Acta*. **2000**, 1477, 98–111.

48. Buck, M.R.; Karustis, D.G.; Day, N.A.; *et al.* Degradation of extracellular-matrix proteins by human cathepsin B from normal and tumour tissues. *Biochem. J.* **1992**, 282, 273–278.

49. Mai, J.; Sameni, M.; Mikkelsen, T.; *et al.* Degradation of extracellular matrix protein tenascin-C by cathepsin B: an interaction involved in the progression of gliomas. *Biol. Chem.* **2002**, 383, 1407–1413.

50. Barthel, B.L.; Zhang, Z.; Rudnicki, D.L.; *et al.* Preclinical efficacy of a carboxylesterase 2-activated prodrug of Doxazolidine. *J. Med. Chem*. **2009**, 52, 7678-7688.

51. Barthel, B.L.; Torres, R.C.; Hyatt, J.L.; *et al.* Identification of human intestinal carboxylesterase as the primary enzyme for activation of a doxazolidine carbamate prodrug. *J. Med. Chem.* **2008**, 51, 298-304. Epub 2008 Jan 4.

52. Burkhart, D.J.; Barthel, B.L.; Post, G.C.; *et al.* Design, Synthesis, and Preliminary Evaluation of Doxazolidine Carbamates as Prodrugs Activated by Carboxylesterases. *J. Med. Chem*. **2006**, 49, 7002-7012.

53. Burke, P.J.; Koch, T.H. Design, synthesis, and biological evaluation of doxorubicin-formaldehyde conjugates targeted to breast cancer cells. *J. Med. Chem*. **2004**, 47, 1193-1206.

54. Burke, P.J.; Koch, T.H. Doxorubicin-formaldehyde conjugate, doxoform: induction of apoptosis relative to doxorubicin. *Anticancer. Res*. **2001**, 21, 2753-2760.

55. Walko, C.M.; Lindley, C. Capecitabine: a review. *Clin. Ther*. **2005**, 27, 23-44.

56. Parker, W.B.; Y.C. Cheng. Metabolism and mechanism of action of 5-fluorouracil. *Pharmacol. Ther*. **1990**, 48, 381-95.

57. Wagstaff, A.J.; Ibbotson, T.; Goa, K.L. Capecitabine: a review of its pharmacology and therapeutic efficacy in the management of advanced breast cancer. *Drugs*. **2003**, 63, 217-236.

58. Post, G. C.; Barthel, B. L.; Burkhart, D. J.; Hagadorn, J. R.; Koch, T. H. Doxazolidine, a proposed active metabolite of doxorubicin that cross-links DNA. *J Med Chem*. **2005**, 48, 7648-57.

59. Gude, M.; Ryf, J.; White, P. An accurate method for quantitation of Fmoc-derivitized solid phase supports. *Letters in Peptide Science*. **2002**, 9, 203-206.

60. Rusiecki, V.K.; Warne,S.A. Synthesis of N_{α}-Fmoc-N_{ε}-Nvoc-Lysine and use in the preparation of selectively functionalized peptides. *Bioorg. Med. Chem*. Lett. **1993**. 3, 707-710.

Collected Bibliography

Chapter 1 Introduction

1. Weiss, R.B. The anthracyclines: will we ever find a better doxorubicin?. *Semin. Oncol.* **1992**, 19, 670-686.

2. Tan, C.; Tasaka, H.; Yu, K.P.; Murphy, M.L.; *et al.* Daunomycin, an antitumor antibiotic, in the treatment of neoplastic disease. Clinical evaluation with special reference to childhood leukemia. *Cancer.* **1967**, 20, 333-353.

3. Arcamone, F.; Cassinelli, G.; Fantini, G.; *et al.* Adriamycin, 14-hydroxydaunomycin, a new antitumor antibiotic from *S. peucetius* var. *caesius*. *Biotechnol. Bioeng.* **1969**, 11, 1101-1110.

4. Di Marco, A.; Gaetani, M.; Scarpinato, B. Adriamycin (NSC-123,127): a new antibiotic with antitumor activity. *Cancer. Chemother. Rep.* **1969**, 53, 33-37.

5. Young, R.C.; Ozols, R.F.; Myers, C.E. The anthracycline antineoplastic drugs. *N. Engl. J. Med.* **1981**, 305, 139-153.

6. Merck pharmaceuticals Home Page. http://Merck.com (accessed January 2012).

7. Von Hoff, D.D.; Layard, M. Risk factors for the development of daunorubicin cardiotoxicity. *Cancer. Treat. Rep.* **1982**, 65, 19-24.

8. Bristow, M.R.; Mason, J.W.; Billingham, M.E.; *et al*: Doxorubicin cardiomyopathy: Evaluation by phonocardiography, endomyocardial biopsy, and cardiac catheterization. *Ann. Intern. Med.* **1978**, 88, 168-175.

9. Von Hoff, D.D.; Layard, M.W.; Basa, P.; *et al*. Risk factors for doxorubicin-induced congestive heart failure. *Ann. Intern. Med*. **1979**, 91, 710-717.

10. Praga, C.; Beretta, G.; Vigo, P.L.; *et al*. Adriamycin cardiotoxicity: A survey of 1,273 patients. *Cancer. Treat. Rep*. **1979**, 63, 827-834.

11. Suzuki, T.; Kanda, H.; Kawai, Y.; *et al.* Cardiotoxicity of anthracycline antineoplastic drugs-Clinicopathological and experimental studies. *Jpn. Circ. J*. **1979**, 43, 1000-1008.

12. Gralla, E.J.; Fleischman, R.W.; Luthra, Y.K.; *et al*. The dosing schedule dependent toxicities of Adriamycin in beagle dogs and rhesus monkeys. *Toxicology*. **1979**, 13, 263-273.

13. Chlebowski, R.T.; Paroly, W.S.; Pugh, R.P.; *et al*. Adriamycin given as a weekly schedule without a loading dose: Clinically effective with reduced incidence of cardiotoxicity. *Cancer. Treat. Rep*. **1980**, 64, 47-51.

14. Minow, R.A.; Benjamin, R.S.; Gottlieb, J.A. Adriamycin (NSC-123127) cardiomyopathy-An overview with determination of risk factors. *Cancer. Chemother. Rep*. **1975**, 6, 195-201.

15. Buzdar, A.U.; Legha, S.S.; Tashima, C.K.; *et al*. Adriamycin and mitomycin C: Possible synergistic cardiotoxicity. *Cancer. Treat. Rep*. **1978**, 62, 1005-1008.

16. Bhanot, P.; Cushing, B.; Philippart, A.; *et al*. Hepatic irradiation and adriamycin cardiotoxicity. *J. Pediatr*. **1979**, 95, 561-563.

17. Beretta, G.; Villani, F. Cardiomyopathy in adults after combination Adriamycin and D1IC (Letter). *Cancer. Treat. Rep*. **1980**, 64, 353.

18. Mosijczuk, A.D.; Ruymann, F.B.; Mease, A.D.; *et al*. Anthracycline cardiomyopathy in children:report of two cases. *Cancer*. **1979**, 44, 1582-1587.

19. Steinherz, L.J.; Steinherz, P.G.; Mangiacasale, D.; *et al*. Cardiac abnormalities after AMSA administration. *Cancer. Treat. Rep*. **1982**, 66, 483-488.

20. Gottlieb, S.L.; Edmiston, A.; Haywood, l.J. Late, late doxorubicin cardiotoxicity. *Chest* **1980**, 78, 880-882.

21. Lefrak, E.A.; Pitha, J.; Rosenheim, S., *et al*. Adriamycin (NSC-123127) cardiomyopathy. *Cancer. Chemother. Rep*. **1975**, 6, 203-208.

22. Doroshow, J.H.; Locker, G.Y.; Myers, C.E. Experimental animal models of adriamycin cardiotoxicity. *Cancer. Treat. Rep*. **1979**, 63, 855-860.

23. Doroshow, J.H.; Locker, G.Y.; Myers, C.E. Enzymatic defenses of the mouse heart against reactive oxygen metabolites: alterations produced by doxorubicin. *J. Clin. Invest*. **1980**, 65, 128-135.

24. Myers, C.E.; McGuire, W.P.; Liss, R.H.; *et al*. Adriamycin: The role of the lipid peroxidation in cardiac toxicity and tumor response. *Science.* **1977**, 197, 165-167.

25. Stuart, M.J.; deAlarcon, P.A.; Oski, F.A. Inhibition of Adriamycin(ADR) induced lipid peroxidation by α-tocopherol (α-T) and acetylsalicylic acid (ASA) (abstr). *Pediatr. Res*. **1978**, 12, 474.

26. Flohé, L.; Zimmermann, R. The role of GSH peroxidase in protecting the membrane of rat liver mitochondria. *Biochem. Biophys. Acta*. **1970**, 223, 210-213.

27. Chow, C.K.; Tappel, A.L. Response of glutathione peroxidase to dietary selenium in rats. *J. Nutr*. **1974**, 104, 444-451.

28. Thayer, W.S. Adriamycin stimulated superoxide formation in submitochondrial particles. *Chem. Biol. Interact*. **1977**, 19, 265-278.

29. Olson, R.D.; MacDonald, J.S.; vanBoxtel, C.J.; *et al*. Regulatory role of glutathione and soluble sulfhydryl groups in the toxicity of adriamycin. *J. Pharmacol. Exp. Ther*. **1980**, 215, 450-454.

30. Kosower, E.M. A role for glutathione in muscle contraction. *Experientia.* **1970**, 26, 760-761.

31. Kishi, T.; Folkers, K. Prevention by coenzyme Q1O (NSC-140865) of the inhibition by adriamycin (NSC-123127) of coenzyme Q10 enzymes (Letter). *Cancer. Treat. Rep*. **1976**, 60, 223-224.

32. Kishi, T.; Watanabe, T.; Folkers, K. Bioenergetics in clinical medicine: Prevention by forms of coenzyme Q of the inhibition by adriamycin of coenzyme Q10-enzymes in mitochondria of the myocardium. *Proc. Natl. Acad. Sci .USA*. **1976**, 73, 4653-4656.

33. Minotti, G; Recalcati, S; Mordente, A.; *et al*. The secondary alcohol metabolite of doxorubicin irreversibly inactivates aconitase/iron regulatory protein-1 in cytosolic fractions from human myocardium. *Faseb J.* 1998, 12, 541-552.

34. Hentze, M.W.; Kühn, L.C. Molecular control of vertebrate iron metabolism: mRNA-based regulatory circuits operated by iron, nitric oxide, and oxidative stress. *Proc. Natl. Acad. Sci. USA.* **1996**, 93, 8175–8182.

35. Minotti, G.; Cavaliere, A.F.; Mordente, A.; *et al*. Secondary alcohol metabolites mediate iron delocalization in cytosolic fractions of myocardial biopsies exposed to anticancer anthracyclines Novel linkage between anthracycline metabolism and iron-induced cardiotoxicity. *J. Clin. Invest.* **1995**, 95, 1595–1605.

36. Minotti, G.; Cairo, G.; Monti, E. Role of iron in anthracycline cardiotoxicity: new tunes for an old song?. *Faseb J*. **1999**, 13, 199-212.

37. Kühn, L.C.; Hentze, M.W. Coordination of cellular iron metabolism by post-transcriptional gene regulation. J*. Inorg. Biochem*. **1992**, 47, 183-195.

38. Mascotti, D.P.; Rup, D.; Thach, R.E. Regulation of iron metabolism: translational effects mediated by iron, heme, and cytokines. *Annu. Rev. Nutr.* **1995**, 15, 239-261.

39. Taatjes, D.J.; Gaudiano, G.; Koch, T.H. Production of formaldehyde and DNA-adriamycin or DNA-daunomycin adducts, initiated through redox chemistry of dithiothreitol/iron, xanthine oxidase/NADH/iron, or glutathione/iron. *Chem. Res. Toxicol.* **1997**, 10, 953-961.

40. Capranico, G.; Zunino, F. DNA topoisomerase-trapping antitumor drugs. *Eur. J. Cancer*. **1992**, 28, 2055-2060.

41. Zunino, F.; Capranico, G. Sequence-selective groove binders. In: Tericher B (ed) Cancer therapeutics: experimental and clinical agents(Humana press, Totowa New Jersey 1997).

42. Capranico, G.; Binaschi, M.; Borgnetto, M.E.; *et al*. A protein-mediated mechanism for the DNA sequence-specific action of topoisomerase II poisons. *Trends. Pharmacol. Sci.* **1997**, 18, 323-329.

43. Gewirtz, D.A. A critical evaluation of the mechanisms of action proposed for the antitumor effects of the anthracycline antibiotics adriamycin and daunorubicin. *Biochem. Pharmacol.* **1999**, 57, 727-741.

44. Yoda, Y.; Nakazawa, M.; Abe T.; *et al.* Prevention of doxorubicin myocardial toxicity in mice by reduced glutathione. *Cancer. Res*. **1986**, 46, 2551-2556.

45. Cervantes, A.; Pinedo, H.M.; Lankelma, J.; Schuurhuis, G.J. The role of oxygen-derived free radicals in the cytotoxicity of doxorubicin in multidrug resistant and sensitive human ovarian cancer cells. *Cancer. Lett*. **1988**, 41, 169-177.

46. Shimpo, K.; Nagatsu, T.; Yamada, K.; *et al.* Ascorbic acid and adriamycin toxicity. *Am. J. Clin. Nutr*. **1991**, 54, 1298S-1301S.

47. Myers, C.; Bonow, R.; Palmeri, S.; *et al.* A randomized controlled trial assessing the prevention of doxorubicin cardiomyopathy by N-acetylcysteine. *Semin. Oncol.* **1983**, 10, Suppl 1, 53-55.

48. Wang, A.H.; Gao, Y.G.; Liaw, Y.C.; Li, Y.K. Formaldehyde cross-links daunorubicin and DNA efficiently: HPLC and X-ray diffraction studies. *Biochemistry*. **1991**, 30, 3812-3815.

49. Podell, E.R.; Harrington, D.J.; Taatjes, D.J.; Koch T.H. Crystal structure of epidoxorubicin-formaldehyde virtual crosslink of DNA and evidence for its formation in human breast-cancer cells. *Acta. Crystallogr. D. Biol. Crystallogr*. **1999**, 55, Pt 9, 1516-1523.

50. Taatjes, D.J.; Gaudiano, G.; Resing, K.; Koch T.H. Alkylation of DNA by the anthracycline, antitumor drugs adriamycin and daunomycin. *J. Med. Chem*. **1996**, 39, 4135-4138.

51. Swift, L.P.; Rephaeli, A.; Nudelman, A.; *et al.* Doxorubicin-DNA adducts induce a non-topoisomerase II-mediated form of cell death. *Cancer. Res*. **2006**, 66, 4863-4871.

52. Nielsen, D.; Maare, C.; and Skovsgaard, T. Cellular resistance to anthracyclines. *Gen. Pharmacol.* **1996**, 27, 251-255.

53. Longley, D.B.; Johnston, P.G. Molecular mechanisms of drug resistance. *J. Pathol*. **2005**, 205, 275-292.

54. Higgins, C.F. ABC transporters: from microorganisms to man. *Annu. Rev. Cell. Biol*. **1992**, 8, 67-113.

55. Gottesman, M.M.; Pastan, I. Biochemistry of multidrug resistance mediated by the multidrug transporter. *Annu. Rev. Biochem*. **1993**, 62, 385-427.

56. Arcamone, F. Doxorubicin Anticancer Antibiotics: Medicinal Chemistry, a Series of Medicinal Chemistry, Vol 17, (Academic Press, New York, 1981)

57. Kharsaw, M.; Bell, R.; Dang, C. Epirubicin: Is it like doxorubicin in breast cancer? A clinical review. *Breast*. **2012**, 21, 142-149. Jan 17 [Epub ahead of print].

58. Fields, S.M.; Koeller, J.M. Idarubicin: a second-generation anthracycline. *Dicp*, **199,**. 25, 505-517.

59. Mross, K.B.; Langenbuch, T.; Burk, K.;. Hossfeld, D.K. [Iodo-doxorubicin, a new anthracycline derivative. Current state of progress]. *Onkologie*, **1990,** 13, 346-351.

60. Koeller, J.; Eble, M. Mitoxantrone: a novel anthracycline derivative. *Clin Pharm*, **1988**, 7 574-581.

61. Onrust, S.V. and H.M. Lamb, Valrubicin. *Drugs Aging*, **1999,** 15, 69-75.

62. Goebel, M., Oral idarubicin--an anthracycline derivative with unique properties. *Ann Hematol*, **1993,** 66, 33-43.

63. Yoo, H.S.; Park, T.G. Folate receptor targeted biodegradable polymeric doxorubicin micelles. *J. Control. Release.* **2004**, 96, 273-283.

64. Shmeeda, H.; Mak, L.; Tzemach, D.; *et al.* Intracellular uptake and intracavitary targeting of folate-conjugated liposomes in a mouse lymphoma model with up-regulated folate receptors. *Mol. Cancer. Ther*. **2006**, 5, 818-824.

65. Xiong, X.B.; Huang, Y.; Lu, W.L.; *et al.* Enhanced intracellular delivery and improved antitumor efficacy of doxorubicin by sterically stabilized liposomes modified with a synthetic RGD mimetic. *J. Control. Release.* **2005**, 107, 262-275.

66. Schiffelers, R.M.; Koning, G.A.; ten Hagen, T.L.; *et al.* Anti-tumor efficacy of tumor vasculature-targeted liposomal doxorubicin. *J. Control. Release*. **2003**, 91, 115-122.

67. Dvorak, H.F. Leaky tumor vessels: consequences for tumor stroma generation and for solid tumor therapy. *Prog. Clin. Biol. Res.* **1990**, 354A, 317-330.

68. Maeda, H.; Wu, J.; Sawa, T.; *et al.* Tumor vascular permeability and the EPR effect in macromolecular therapeutics: a review. *J. Control. Release*. **2000**, 65, 271-284.

69. Fang, J.; Nakamura, H.; Maeda, H. The EPR effect: Unique features of tumor blood vessels for drug delivery, factors involved, and limitations and augmentation of the effect. *Adv. Drug. Deliv. Rev.* **2011**, 63, 136-151.

70. Florent, J.C.; Monneret, C. Doxorubicin Conjugates for Selective Delivery to Tumors. *Top. Curr. Chem.* **2008**, 283, 99-140.

71. Trail, P.A.; King, H.D.; Dubowchik, G.M. Monoclonal antibody drug immunoconjugates for targeted treatment of cancer. *Cancer. Immunol. Immunother*. **2003**, 52, 328-337.

72. Dubowchik, G.M.; Radia, S.; Mastalerz, H.; *et al.* Doxorubicin immunoconjugates containing bivalent, lysosomally-cleavable dipeptide linkages. *Bioorg. Med. Chem. Lett*. **2002**, 12, 1529-1533.

73. Denny, W.A. Tumor activated prodrugs-a new approach to cancer therapy. *Cancer. Invest*. **2004**, 22, 604-619.

74. Dang, L.H.; Bettegowda, C.; Huso, D.L.; *et al.* Combination bacteriolytic therapy for the treatment of experimental tumors. *Proc. Natl. Acad. Sci. USA*. **2001**, 98, 15155-15160.

75. Chakravarty, P.K.; Carl, P.L.; Weber, M.J.; and Katzenellenbogen, J.A. Plasmin-activated prodrugs for cancer chemotherapy. 2. Synthesis and biological activity of peptidyl derivatives of doxorubicin. *J. Med. Chem*. **1983**, 26, 638-644.

76. de Groot, F.M.; de Bart, A.C.; Verheijen, J.H.; *et al.* Synthesis and biological evaluation of novel prodrugs of anthracyclines for selective activation by the tumor-associated protease plasmin. *J. Med. Chem*. **1999**, 42, 5277-5283.

77. Albright, C.F.; Graciani, N.; Han, W.; *et al.* Matrix metalloproteinase–activated doxorubicin prodrugs inhibit HT1080 xenograft growth better than doxorubicin with less toxicity. *Mol. Cancer. Ther*. **2005**, 4, 751-760.

78. Liu, C.; Sun, C.; Huang, H.; *et al.* Overexpression of legumain in tumors is significant for invasion/metastasis and a candidate enzymatic target for prodrug therapy. *Cancer. Res*. **2003**, 63, 2957-2964.

79. Kato, S.; Burke, P. J.; Koch, T.H.; *et al.* Mass spectrometric measurement of formaldehyde generated in breast cancer cells upon treatment with anthracycline antitumor drugs. *Chem. Res. Toxicol.* **2000**, *13*, 509-516.

80. Post, G. C.; Barthel, B. L.; Koch, T.H.; *et al.* Doxazolidine, a proposed active metabolite of doxorubicin that cross-links DNA. *J. Med. Chem.* **2005**, *48*, 7648-7657.

81. Kato, S.; Burke, P. J.; Koch, T.D.; *et al.* Mass spectrometric measurement of formaldehyde generated in breast cancer cells upon treatment with anthracycline antitumor drugs. *Chem. Res. Toxicol.* **2000**, *13*, 509-516.

82. Fenick, D. J.; Taatjes, D. J.; Koch, T. H. Doxoform and Daunoform: Anthracycline-formaldehyde conjugates toxic to resistant tumor cells. *J. Med. Chem.* **1997**, *40*, 2452-2461.

83. Cogan, P. S.; Fowler, C. R.; Post, G. C.; Koch, T. H. Doxsaliform: A novel N-Mannich base prodrug of a doxorubicin formaldehyde conjugate. *Lett. Drug Des. Dis.* **2004**, *1*, 247-255.

84. Meyer, A.; Auernheimer, J.; Modinger, A.; *et al.* Targeting RGD recognizing integrins: drug development, biomaterial research, tumor imaging and targeting. **2006**, 12, 2723-2747.

85. Kalet, B.T.; McBryde, M.B.; Espinosa, J.M.; Koch, T.H. Doxazolidine induction of apoptosis by a topoisomerase II independent mechanism. *J. Med. Chem*. **2007**, 50, 4493-4500.

Chapter 2 Protease Activated Prodrugs of Doxazolidine

1. López-Otín, C.; Matrisian, L.M. Emerging roles of proteases in tumour suppression. *Nat. Rev. Cancer*. **2007**, 7, 800-808.

2. Gabriel, D.; Zuluaga, M.F.; van den Bergh, H.; *et al*. It is all about proteases: From drug delivery to in vivo imaging and photomedicine. *Curr. Med. Chem*. **2011**, 18, 1785–1805.

3. Pollard, J.W. Tumour-educated macrophages promote tumour progression and metastasis. *Nat. Rev. Cancer*. **2004**, 4, 71–78.

4. Coussens, L.M.; Werb, Z. Inflammation and cancer. *Nature*. **2002**, 420, 860–867.

5. Nyberg, P.; Salo, T.; Kalluri, R. Tumor microenvironment and angiogenesis. *Front. Biosci*. **2008**, 13, 6537-6553.

6. Borgoño, C.A.; Diamandis, E.P. The emerging roles of human tissue kallikreins in cancer. *Nat. Rev. Cancer*. **2004**, 4, 876–890.

7. Kalluri, R. Basement membranes: structure, assembly and role in tumour angiogenesis. Nat. Rev. Cancer. **2003**, 3, 422-433.

8. Sund, M.; Xie, L.; Kalluri, R. The contribution of vascular basement membranes and extracellular matrix to the mechanics of tumor angiogenesis. *Apmis*, **2004**, 112, 450- 462.

9. Bernik, M.B.; Kwaan, H.C. Plasminogen activator activity in cultures from human tissues. An immunological and histochemical study. *J. Clin. Invest.* **1969**, 48, 1740–1753.

10. Bernik, M.B.; Kwaan, H.C. Origin of fibrinolytic activity in cultures of the human kidney. *J. Lab. Clin. Med*. **1967**, 70, 650–661.

11. Blasi, F.; Carmeliet, P. uPAR: a versatile signalling orchestrator. *Nat. Rev. Mol. Cell. Biol.* **2002**, 3, 932–943.

12. Wall, M.E.; Wani, M.C.; Cook, C.E.; *et al.* Plant antitumor agents, I: the isolation and structure of camptothecin, a novel alkaloidal leukemia and tumor inhibitor from Camptotheca acuminate. *J. Am. Chem. Soc.* **1966**, 88, 3888-3890.

13. Hsiang, Y.H.; Hertzberg, R.; Hecht, S.; *et al*. Camptothecin induces protein-linked DNA breaks via mammalian DNA topoisomerase I. *J. Biol. Chem.* **1985**, 260, 14873-14878.

14. Rivory, L.P.; Bowles, M.R.; Robert, J.; *et al.* Conversion of irinotecan (CPT-11) to its active metabolite, 7-ethyl-10-hydroxycamptothecin (SN-38), by human liver carboxylesterase. *Biochem. Pharmacol*. **1996,** 52, 1103-1111.

15. Bencharit, S.; Morton, C.L.; Xue, Y.; *et al. St*ructural basis of heroin and cocaine metabolism by a promiscuous human drug-processing enzyme. *Nat. Struct. Biol.* **2003**, 10, 349-356.

16. Sanghani, S.P.; Quinney, S.K.; Fredenburg, T.B.; *et al.* Hydrolysis of irinotecan and its oxidative metabolites, 7-ethyl-10-[4-N-(5-aminopentanoic acid)-1-piperidino] carbonyloxycamptothecin and 7-ethyl-10-[4-(1-piperidino)-1-amino]-carbonyloxycamptothecin, by human carboxylesterases CES1A1, CES2, and a newly expressed carboxylesterase isoenzyme, CES3. *Drug. Metab. Dispos*. **2004**, 32, 505-511.

17. Durand, M.K.; Bødker, J.S.; Christensen, A.; *et al*. Plasminogen activator inhibitor-I and tumour growth, invasion, and metastasis. *Thromb. Haemost*. **2004**, 91, 438–449.

18. Mignatti, P.; Rifkin, DB. Biology and biochemistry of proteinases in tumor invasion. *Physiol. Rev.* **1993**, 73, 161–195.

19. Kwaan, HC. The plasminogen-plasmin system in malignancy. *Cancer. Metastasis. Rev*. **1992**, 11, 291–311.

20. Danø, K.; Andreasen, P.A.; Grøndahl –Hansen, J.; *et al.* Plasminogen activators, tissue degradation, and cancer. *Adv. Cancer. Res.* **1985**, 44, 139–266.

21. Kirchheimer, J.C.; Wojta, J.; Christ, G.; *et al*. Proliferation of a human epidermal tumor cell line stimulated by urokinase. *Faseb.J*. **1987**, 1, 125–128.

22. Kirchheimer, J.C.; Wojta, J.; Hienert, G.; *et al*. Effect of urokinase on the proliferation of primary cultures of human prostatic cells. *Thromb. Res*. **1987**, 48, 291–298.

23. Kwaan, H.C.; Wang, J.; Svoboda, K.; *et al*. Plasminogen activator inhibitor 1 may promote tumour growth through inhibition of apoptosis. *Br. J. Cancer*. **2000**, 82, 1702–1708.

24. Soff, G.A.; Sanderowitz, J.; Gately, S.; *et al*. Expression of plasminogen activator inhibitor type 1 by human prostate carcinoma cells inhibits primary tumor growth, tumorassociated angiogenesis, and metastasis to lung and liver in an athymic mouse model. *J. Clin. Invest.* **1995**, 96, 2593–2600.

25. Madsen, C.D.; Ferraris, G.M.; Andolfo, A.; *et al.* uPAR-induced cell adhesion and migration: vitronectin provides the key. *J. Cell. Biol.* **2007**, 177, 927–939.

26. Caiolfa, V.R.; Zamai, M.; Malengo, G.; *et al.* Monomer dimer dynamics and distribution of GPI-anchored uPAR are determined by cell surface protein assemblies. *J. Cell. Biol.* **2007**, 179, 1067–1082.

27. Cunningham, O.; Andolfo, A.; Santovito, M.L.; *et al.* Dimerization controls the lipid raft partitioning of uPAR/CD87 and regulates its biological functions. *EMBO. J.* **2003**, 22, 5994–6003.

28. Choi, K.Y.; Swierczewska, M.; Lee, S.; *et al.* Protease-Activated Drug Development. *Theranostics.* **2012**, 2, 156–178.

29. Cao, Y.; Cao, R.; Veitonmäki, N. Kringle structures and antiangiogenesis. *Curr. Med. Chem. Anticancer. Agents*. **2002**, 2, 667-681.

30. Albright, C.F.; Graciani, N.; Han, w.; *et al.* Matrix metalloproteinase-activated doxorubicin prodrugs inhibit HT1080 xenograft growth better than doxorubicin with less toxicity. *Mol. Cancer. Ther.* **2005**, 4, 751-760.

31. Kline, T.; Torgov, M.Y.; Mendelsohn, B.A.; *et al.* Novel antitumor prodrugs designed for activation by matrix metalloproteinases-2 and -9. *Mol. Pharm*. **2004**, 1, 9-22.

32. Kratz, F.; Drevs, J.; Bing, G.; *et al.* Development and in vitro efficacy of novel MMP2 and MMP9 specific doxorubicin albumin conjugates. *Bioorg. Med. Chem. Lett.* **2001**, 11, 2001-2006.

33. Dubowchik, G.M.; Mosure, K.; Knipe, J.O.; *et al.* Cathepsin B-sensitive dipeptide prodrugs. 2. Models of anticancer drugs paclitaxel (Taxol), mitomycin C and doxorubicin. *Bioorg. Med. Chem. Lett*. **1998**, 8, 3347-3352.

34. Warnecke, A.; Fichtner, I.; Sass, G.; *et al.* Synthesis, cleavage profile, and antitumor efficacy of an albumin-binding prodrug of methotrexate that is cleaved by plasmin and cathepsin B. *Arch Pharm (Weinheim).* **2007**, 340, 389-395.

35. Chakravarty, P.K.; Carl, P.L.; Weber, M.J.; *et al.* Plasmin-activated prodrugs for cancer chemotherapy. 2. Synthesis and biological activity of peptidyl derivatives of doxorubicin. *J. Med. Chem*. **1983**, 26, 638-644.

36. de Groot, F.M.; de Bart, A.C.; Verheijen, J.H.; *et al.* Synthesis and biological evaluation of novel prodrugs of anthracyclines for selective activation by the tumor-associated protease plasmin. *J. Med. Chem*. **1999**, 42, 5277-5283.

37. Devy, L.; de Groot, F.M.; Blacher, S.; *et al.* Plasmin-activated doxorubicin prodrugs containing a spacer reduce tumor growth and angiogenesis without systemic toxicity. *Faseb. J.* **2004**, 18, 565-567.

38. Post, G. C.; Barthel, B. L.; Burkhart, D. J.; Hagadorn, J. R.; Koch, T. H. Doxazolidine, a proposed active metabolite of doxorubicin that cross-links DNA. *J Med Chem*. **2005**, 48, 7648-57.

39. Gude, M.; Ryf, J.; White, P. An accurate method for quantitation of Fmoc-derivitized solid phase supports. *Letters in Peptide Science*. **2002**, 9, 203-206.

40. Low, T. L.; Goldstein, A. L. The chemistry and biology of thymosin. II. Amino acid sequence analysis of thymosin alpha1 and polypeptide beta1. *J. Biol. Chem.* **1979**, 254, 987-95.

41. Abiko, T.; Sekino, H. Synthesis of an immunologically active fragment analog of prothymosin alpha with enhanced enzymatic stability. *Chem Pharm Bull (Tokyo).* **1991**, 39, 752-756.

42. Nguyen, L. T.; Chau, J. K.; Perry, N. A.; de Boer, L.; Zaat, S. A.; Vogel, H. J. Serum stabilities of short tryptophan- and arginine-rich antimicrobial peptide analogs. *PLoS One.* **2010**, 5.

43. Huang, Y.; Tan, M.; Gosink, M. Wang, K.W.; Sun, Yi. Histone deacetylase 5 is not a p53 target gene, but its overexpression inhibits tumor cell growth and induces apoptosis. *Cancer Res.* **2002.** 62, 2913-2922.

44. Wilson, A.J.; Byun, D.S.; Nasser, S.; *et al.* HDAC4 Promotes growth of colon cancer cells via repression of p21. *Mol. Bio. Cell*. **2008**, 19, 4062-4075.

45. Gallinari, P.; Di Marco, S.; Jones, P.; Pallaoro, M.; Steinkühler, C. HDACs, histone deacetylation and gene transcription: from molecular biology to cancer therapeutics. *Cell Res*. **2007**, 17, 195-211.

46. Matsuoka, H.; Fujimura, T.; Hayashi, M.; *et al*. Disruption of HDAC4/N-CoR complex by histone deacetylase inhibitors leads to inhibition of IL-2 gene expression. *Biochem. Pharm*. **2007**, 74, 465-476.

47. Avvakumov, N. Côté. The MYST family of histone acetyltransferases and their intimate links to cancer. *Oncogene*. **2007**, 26, 5395-5407.

48. Lahm, A.; Paolini, C.; Pallaoro, M.; *et al*. Unraveling the hidden catalytic activity of vertebrate classIIa histone deacetylases. *PNAS*. **2007**, 104, 17335-17340.

49. Dekker, G.J.; Haisma, H.J. Histone acetyl transferases as emerging drug targets. *Drug Discov. Today*. **2009**, 14, 942-948.

Chapter 3 Prodrugs Activated by Hypoxic Conditions

1. Dewhirst, M. W.; Cao, Y; Moeller, B. Cycling hypoxia and free radicals regulate angiogenesis and radiotherapy response. *Nature. Rev. Cancer.* **2008,** 8, 425–437.

2. Wilson, W.R; Hay, M.P. Targeting hypoxia in cancer therapy. *Nature. Rev. Cancer.* 11, 4, 393-410.

3. Erler, J.T.; Cawthorne, C.J.; Williams, K.J.; *et al.* Hypoxia-mediated down-regulation of Bid and Bax in tumors occurs via hypoxia-inducible factor 1-dependent and -independent mechanisms and contributes to drug resistance. *Mol. Cell. Biol.* **2004**, 24, 2875–2889.

4. Cairns, R. A., Harris, I. S.; Mak, T. W. Regulation of cancer cell metabolism. *Nature Rev. Cancer.* **2011**, 11, 85–95.

5. Wang, Y.; Ohh, M. Oxygen-mediated endocytosis in cancer. *J. Cell. Mol. Med.* **2010**, 14, 496–503.

6. Kioi, M.; Vogel, H.; Schultz, G.; *et al.* Inhibition of vasculogenesis, but not angiogenesis, prevents the recurrence of glioblastoma after irradiation in mice. *J. Clin. Invest.* **2010,** 120, 695–705.

7. Hill, R.P.; Marie-Egyptienne, D.T.; Hedley, D.W. Cancer stem cells, hypoxia and metastasis. *Semin. Radiat. Oncol.* **2009**, 19, 106–111.

8. Guzy, R.D.; Hoyos, B.; Robin, E.; *et al.* Mitochondrial complex III is required for hypoxia-induced ROS production and cellular oxygen sensing. *Cell. Metab.* **2005**, 1, 401–408.

9. Bristow, R.G.; Hill, R.P. Hypoxia, DNA repair and genetic instability. *Nat. Rev. Cancer.* **2008,** 8, 180–192.

10. Semenza, G.L. Targeting HIF-1 for cancer therapy. *Nature Rev. Cancer*. **2003**, 3, 721–732.

11. Li, F.; Sonveaux, P.; Rabbani, Z.N.; *et al.* Regulation of HIF-1α stability through S-nitrosylation. *Mol. Cell.* **2007**, 26, 63–74.

12. Chandel, N.S.; McClintock, D.S.; Feliciano, C.E.; *et al.* Reactive oxygen species generated at mitochondrial complex III stabilize hypoxia-inducible factor-1α during hypoxia: a mechanism of O2 sensing. *J. Biol. Chem.* **2000**, 275, 25130–25138.

13. Tozer, G.M.; Everett, S.A. Nitric oxide in tumor biology and cancer therapy. Part 2: Therapeutic implications. *Clin. Oncol. (R. Coll. Radiol).* **1997**, 9, 357–364.

14. Tozer, G.M.; Everett, S.A. Nitric oxide in tumour biology and cancer therapy. Part 1: Physiological aspects. *Clin. Oncol. (R. Coll. Radiol).* **1997,** 9, 282–293.

15. Bell, E.L.; Klimova, T.A.; Eisenbart, J.: *et al.* The Qo site of the mitochondrial complex III is required for the transduction of hypoxic signaling via reactive oxygen species production. *J. Cell Biol.* **2007**, 177, 1029–1036.

16. Brown, J. M. Clinical trials of radiosensitizers: what should we expect? *Int. J. Radiat. Oncol. Biol. Phys.* **1984,** 10, 425–420.

17. Connors, T.A.; Whisson, M.E. Cure of mice bearing advanced plasma cell tumours with aniline mustard: the relationship between glucuronidase activity and tumour sensitivity. *Nature.* **1966,** 210, 866–867.

18. Knox, R.J.; Boland, M.P.; Friedlos F.; *et al.* The nitroreductase enzyme in Walker cells that activates 5-(aziridin-1-yl)-2,4-dinitro-benzamide (CB 1954) to 5-(aziridin-1-yl)-4-hydroxylamino-2-nitrobenzamide is a form of NAD(P)H dehydrogenase (quinone) (EC 1.6.99.2). *Biochem. Pharmacol.* **1988**, 37, 4671–4677.

19. Long, D.J.; Jaiswal, A.K. NRH: quinone oxidoreductase2 (NQO2) *Chemino-Biol. Interact.* **2000**, *129*, 99-112.

20. Skelly, J.V.; Knox, R.J.; Jenkins, T.C. Aerobic nitroreduction by flavoproteins: enzyme structure, mechanism and role in cancer chemotherapy. *Mini. Rev. Med. Chem.* **2001**, *1*, 293-306.

21. Bianchet, M.A.; Faig, M.; Amzel, L.M. Structure and mechanism of NAD(P)H: quinone accpetor oxidoreductases (NQO). *Methods. Enzymol.* **2004**, *382*, 144-174.

22. Niculescu-Duvaz, I.; Cooper, R.G.; Stribbling, S.M.; *et al.* Recent developments in genedirected enzyme prodrug therapy (GDEPT) for cancer. *Curr. Opin. Mol. Ther.* **1999**, *4*, 480-486.

23. Knox, R.J.; Jenkins, T.C.; Hobbs, S.M.; *et al.* Bioactivation of 5-(Aziridine-1-yl)-2,4-dinitrobenzamide (CB1954) by human NADPH Quinone Oxidoreductase 2: A Novel Cosubstrate-mediated Antitumor Prodrug Therapy. *Cancer. Res.* **2000**, *60*, 4179-4186.

24. Knox, J.R.; Burke, P.J.; Chen, S.; *et al.* CB 1954: from the Walker tumor to NQO2 and VDEPT. *Curr. Pharm. Des.* **2003**, *9*, 2091-2104.

25. AbuKhader, M.; Heap, J.; De Matteis, C.; *et al.* Binding of the anticancer prodrug CB1954 to the activating enzyme NQO2 revealed by the crystal structure of their complex. *J. Med. Chem*. **2005**, 48, 7714-7719.

26. Patterson, A.V.; Ferry, D.M.; Edmunds, S.J.; *et al.* Mechanism of action and preclinical antitumor activity of the novel hypoxia-activated DNA cross-linking agent PR-104. *Clin. Cancer. Res*. **2007**, 13, 3922-3932.

27. McKeage, M.J.; Gu, Y.; Wilson, W.R.; Hill, A.; Amies, K.; Melink, T.J.; Jameson, M.B. McKeage et al. *BMC Cancer* **2011**, 11, 432-446.

28. Guise, C.P.; Abbattista, M.R.; Singleton, R.S.; *et al.* The bioreductive prodrug PR-104A is activated under aerobic conditions by human aldo-keto reductase 1C3. *Cancer. Res.* **2010,** 70, 1573–1584.

29. Birtwistle, J.; Hayden, R.E.; Khanim, F.L.; *et al.* The aldo-keto reductase AKR1C3 contributes to 7,12-dimethylbenz(a) anthracene-3,4-dihydrodiol mediated oxidative DNA damage in myeloid cells: implications for leukemogenesis. *Mutat. Res.* **2009**, 662, 67–74.

30. Guise, C.P. *et al.* Identification of human oxidoreductases involved in the hypoxia-dependent activation of bioreductive prodrugs. *Proc. Am. Assoc. Cancer. Res.* **2010**, 51, Abstract 453.

31. Hodnick, W.F.; Sartorelli, A. C. Reductive activation of mitomycin C by NADH:cytochrome *b*5 reductase. *Cancer. Res.* **1993**, 53, 4907–4912.

32. Miskiniene, V.; Dickancaite, E.; Nemeikaite, A.; *et al.* Nitroaromatic betulin derivatives as redox cycling agents. *Biochem. Mol. Biol. Int.* **1997**, 42, 391–397.

33. Yan, C.; Kepa, J.K.; Siegel, D.; *et al.* Dissecting the role of multiple reductases in bioactivation and cytotoxicity of the antitumor agent 2, 5-diaziridinyl-3-(hydroxymethyl)-6-methyl-1,4-benzo quinone (RH1). *Mol. Pharmacol.* **2008**, 74, 1657–1665.

34. Kutcher, W.W.; McCalla, D.R. Aerobic reduction of 5-nitro-2-furaldehyde semicarbazone by rat liver xanthine dehydrogenase. *Biochem. Pharmacol.* **1984**, 33, 799–805.

35. Seow, H.A.; Penketh, P.G.; Shyam, K.; *et al.* A.C. 1,2-Bis(methylsulfonyl)-1-(2-chloroethyl)-2-[[1-(4-nitrophenyl)ethoxy]carbonyl]hydrazine: an anticancer agent targeting hypoxic cells. *Proc. Natl. Acad. Sci*. *USA*. **2005**, 102, 9282-9287.

36. Erler, J.T.; Giaccia, A.J. Lysyl oxidase mediates hypoxic control of metastasis. *Cancer Res*. **2006**, 66, 10238–10241.

37. Dawson, D.A.; Rinaldi, A.C.; Pöch, G. Biochemical and toxicological evaluation of agent-cofactor reactivity as a mechanism of action for osteolathyrism. *Toxicology*. **2002**, 177, 267–284.

38. Bachhuber, T.E.; Lalich, J.J.; Angevine, D.M.; Schilling, E.D.; Strong, F.M. Lathyrus factor activity of beta-aminopropionitrile and related compounds. *Proc. Soc. Exp. Biol. Med*. **1955**, 89, 294–297.

39. Granchi, C.; Funaioli, T.; Erler, J.T.; *et al.* Bioreductively activated lysyl oxidase inhibitors against hypoxic tumours. *Chem. Med. Chem*. **2009**, 4, 1590–1594.

40. Giglio, J.; Patsis, G.; Pirmettis, I.; *et al.* Preparation and characterization of technetium and rhenium tricarbonyl complexes bearing the 4-nitrobenzyl moiety as potential bioreductive diagnostic radiopharmaceuticals. In vitro and in vivo studies. *Eur. J. Med. Chem.* **2008**, 43, 741-748.

41. Mauger, A.B.; Burke, P.J, Somani, H.H.; *et al*. Self-Immolative prodrugs: Candidates for Antibody-Directed Enzyme Prodrug Therapy in Conjunction with a Nitroreductase Enzyme. *J. Med. Chem.* **1994**, 37, 3452-3458.

42. Hay, M.P.; Wilson, W.R.; Denny, W.A. Nitroarylmethylcarbamate prodrugs of doxorubicin for use with nitroreductase gene-directed enzyme prodrug therapy. *Bioorg. Med. Chem*. **2005**, 13, 4043–4055.

43. Post, G.P.; Barthel, B.L.; Koch, T.H.; *et al.* Doxazolidine, a proposed active metabolite of Doxorubicin that cross-links DNA. *J. Med. Chem*. **2005**, 48, 7648-7657.

Chapter 4 Prodrug Albumin Conjugates

1. Elsadek, B.; Kratz, F. Impact of albumin on drug delivery — New applications on the horizon. *J. Control. Release*. **2012**, 157, 4–28.

2. Kratz, F. Albumin as a drug carrier: design of prodrugs, drug conjugates and nanoparticles. *J. Control. Release*. **2008**, 132, 171–183.

3. Park, K. Albumin: A versatile carrier for drug delivery. *J. Control. Release*. **2012**, 157, 3. (Epub 2011.

4. Kratz, F.; Roth, T.; Fichiner, I.; *et al.* In vitro and in vivo efficacy of acid-sensitive transferrin and albumin doxorubicin conjugates in a human xenograft panel and in the MDA-MB-435 mamma carcinoma model, *J. Drug. Target*. **2000**, 8, 305–318.

5. Maeda, H.; Ueda, M.; Morinaga, T.; *et al.* Conjugation of poly(styrene-comaleic acid) derivatives to the antitumor protein neocarzinostatin: pronounced improvements in pharmacological properties. *J. Med. Chem*. **1985**, 28, 455–461.

6. Matsumura, Y.; Maeda, H. A new concept for macromolecular therapeutics in cancer chemotherapy: mechanism of tumoritropic accumulation of proteins and the antitumor agent smancs. *Cancer. Res*. **1986**, 46, 6387–6392.

7. Lindholm, A. New insulins in the treatment of diabetes mellitus. *Best. Pract. Res. Clin. Gastroenterol*. **2002**, 16, 475-492.

8. Hamilton-Wessler, M.; Ader, M.; Dea, M.; *et al*. Mechansim of protracted metabolic effects of fatty acid acylated insulin, NN304, in dogs: retention of NN304 by albumin. *Diabetologia.* **1999**, 42, 1254-1263.

9. Standl, E. Insulin analogues - state of the art. *Horm. Res*. **2002**, 57, Suppl 1:40-45.

10. Wootten, D.; Savage, E.E.; Valant, C.; *et al.* Allosteric modulation of endogenous metabolites as an avenue for drug discovery. *Mol. Pharmacol*. **2012**, May 10. [Epub ahead of print].

11. Flisiak, R.; Flisiak, I. Albinterferon-alpha 2b: a new treatment option for hepatitis C. *Expert. Opin. Biol. Ther.* **2010**, 10, 1509–1515.

12. Nelson, D.R.; Benhamou, Y.; Chuang, W.L.; *et al.* Albinterferon Alfa-2b was not inferior to pegylated interferon-alpha in a randomized trial of patients with chronic hepatitis C virus genotype 2 or 3. *Gastroenterology*. **2010**, 139, 1267–1276.

13. Zeuzem, S.; Sulkowski, M.S.; Lawitz, E.J.; *et al.* Albinterferon Alfa-2b was not inferior to pegylated interferon-alpha in a randomized trial of patients with chronic hepatitis C virus genotype 1. *Gastroenterology.* **2010**, 139, 1257–1266.

14. Gradishar WJ. Albumin-bound paclitaxel: a next-generation taxane. *Expert Opin Pharmacother*. **2006**. 7, 1041-1053.

15. Cortes J.; Saura C. Nanopartcle albumin-bound (nab™)-paclitaxel: improving efficacy and tolerability by targeted drug delivery in metastatic breast cancer. *Eur. J. Cancer. Suppl*. **2010**, 8, 1-10.

16. Taxotere (docetaxel) Injection Concentrate [Package Insert]. Aventis Pharmaceutical Products, Inc.; Bridgewater, NJ: 2003.

17. Taxol (paclitaxel) Injection [Package Insert]. Brystol-Meyers Squibb Co.; Princeton, NJ: 2003.

18. Weiss, R.B.; Donehower, R.C.; Wiernik, P.H.; *et al*. Hypersensitivity reactions from taxol. *J. Clin. Oncol.* **1990**, 8, 1263-1268.

19. ten Tije, A.J.; Verweij, J.; Loos, W.J.; *et al.* Pharmacological effects of formulation vehicles: implications for cancer chemotherapy. *Clin. Pharmacokinet*. **2003**, 42, 665-685.

20. Authier, N.; Gillet, J.P.; Fialip, J.; *et al*. Assessment of neurotoxicity following repeated cremophor/ethanol injections in rats. *Neurotox. Res.* **2001**, 3, 301-306.

21. Postma, T.J.; Vermorken, J.B.; Liefting, A.J.M.; *et al*. Paclitaxel-induced neuropathy. *Ann. Oncol*. **2004**, 6, 484-494.

22. Gelderblom, H.; Verweij, J.; Nooter, K.; *et al*. Cremophor EL: the drawbacks and advantages of vehicle selection for drug formulation. *Eur. J. Cancer*. **2001**, 37, 1590-1598.

23. Winer, E.P.; Berry, D.A.; Woolf, S.; *et al*. Failure of higher-dose paclitaxel toimprove outcome in patients with metastatic breast cancer: cancer and leukemia group B trial 9342. J. Clin. Oncol. **2004**, 22, 2061-2068.

24. Gradishar, W.J.; Krasnojon, D.; Cheporov, S.; *et al.* Significantly longer progression-free survival with nab-paclitaxel compared with docetaxel as first-line therapy for metastatic breast cancer. *J. Clin*. *Oncol*. **2009**, 27, 3611–3619.

25. Hawkins, M.J.; Soon-Shiong, P.; Desai, N. Protein nanoparticles as drug carriers in clinical medicine. *Adv. Drug. Deliv. Rev.* **2008**, 60, 876–885.

26. Desai, N.; Trieu, V.; Damascelli, B.: *et al.* SPARC expression correlates with tumor response to albumin-bound paclitaxel in head and neck cancer patients. *Transl. Oncol.* **2009**, 2, 59–64.

26. Tiruppathi, C.; Song, W.; Bergenfeldt, M.; *et al.* Gp60 activation mediates albumin transcytosis in endothelial cells by tyrosine kinase-dependent pathway. *J. Biol. Chem*. **1997**, 272, 25968–25975.

27. Schnitzer, J.E. gp60 is an albumin-binding glycoprotein expressed by continuous endothelium involved in albumin transcytosis. *Am. J. Physiol*. **1992**, 262, (1 Pt 2) H246–H254.

28. Wang, Z.; Tiruppathi, C.; Minshall, R.D.; *et al.* Size and dynamics of caveolae studied using nanoparticles in living endothelial cells. *ACS. Nano*. **2009**, 3, 4110–4116.

29. Sage, H.; Johnson, C.; Bornstein, P. Characterization of a novel serum albuminbinding glycoprotein secreted by endothelial cells in culture. *J. Biol. Chem.* **1984**, 259, 3993–4007.

30. Podhajcer, O.L.; Benedetti, L.G.; Girotti, M.R.; *et al.* The role of the matricellular protein SPARC in the dynamic interaction between the tumor and the host. *Cancer. Metastasis. Rev*. **2008**, 27, 691–705.

31. Kratz, F.; Müller-Driver, R.; Hofmann.; *et al.* A novel macromolecular prodrug concept exploiting endogenous serum albumin as a drug carrier for cancer chemotherapy. *J. Med. Chem*. **2000**, 43, 1253–1256.

32. Kratz, F.; Warnecke, K.; Scheuermann, C.; *et al.* Probing the cysteine-34 position of endogenous serum albumin with thiol-binding doxorubicin derivatives. Improved efficacy of an

acid-sensitive doxorubicin derivative with specific albumin-binding properties compared to that of the parent compound. *J. Med. Chem*. **2002**, 45, 5523–5533.

33. Graeser, R.; Esser, N.; Unger, H.; *et al.* INNO-206, the (6-maleimidocaproyl hydrazone derivative of doxorubicin), shows superior antitumor efficacy compared to doxorubicin in different tumor xenograft models and in an orthotopic pancreas carcinoma model. *Invest. New. Drugs.* **2010**, 28, 14–19. Epub 2009, Jan 8.

34. Unger, C.; Häring, B.; Medinger, M.; *et al.* Phase I and pharmacokinetic study of the (6-maleimidocaproyl) hydrazone derivative of doxorubicin. *Clin. Cancer. Res*. **2007**, 13, 4858–4866.

35. Kratz, F.; Fichtner, I.; Graeser, R. Combination therapy with the albumin-binding prodrug of doxorubicin (INNO-206) and doxorubicin achieves complete remissions and improves tolerability in an ovarian A2780 xenograft model. *Invest. New. Drugs*. **2011**, [Epub ahead of print].

36. Calderón, M.; Welker, P.; Licha,K.; *et al.* Development of efficient acid cleavable multifunctional prodrugs derived from dendritic polyglycerol with a poly(ethylene glycol) shell. *J. Control. Release*. **2011**, 151, 295–301.

37. Hofmann, U.B.; Westphal, J.R.; van Muijen, G.N.P.; *et al.* Matrix metalloproteinases in human melanoma. *J. Investig. Dermatol.* **2000**, 115, 337–344.

38. Curran, S.; Murray, G.I. Matrix metalloproteinases in tumour invasion and metastasis. *J. Pathol.* **1999**, 189, 300–308.

39. Chambers, A.F.; Matrisian, L. M. Changing views of the role of matrix metalloproteinases in metastasis*. J. Natl. Cancer. Inst*. **1997**, 89, 1260–1270.

40. Hofmann, U.B.; Westphal, J.R.; Waas, E.T.; *et al.* Matrix metalloproteinases in human melanoma cell lines and xenografts: increased expression of activated matrix metalloproteinase-2 (MMP-2) correlates with melanoma progression. *Br. J. Cancer*. **1999**, 81, 774–782.

41. Sun, W.; Schuchter, L.M. Metastatic melanoma. *Curr. Treat. Options. Oncol*. **2001**, 2, 193–202.

42. Kurschat, P.; Zigrino, P.; Nischt, R.; *et al.* Tissue inhibitor of matrix metalloproteinase-2 regulates matrix metalloproteinase-2 activation by modulation of membrane-type 1 matrix metalloproteinaseactivity in high and low invasive melanoma cell lines. *J. Biol. Chem*. **1999**, 274, 21056–21062.

43. Fiebig, H.H.; Klostermeyer, A.; Schüler, J.B.; *et al.* Characterization of matrix metalloproteinases in 47 human tumor xenografts show high expression of MMP-2 in melanomas and sarcomas. *Proc. Am*. *Assoc. Cancer. Res*. **1999**, 40, 463.

44. Väisänen, A.; Tuominen, H.; Kallioinen, M.; *et al.* Matrix metalloproteinase-2 (72 kD type IV collagenase) expression occurs in the early stage of human melanocytic tumour progression and may have prognostic value. *J. Pathol*. **1996**, 180, 283–289.

45. Mansour, A.M.; Drevs, J.; Esser, N.; *et al.* A New Approach for the Treatment of Malignant Melanoma: Enhanced Antitumor Efficacy of an Albumin-binding Doxorubicin Prodrug That Is Cleaved by Matrix Metalloproteinase 2. *Cancer. Res*. **2003**, 63, 4062-4066.

46. Abu Ajaj, K.; Graeser, R.; Fichtner, I.; *et al.* In vitro and in vivo study of an albumin-binding prodrug of doxorubicin that is cleaved by cathepsin B. *Cancer. Chemother. Pharmacol*. **2009**, 64, 413–418.

47. Turk, B.; Turk, D.; Turk, V. Lysosomal cysteine proteases: more than scavengers. *Biochim*. *Biophys. Acta*. **2000**, 1477, 98–111.

48. Buck, M.R.; Karustis, D.G.; Day, N.A.; *et al.* Degradation of extracellular-matrix proteins by human cathepsin B from normal and tumour tissues. *Biochem. J.* **1992**, 282, 273–278.

49. Mai, J.; Sameni, M.; Mikkelsen, T.; *et al.* Degradation of extracellular matrix protein tenascin-C by cathepsin B: an interaction involved in the progression of gliomas. *Biol. Chem.* **2002**, 383, 1407–1413.

50. Barthel, B.L.; Zhang, Z.; Rudnicki, D.L.; *et al.* Preclinical efficacy of a carboxylesterase 2-activated prodrug of Doxazolidine. *J. Med. Chem*. **2009**, 52, 7678-7688.

51. Barthel, B.L.; Torres, R.C.; Hyatt, J.L.; *et al.* Identification of human intestinal carboxylesterase as the primary enzyme for activation of a doxazolidine carbamate prodrug. *J. Med. Chem.* **2008**, 51, 298-304. Epub 2008 Jan 4.

52. Burkhart, D.J.; Barthel, B.L.; Post, G.C.; *et al.* Design, Synthesis, and Preliminary Evaluation of Doxazolidine Carbamates as Prodrugs Activated by Carboxylesterases. *J. Med. Chem*. **2006**, 49, 7002-7012.

53. Burke, P.J.; Koch, T.H. Design, synthesis, and biological evaluation of doxorubicin-formaldehyde conjugates targeted to breast cancer cells. *J. Med. Chem*. **2004**, 47, 1193-1206.

54. Burke, P.J.; Koch, T.H. Doxorubicin-formaldehyde conjugate, doxoform: induction of apoptosis relative to doxorubicin. *Anticancer. Res*. **2001**, 21, 2753-2760.

55. Walko, C.M.; Lindley, C. Capecitabine: a review. *Clin. Ther*. **2005**, 27, 23-44.

56. Parker, W.B.; Y.C. Cheng. Metabolism and mechanism of action of 5-fluorouracil. *Pharmacol. Ther*. **1990**, 48, 381-95.

57. Wagstaff, A.J.; Ibbotson, T.; Goa, K.L. Capecitabine: a review of its pharmacology and therapeutic efficacy in the management of advanced breast cancer. *Drugs*. **2003**, 63, 217-236.

58. Post, G. C.; Barthel, B. L.; Burkhart, D. J.; Hagadorn, J. R.; Koch, T. H. Doxazolidine, a proposed active metabolite of doxorubicin that cross-links DNA. *J Med Chem*. **2005**, 48, 7648-57.

59. Gude, M.; Ryf, J.; White, P. An accurate method for quantitation of Fmoc-derivitized solid phase supports. *Letters in Peptide Science*. **2002**, 9, 203-206.

60. Rusiecki, V.K.; Warne,S.A. Synthesis of N_{α}-Fmoc-N_{ε}-Nvoc-Lysine and use in the preparation of selectively functionalized peptides. *Bioorg. Med. Chem*. Lett. **1993**. 3, 707-710.

Appendix I Selected NMR Spectra

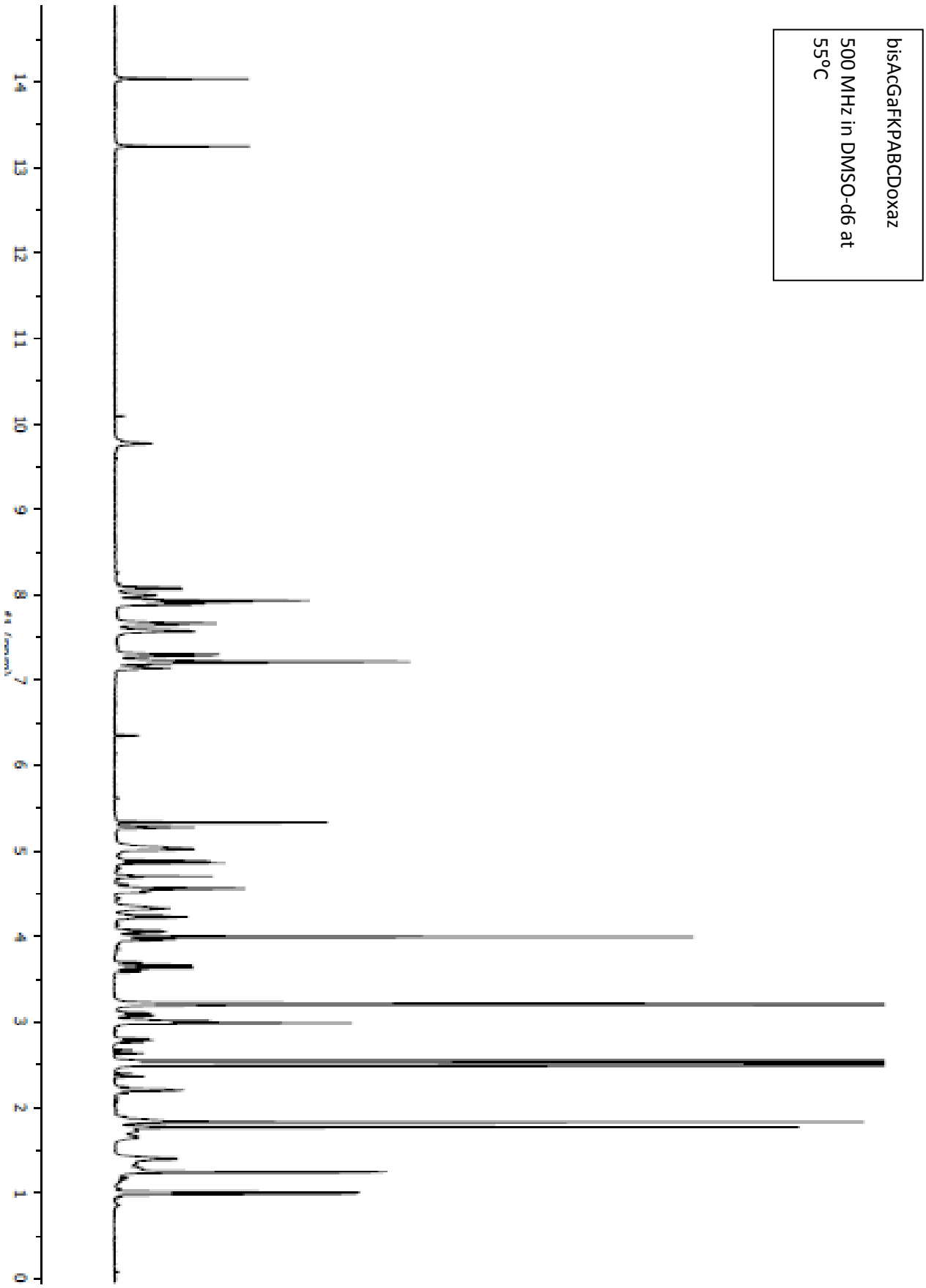
bisAcGaFKPABCDoxaz
500 MHz in DMSO-d6 at 55°C
f1 /ppm

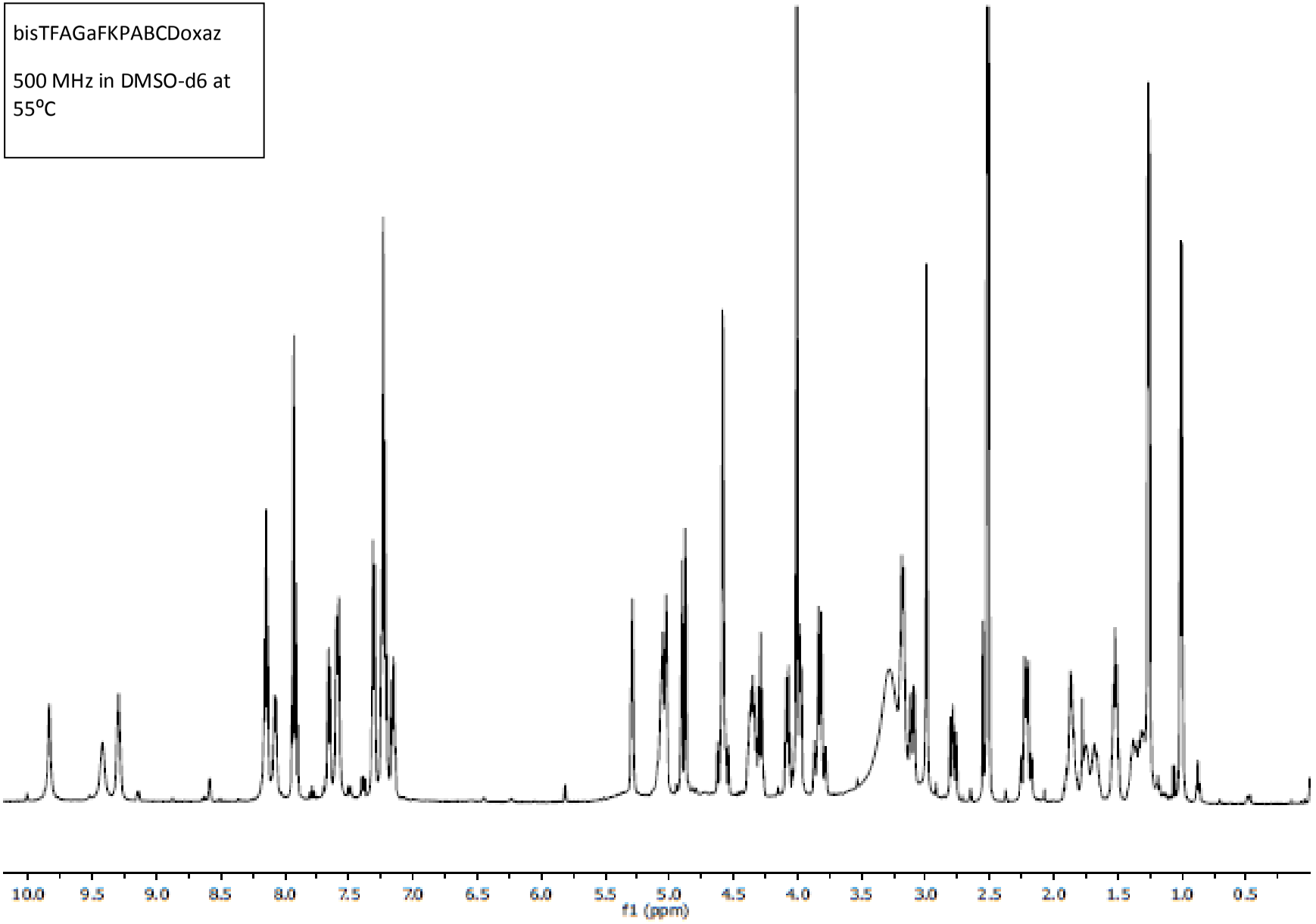
bisTFAGaFKPABCDoxaz
500 MHz in DMSO-d6 at 55°C
10.0
9.5
9.0
8.5
8.0
7.5
7.0
6.5
6.0
5.5
5.0
4.5
4.0
3.5
3.0
2.5
2.0
1.5
1.0
0.5
f1 (ppm)

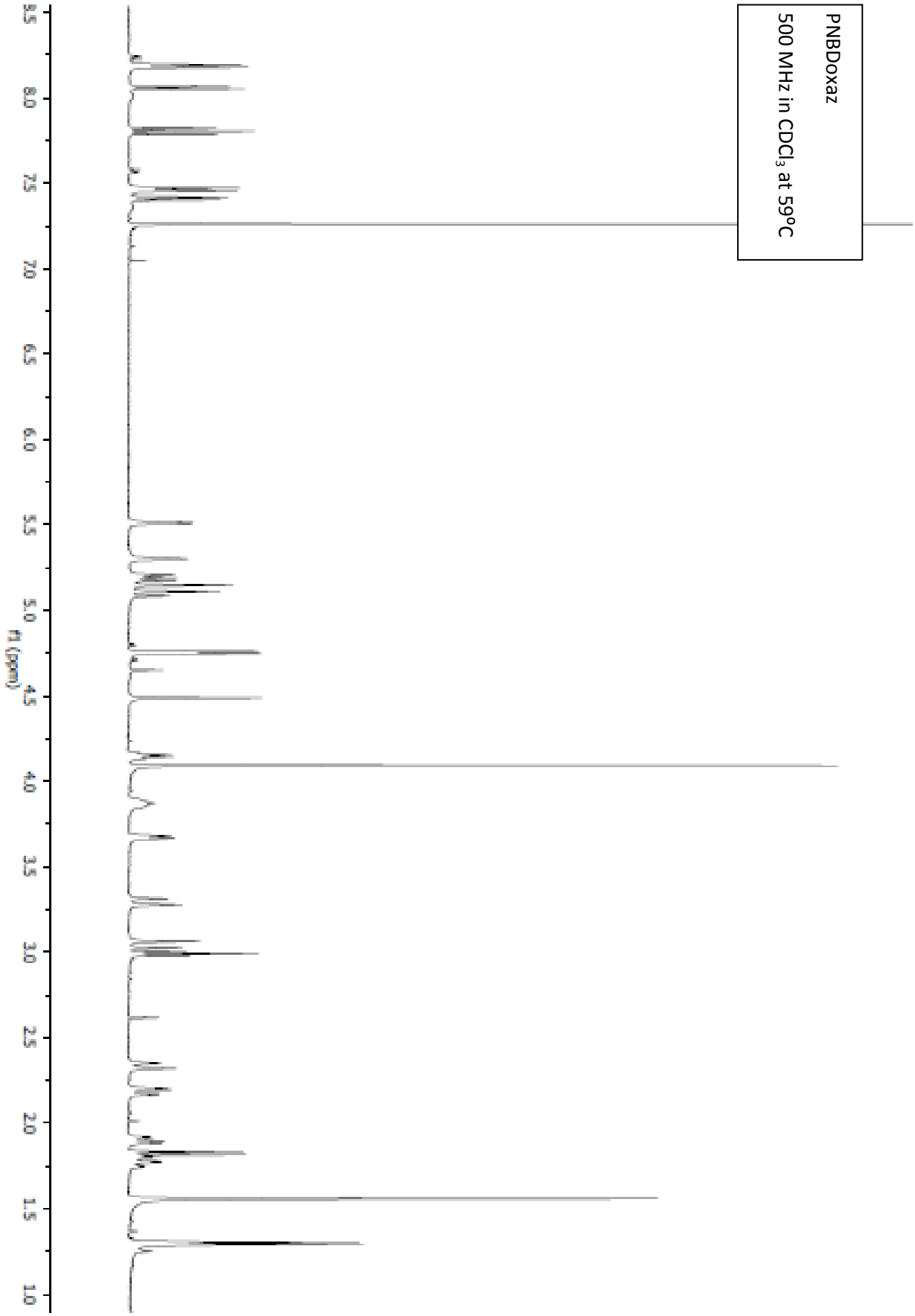
PNBDoxaz
500 MHz in CDCl3 at 59°C
f1 (ppm)
8.5
8.0
7.5
7.0
6.5
6.0
5.5
5.0
4.5
4.0
3.5
3.0
2.5
2.0
1.5
1.0

PNBPABADoxaz

500 MHz in $CDCl_3$ at 59°C

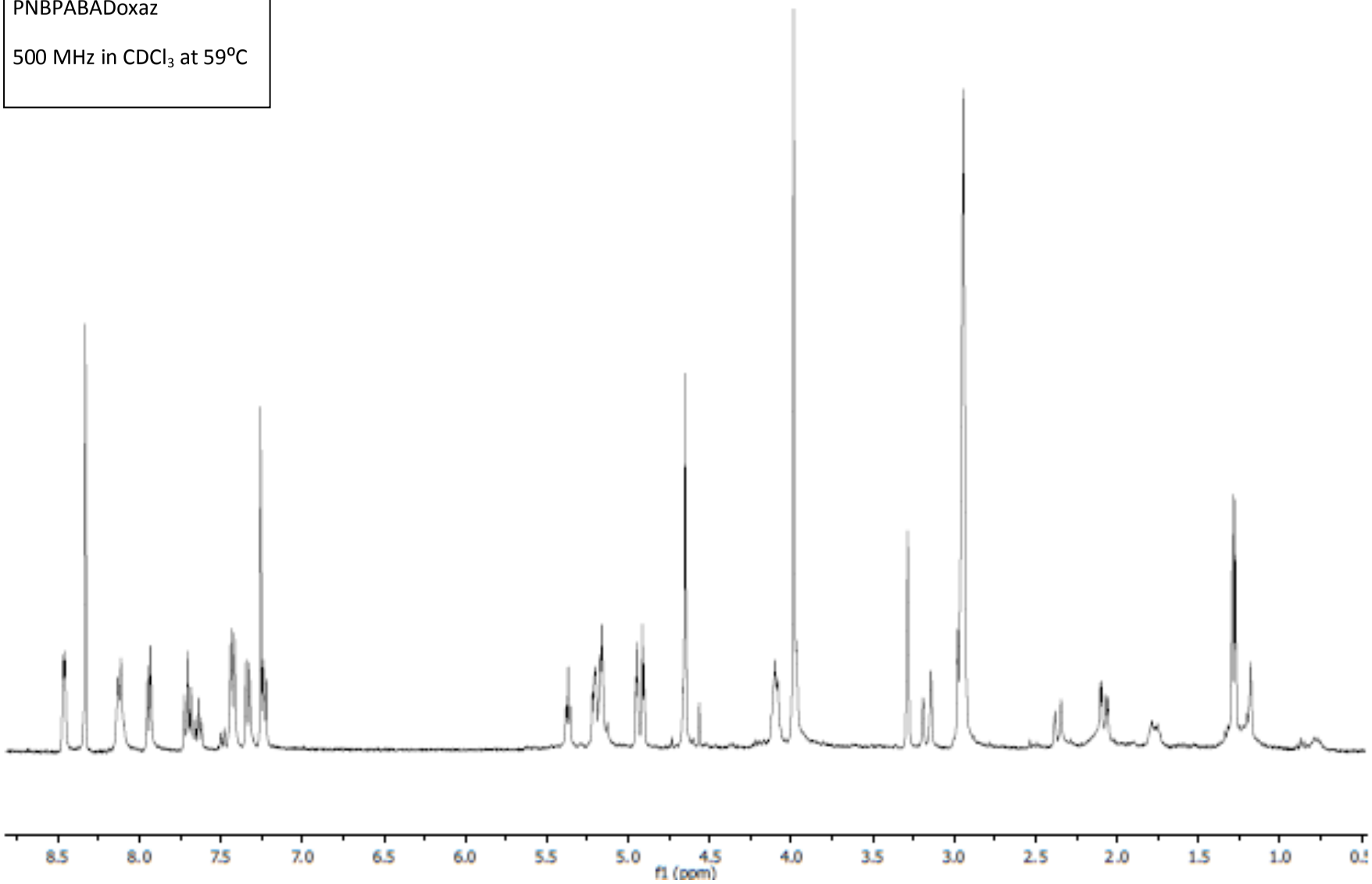

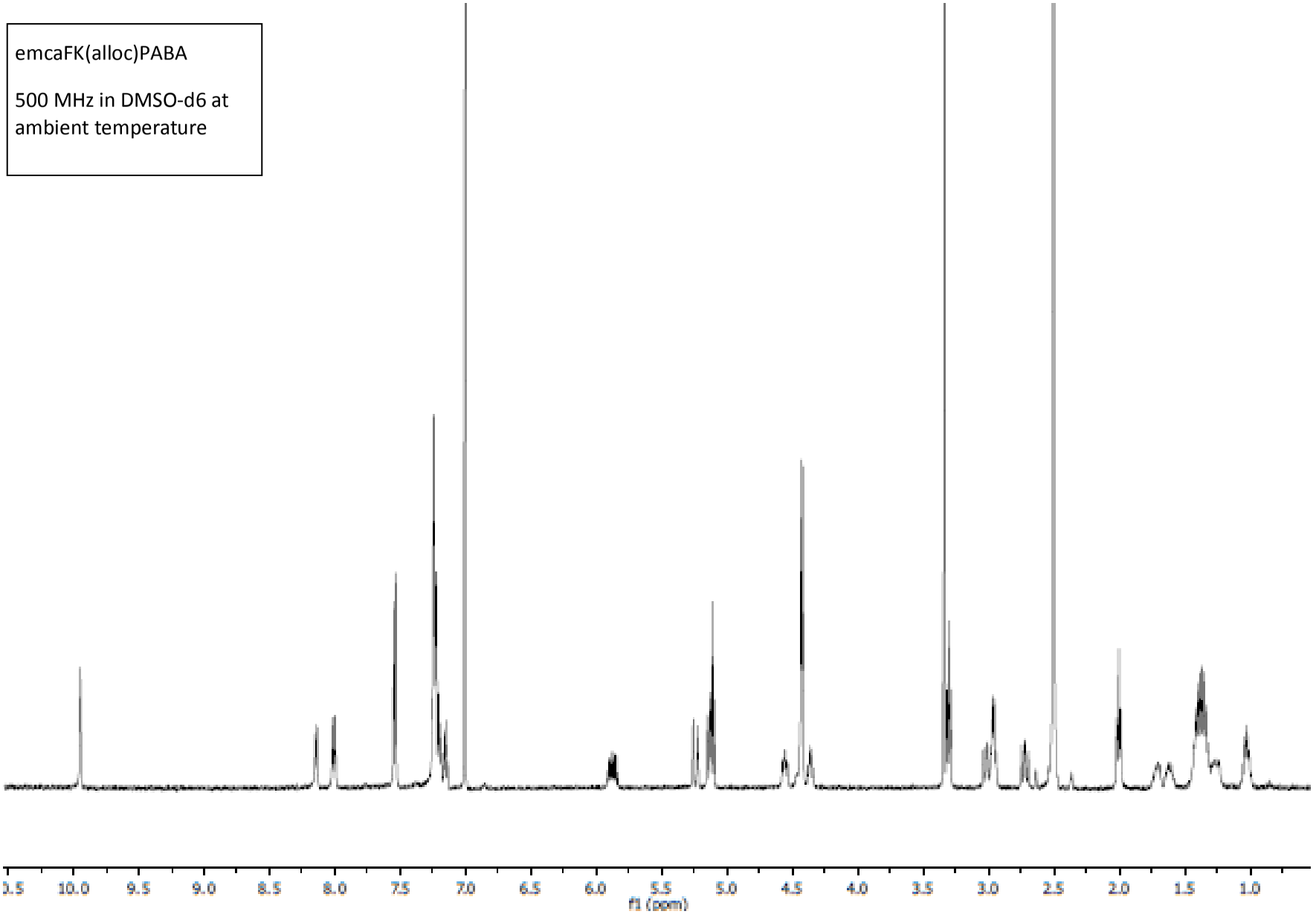
emcaFK(alloc)PABA
500 MHz in DMSO-d6 at ambient temperature
10.0
9.5
9.0
8.5
8.0
7.5
7.0
6.5
6.0
5.5
5.0
4.5
4.0
3.5
3.0
2.5
2.0
1.5
1.0
f1 (ppm)

emcaFK(alloc)PABAPNP

500 MHz in DMSO-d6 at ambient temperature

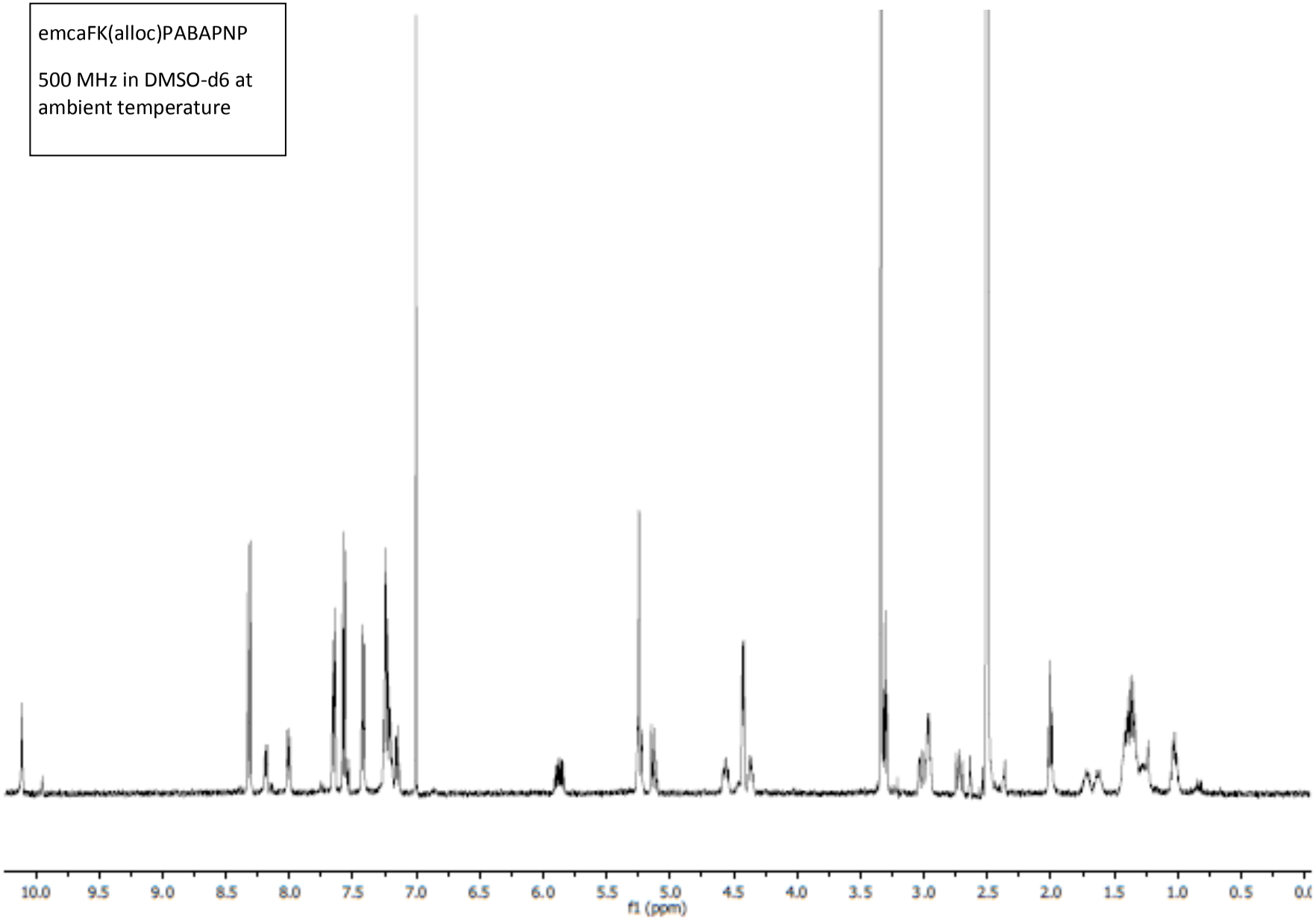

emcaFK(alloc)PABCDoxaz

500 MHz in DMSO-d6 at 55°C

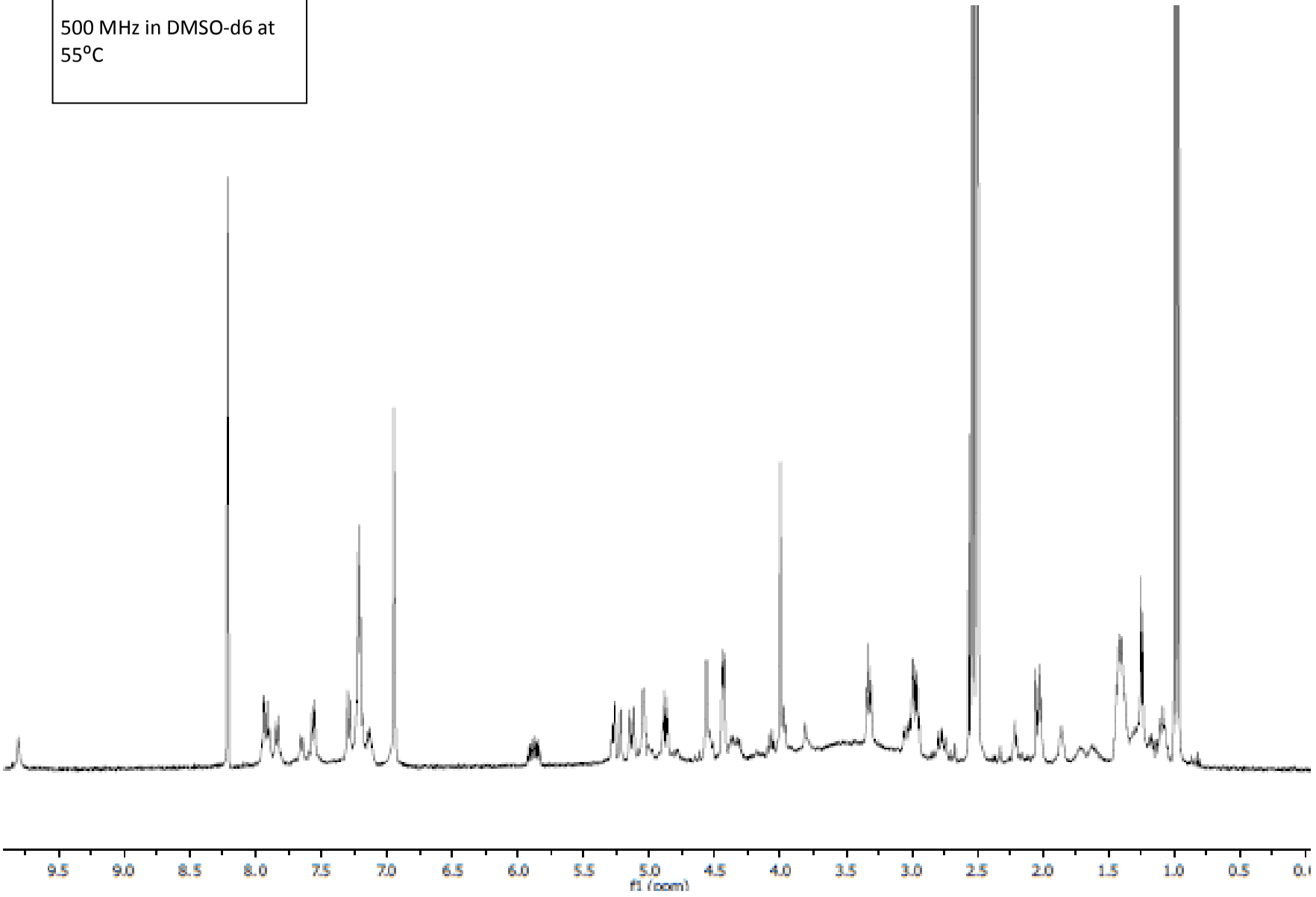

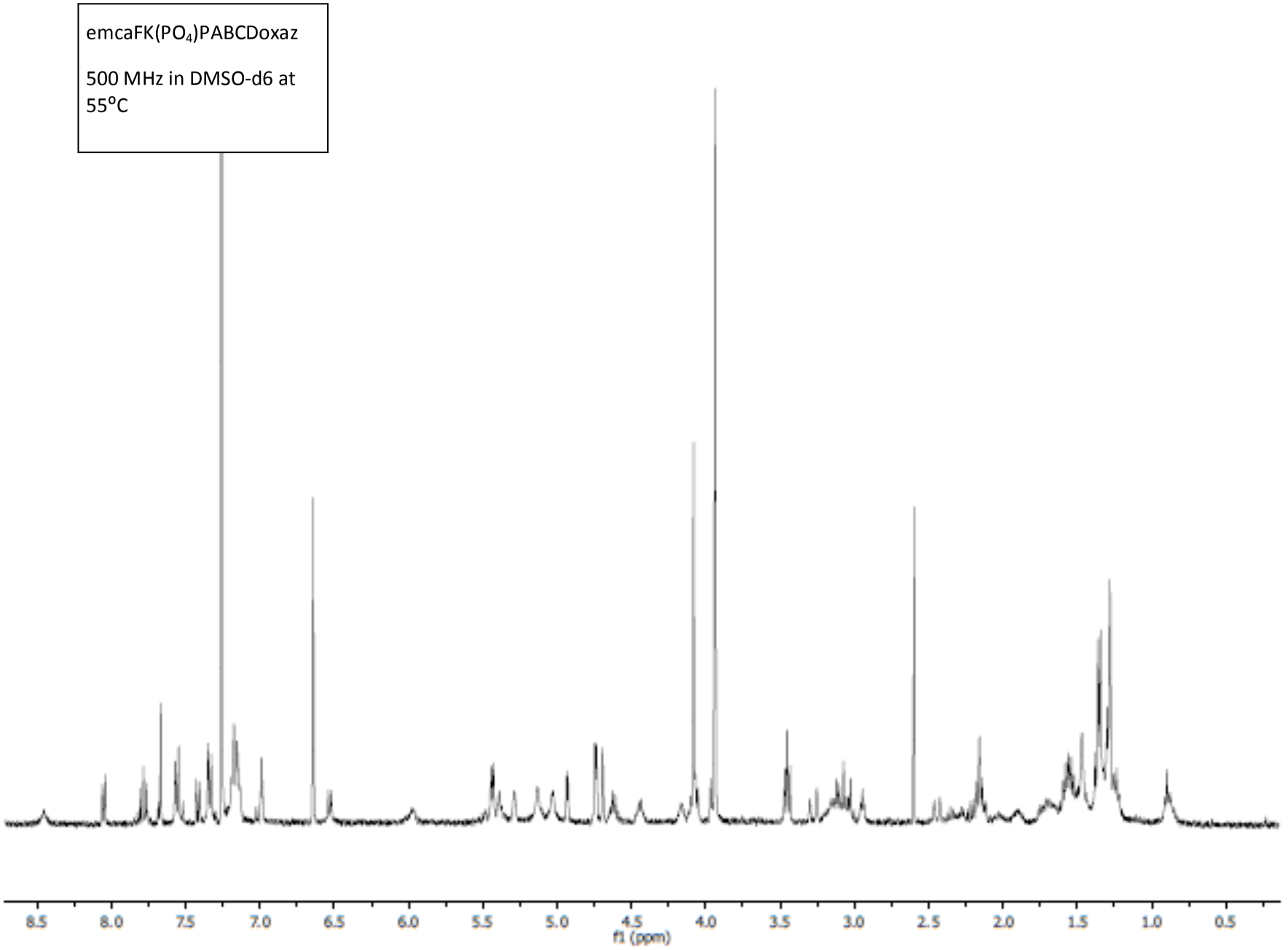
emcaFK(PO4)PABCDoxaz
500 MHz in DMSO-d6 at 55°C
8.5
8.0
7.5
7.0
6.5
6.0
5.5
5.0
4.5
4.0
3.5
3.0
2.5
2.0
1.5
1.0
0.5
f1 (ppm)

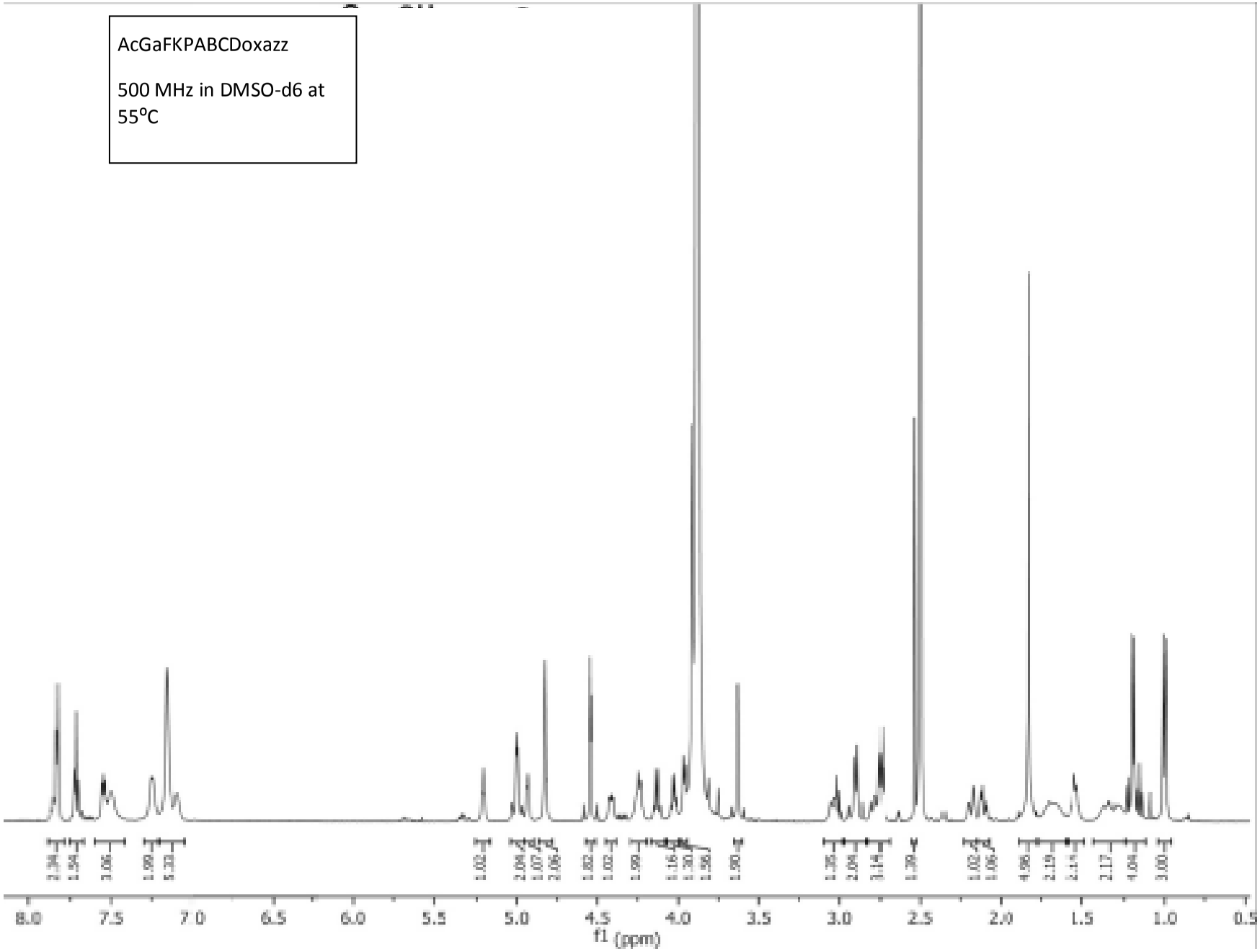
AcGaFKPABCDoxazz
500 MHz in DMSO-d6 at 55°C
8.0
7.5
7.0
6.5
6.0
5.5
5.0
4.5
4.0
3.5
3.0
2.5
2.0
1.5
1.0
0.5
f1 (ppm)

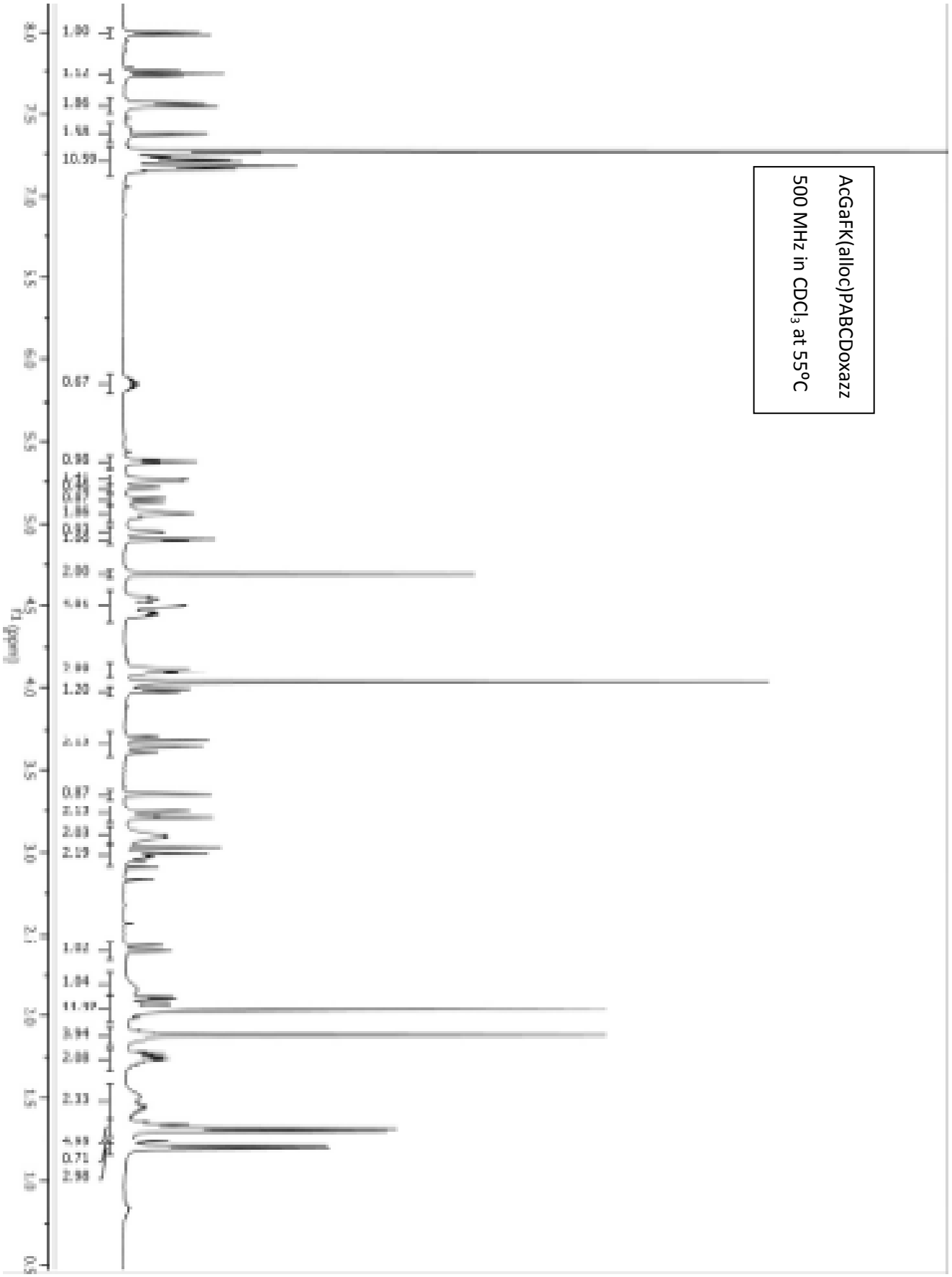
AcGaFK(alloc)PABCDoxazz
500 MHz in $CDCl_3$ at 55°C